
**Exactly Solvable Models of Strongly Correlated Systems:
Application to One-dimensional Cold Gases and Quantum
Impurity Problems**

Der Fakultät für Mathematik und Physik der
Gottfried Wilhelm Leibniz Universität Hannover
zur Erlangung des Grades
Doktor der Naturwissenschaften
Dr. rer. nat.
genehmigte Dissertation

von
M. Sc. Guillaume Palacios
geboren am 20. März 1980 in Enghien-les-Bains (Frankreich)

Oktober 2007

Referent: Prof. Dr. Holger Frahm
Korreferent: Prof. Dr. Luis Santos
Tag der Promotion: 14 November 2007

A mes parents, Christiane et Jean-Luc

Zusammenfassung

In dieser Arbeit wird der Bethe-Ansatz herangezogen, um physikalische Eigenschaften zweier weithin untersuchter Systemklassen zu bestimmen: kalte Gase und Quantenstörstellen.

In Teil I werden aus den *finite-size* Korrekturen des Modellspektrums die kritischen Exponenten der Modelle am Quanten-kritischen Punkt bestimmt und aus bekannten Resultaten der Konformen Feldtheorie das asymptotische Verhalten von Korrelationsfunktionen ermittelt. Letzteres konnte sogar Bose-Fermi Gasgemische in einer Raumdimension erweitert werden. Ein nichttriviales Ergebnis dieser Analyse ist das Auftreten (bislang nicht beobachteter) Singularitäten in der Impulsverteilungsfunktion. Sie wären ein klares Indiz für starke Korrelationen in zukünftigen Experimenten.

Teil II beschäftigt sich mit der Physik von Randeffekten und Störstellen in stark korrelierten Systemen. Die Quanten-Inverse-Streumethode bietet hier ein leistungsfähiges Werkzeug zur Konstruktion zweier physikalisch interessanter Störstellenmodelle für die t - J Kette. Das erste dieser Modelle trägt eine Anderson-artige Störstelle, deren lokales Spektrum über einen Randparameter kontrolliert werden kann. Im thermodynamischen Limes kann hier eine Sequenz gebundener Randzustände ausgemacht werden. Im Limes schwacher Ankopplung der Störstellen an den Bulk konnte Kondo-artiges Verhalten nachgewiesen werden, welches durch einen Übergang von linearem Verhalten zu Sättigungsverhalten der Störstellenmagnetisierung charakterisiert wird. Die Kondo-Skala ist dabei als Funktion der Störstellenparameter bestimmt worden. Schließlich konnte durch eine Projektionsmethode direkt ein zweites integrables Modell mit Kondo-Störstelle erzeugt werden. Diese Projektionsmethode ähnelt einer Schrieffer-Wolf Transformation zwischen Anderson- und Kondo-Störstelle. Auch hier konnte klares Kondo-Verhalten in der Störstellenmagnetisierung bei schwacher antiferromagnetischer Ankopplung an der Bulk nachgewiesen werden, mit klarer Unterscheidung der Fixpunkt für $s = 1/2$ und $s > 1/2$ im Niederfeldlimes. Sowohl im ferromagnetischen als auch im *under-screened* Sektor zeigt das System eine Divergenz der magnetischen Suszeptibilität.

Schlagworte: Bethe Ansatz lösbare Modelle – stark korrelierte Systeme – Kondo Physik

Abstract

In this thesis we use Bethe-ansatz solvable models to describe the properties of two types of systems widely studied in contemporary physics: one-dimensional cold gases and quantum impurities.

In Part I, we show how the computation of the finite-size spectrum from the Bethe ansatz can be used to extract the critical exponents of the underlying theory. Based on results borrowed from conformal field theory, we review how the asymptotic behaviour of the correlation functions in the δ -Bose gas can be calculated, and make the connection with the Tomonaga-Luttinger picture. We then extend this approach to the case of several degrees of freedom through the specific example of the one-dimensional Bose-Fermi mixture. We present some original computations of the critical exponents of such systems and argue on the experimental relevance of our results. Of particular interest is the prediction, from our analysis, of non-trivial singularities in the momentum distribution function of the mixture that should be observable as a signature of the strongly interacting nature of the system.

In Part II, the issue of boundaries and impurities in models of correlated electrons is considered. Within the quantum inverse scattering method, we construct two models of impurities in the supersymmetric t - J model. We first describe an Anderson-like impurity whose local spectrum can be controlled through a continuous parameter without breaking integrability. Analysing the Bethe-ansatz equations in the thermodynamic limit, we exhibit in the spectrum a sequence of boundary bound states that we describe with precision. The impurity magnetization, susceptibility and compressibility are calculated exactly. For small enough hybridization, we show that the system exhibits a Kondo-like behaviour characterised by a crossover from a linear to a saturated dependence of the magnetization. The Kondo regime is governed by an intrinsic Kondo scale function of the impurity parameters. Finally, we construct a model of a Kondo (spin- s) impurity still taking the t - J model as the correlated host. We calculate the finite-size spectrum and the impurity magnetization. For small anti-ferromagnetic Kondo coupling, the system features a screening of the impurity at low-energy. A clear difference between the $s = 1/2$ fixed point, which is a singlet state, and the $s > 1/2$ under-screened case is established on behalf of an explicit calculation of the low-field impurity magnetization.

Keywords: Bethe Ansatz solvable models – strongly correlated systems – Kondo physics

Preface

Motivations

It appears that it is rather difficult to give a satisfactory mathematical definition of quantum exactly solvable models, but generally one could say that they constitute a class of models whose eigenstates, spectrum, and expectation values of interest are known exactly. Exactly solvable models are "toy models", stripped down to the most accessible non-trivial form, which displays nevertheless a rich physics. Historically, the first interacting quantum model which has been solved exactly was the Heisenberg spin chain. To tackle this problem, Bethe introduced an *ansatz*¹ which today is bearing his name [25]. Because of the nature of the interactions coupling only nearest-neighbours sites, Bethe came up with a clever eigenfunction which is almost like a free plane wave of the form $\exp(ikx)$, the effect of the interactions being simply encoded into a two-body scattering phase. In fact, all integrable theories share the property that the N -body scattering is purely elastic and the full S -matrix is completely determined by the computation of the two-body operator. Today, many other quantum many body systems are known to be solvable by some variant of the Bethe ansatz, and the method has been generalized and expanded far beyond its original scope. But here we should say that, despite the promise made by Bethe² at the end of its original paper, the Bethe ansatz technique remains limited to one-dimensional (1D) systems. Therefore, in this thesis, we will restrict ourselves to the study of systems in 1+1 (space+time) dimension only.

1D systems have been intensively investigated in the last decades and have been proved to be very peculiar compared to 2D or 3D systems. In 1D, even the smallest amount of interaction is known to have drastic effects leading to a physics which cannot be captured by standard perturbation theory. In the context of electronic systems, the Landau Fermi Liquid picture, based on a one-to-one correspondence between electrons and low energy modes or quasiparticles, breaks down in 1D. Instead, 1D electrons are conceptually described by a Tomonaga-Luttinger (TL) which exhibits non-trivial physics;

¹In German ansatz means trial function.

²"In einer folgenden Arbeit soll die Methode auf räumliche Gitter ausgedehnt werden"

most surprisingly, the electrons are no longer the central objects of the theory but rather their charge and spin excitations, separately. This phenomenon is known as the *spin-charge separation*. A lot of theoretical efforts have been devoted to the understanding of the peculiar physics which occurs in 1D, with the development of new and specific techniques, e.g. field theory descriptions via the bosonization prescription [64, 62], conformal field theory (CFT) techniques, and numerics. We want to emphasize, since it will be the core of the present work, that Bethe-ansatz solvable models provide, by essence, a non-perturbative approach to strongly correlated systems.

Not only they give us a good understanding of the elementary excitations of such systems, but exactly solvable models are also a benchmark for the numerics like numerical and density matrix renormalization group algorithms. We would like to note that the Bethe-Ansatz solution of the XXZ spin-1/2 chain has also permitted to fix the values of the renormalized couplings entering the low-energy field theory [102, 27]. Recently, a more exotic (or better saying unexpected) connection was pointed up: the anomalous scaling dimensions of certain supersymmetric gauge theories can be derived from the spectrum of an integrable spin chain [21, 23, 22]. Thus, integrable models have become very trendy among string theorists in the context of the now famous AdS/CFT correspondence [104]. Last but not least, integrable models have true realizations in nature, e.g. certain 1D magnets are accurately represented by an Heisenberg spin chain. For these systems, in recent works [28] the Bethe ansatz has permitted to determine the dynamical structure factor of the spin excitations

$$S^{\alpha\alpha}(q, \omega) = \int dt e^{i(qx - \omega t)} \langle S^{\alpha}(x, t) S^{\alpha}(0, 0) \rangle$$

with a remarkable accuracy, and comparison with neutron scattering experiments [93] is excellent (see Fig. 0.1)

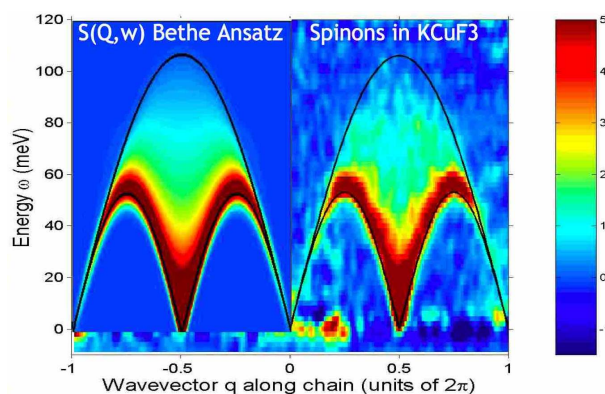


Figure 0.1: Comparison of the dynamic structure factor $S(q, \omega)$ between the experiment realized on the KCuF3 compound (Tennant's group HMI Berlin) and Bethe Ansatz (Caux and Maillet). Extracted from <http://staff.science.uva.nl/~jcaux/ABACUS.html>.

Outline

In this work we will concentrate on two specific physical situations where the Bethe ansatz can be applied successfully: one-dimensional cold gases and quantum impurity problems. The first part, decomposed into four chapters, is dedicated to the study of the critical properties of one-dimensional cold gases. After giving a short introduction to one-dimensional atomic gases in the first chapter, we continue by showing an explicit Bethe-ansatz solution of the δ -interacting Bose gas. Chapter 3 presents an elementary discussion of the link between 1D models and CFT. A special emphasis is put on the relation between the finite-size spectrum of the microscopic model on one hand and the conformal data on the other hand, using the one-dimensional Bose gas as an illustration. We conclude this part in Chapter 4 by presenting the calculation of the exact critical exponents of a 1D Bose-Fermi mixture invoking arguments from CFT introduced in Chapter 3. The second part of the thesis, also divided into four chapters, is dealing with boundaries and impurities in models of correlated electrons. Chapter 5 is a broad introduction to the physics of quantum impurities and the Kondo effect. Chapter 6 contains a rapid description of some model Hamiltonians widely used in condensed matter, namely the Hubbard model and its descendants, the Heisenberg and t - J models. Then, we make a short introduction to the modern language of quantum integrability which goes under the name of the Quantum Inverse Scattering Method (QISM). This technique is afterwards used to construct two models of quantum impurities into a correlated host. More precisely, in Chapter 7, we construct and examine the thermodynamical properties of an Anderson impurity in a t - J model. Finally, in Chapter 8, we will show how to derive an integrable model describing a Kondo impurity in a t - J chain and quantify the influence of this impurity on the magnetic behaviour of the system.

List of related publications

- Holger Frahm and Guillaume Palacios
Correlation functions of one-dimensional Bose-Fermi mixtures
Phys. Rev. A **72** (2005) 061604(R) [cond-mat/0507368]
- Holger Frahm and Guillaume Palacios
Anderson-like impurity in the one-dimensional t - J model: Formation of local states and magnetic behaviour
Phys. Rev. B **73** (2006) 214419 [cond-mat/0603198]
- Holger Frahm and Guillaume Palacios
Integrable Anderson-like impurity in the supersymmetric t - J model
(Proceedings of the Workshop Classical and Quantum Integrable Systems, Protvino, January 2006)
Theor. Math. Phys. **150** (2007) 338–352
- Holger Frahm and Guillaume Palacios
Interplay between a quantum impurity and a boundary field in the SUSY t - J model
J. Stat. Mech. (2007) P05006 [cond-mat/0703339]
- Holger Frahm and Guillaume Palacios
Magnetic properties of a boundary Kondo impurity in the one-dimensional t - J model
in preparation

Other publications

- Julien Vidal, Guillaume Palacios and Rémy Mosseri
Entanglement in a second order quantum phase transition
Phys. Rev. A **69** (2004) 022107 [cond-mat/0305573]
- Julien Vidal, Guillaume Palacios and Claude Aslangul
Entanglement dynamics in the Lipkin-Meshkov-Glick model
Phys. Rev. A **70** (2004) 062304 [cond-mat/0406481]
- Andreas Osterloh, Guillaume Palacios and Simone Montangero
Enhancement of pairwise entanglement from \mathbb{Z}_2 symmetry breaking
Phys. Rev. Lett. **97**, 257201 (2006) [cond-mat/0608244]
chosen for publication in the July 3, 2007 issue of the Virtual Journal of Nanoscale Science & Technology

Acknowledgements

My first thank goes to "chef" Prof. Dr. Holger Frahm, tall by his size and his expertise. To be part of his group was a true pleasure. I thank him for the quality of his guidance, his patience, his trust. In German, there is the expression *Doktorvater* to qualify your PhD's supervisor. Well, in the case of Holger, I find this expression particularly appropriate and I will try my best to make my way in physics using what he taught me. The tradition wants that the apprentice becomes stronger than his master. In that case, I still have a lot to learn!

I am very honoured that such distinguished physicists as Prof. Dr. Luis Santos and Prof. Dr. Rolf Haug accepted to be respectively the co-referee of my thesis and the chairman on the jury. I want to acknowledge *the wise guys* Prof. Dr. Hans-Ulrich Everts and Prof. Dr. Hans-Jürgen Mikeska for their sympathy, their advices, their help. A big *merci* to Prof. Dr. Eric Jeckelmann who gave me the opportunity to practice my French and to make the tutorials for its lecture on Condensed Matter Theory. Honestly, I guess it was even more a benefit for me than for my talented students. Thanks to Dr. Michael Flohr for trusting me for the preparation of the Statistical Mechanics tutorials. Greetings to Prof. Dr. Olaf Lechtenfeld. I enjoyed his nice lectures on QFT. I cheer up with Tobias Wirth, Alexander Seel for reviewing this manuscript, and Jörn Broer. I am so indebted to the dynasty of admins Carsten I the great and Carsten II the prince for their marvelous work in dealing with computers. Hola to the ITP soccer team, *los Columbianos* Arturo and Karen, Philipp, the entangled twins Carsten and Micha, and Garu who joined us during the *mercato*. Hallo to my friends from the Flohr's group Kirsten, Henne, and Lily *the Diva*, to my SUSY partners, Martin Wolf who moved to Imperial College and Robert Wimmer now in Stony Brook, to Klaus Osterloh a.k.a *the spokesman* now trying to make money in the consulting business, to Malcolm Einhellinger and his incomparable laugh.

I want to thank sincerely, my friend and room-mate Dr. Andreas Osterloh a.k.a *the Italian*, with whom I had the chance to collaborate and to talk about the fascinating world of entanglement.

Special thanks to Emma Schwebs, a fantastic secretary. She really helped me a lot at my arrival and during my stay here in Hannover. Without her, I would probably be still struggling with the German administrations. Actually

I should not complain, the French ones are even worst.

Big up to Maciej Lewenstein! I thank him for his interest in our work on the Bose-Fermi mixture, for his invitation to Barcelona, and his support. To the ICFO people in Barcelona especially to Jarek, Armand, and Anja. Respect!

My stay in Hannover wouldn't have been so nice if I haven't met some fantastic people that I consider today as true friends: the excellent Alexei Kolezhuk, the bright Temo Vekua, Alex I, the intellectual, Alex II the N.B.A, the little Joyce, Dorian and Alban, the *Frenchies*, Kadiatou, the *Lituanian chicks* Ieva and Birute. Special mention to my very special friend Sarah, without you life wouldn't be so colourful. Thanks also to my friends in France, Belgium, UK, who still count for me. I'm thinking of Amino, Alaric, Dorothée "Sangoku", the perfect couple Sonia and Marco, Vince and the notorious Stefano.

Words cannot express all my gratitude and affection to my wonderful parents Christiane and Jean-Luc who always supported my choices even the craziest, to my little brother Hugo; remember his name he is going to become a great star! Tata Colette, Elise and JC, Alice and little Vicky, I think of you. My girls in Spain, Tata Marie-France, Anita and Maria, thank you so much for your cards and emails. It was a like a little ray of sun each time.

Contents

| | | |
|-----------|---|-----------|
| I | One-dimensional Cold Gases | 19 |
| 1 | Introduction to one-dimensional atomic gases | 21 |
| 1.1 | Bosons | 21 |
| 1.2 | Fermions and Bose-Fermi mixtures | 23 |
| 2 | The one-dimensional δ-Bose gas | 25 |
| 2.1 | Construction of exact eigenstates | 25 |
| 2.2 | The many-body ground state | 28 |
| 2.3 | Elementary excitations | 31 |
| 3 | Finite-size scaling and conformal field theory | 33 |
| 3.1 | Universality and finite-size spectrum | 33 |
| 3.2 | Correlation functions | 34 |
| 3.3 | Example: correlation functions for the Bose gas | 36 |
| 4 | Critical one-dimensional Bose-Fermi mixtures | 41 |
| 4.1 | Description of the model | 42 |
| 4.2 | Finite-size spectrum | 43 |
| 4.3 | Asymptotics of correlation functions | 45 |
| 4.4 | Experimentally relevant examples | 47 |
| 4.5 | Summary | 50 |
| II | Boundaries/Impurities in correlated electrons models | 55 |
| 5 | Quantum impurities and Kondo effect | 57 |
| 5.1 | Conventional Kondo effect | 58 |
| 5.2 | Kondo effect in nanostructures | 60 |
| 5.3 | Insight from exactly solvable models | 64 |
| 5.4 | Open questions and new trends in quantum impurity problems | 69 |
| 6 | Integrable lattice models of correlated electrons | 73 |
| 6.1 | Models of correlated electrons | 73 |
| 6.2 | Elements of Quantum Inverse Scattering Method | 76 |

| | | |
|----------|---|------------|
| 7 | Anderson impurity in the SUSY t-J model | 89 |
| 7.1 | Presentation of the model | 89 |
| 7.2 | The Bethe Ansatz solution | 92 |
| 7.3 | Characterization of the impurity | 97 |
| 7.4 | Summary | 104 |
| 8 | Kondo impurity in the SUSY t-J model | 107 |
| 8.1 | Hamiltonian | 107 |
| 8.2 | Spectrum and bound states | 109 |
| 8.3 | Reduction to a boundary Kondo problem | 112 |
| 8.4 | Magnetic behaviour of the Kondo impurity | 116 |
| 8.5 | Summary and Outlook | 125 |
| A | The (super)algebra $gl(2 1)$ | 127 |
| A.1 | Generators | 127 |
| A.2 | Irreducible representations | 127 |
| A.3 | Matrix representation | 129 |
| B | Density equations for the open t-J chain | 131 |
| C | The Wiener-Hopf method | 133 |
| C.1 | Wiener-Hopf factorization | 133 |
| C.2 | Applications | 133 |
| D | Derivation of the Hamiltonian (8.1.4) | 137 |
| E | Lai and Sutherland BAE | 141 |
| | Bibliography | 145 |

"As it also may, how useful, not to say how necessary, pictures, and in some cases, models, are wont to be, when engines, houses, ships, and other structures are to be judged of, that they may be approved or improved; but I shall rather take notice that not only mechanical, mathematical, and anatomical things need schemes and pictures to represent them clearly to our conceptions; but many things that are looked upon as more purely physical may, in my opinion, be much illustrated the same way."

Robert Boyle – *Of the Usefulness of Experimental Philosophy*

Part I

One-dimensional Cold Gases

Chapter 1

Introduction to one-dimensional atomic gases

In the first Part of this thesis, we want to discuss a specific realisation of a one-dimensional (1D) system, namely one-dimensional atomic gases. The early studies of such systems, which go back to the 1960's, have been mostly academic. But, in the past years, the technological advances in cooling and trapping of atomic gases have opened the possibility to realize quasi one-dimensional systems with tuneable strength of the interactions in optical lattices. This gives rise to new opportunities for the investigation of the striking phenomena appearing in correlated systems as a consequence of the enhanced quantum fluctuations in reduced spatial dimensions.

1.1 Bosons

In 2003, a true one-dimensional atomic system, consisting of a Bose Einstein condensate (BEC) of rubidium atoms arranged into a thin tube-like shape, has been experimentally demonstrated for the first time, in the ETH lab in Zurich [125]. The ETH researchers began by loading their condensate into an optical lattice, an artificial configuration in which atoms are held and moved about in 3D space by criss-crossing beams of laser light. This experiment succeeded in extruding a condensate into 1000 small needle-like condensates, one dimensional strings of merely 100 atoms (see Fig. 1.1). This experimental breakthrough is an important step towards the understanding of low-temperature 1D atomic systems which behave quite differently from their 2D or 3D counterparts. For example, the 1D Bose gas with repulsive coupling constant becomes more and more interacting as the density of atoms is decreased. This fact is in complete contradiction with what happens in higher dimensions where the more atoms per unit of volume there are, the bigger is the probability that they scatter. In the 1D case, the particles cannot exchange without feeling the interaction. In particular, for an infinite local repulsion,

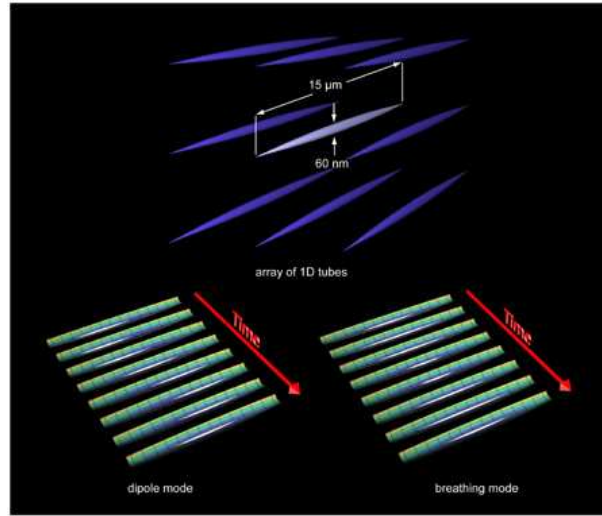


Figure 1.1: Bottom left figure: Time evolution of the 1D gas performing a dipole oscillation in a single tube. Bottom right: Time evolution of the 1D gas after a breathing mode has been excited. Reported by: Moritz et al. [125]

the bosons cannot pass through each other. In this scenario, the 1D Bose gas acquires Fermi-like properties. This case corresponds to the so-called Tonks-Girardeau [128, 63] limit of impenetrable bosons. This highly non-trivial effect can be seen through the Bethe ansatz solution of the Lieb-Liniger [99] model of δ -interacting bosons on a line. Note that contact interactions between the particles is, in the context of atomic physics, an excellent approximation of the leading s -wave scattering process. First solved at zero-temperature, the Lieb and Liniger model was studied at finite temperature in the work of Yang and Yang [140]. Interestingly, in one-dimension, there is no phase transition leading to a BEC even at $T = 0$ ¹. Instead, the system is characterised by continuously varying critical exponents and a power-law decay of the correlation functions. The latter is generally viewed as the appanage of Tomonaga-Luttinger (TL) liquids realized by correlated electrons in 1D lattices. And indeed, Haldane [73] has shown that interacting bosons are, just like fermions, a TL in one dimension. A recent experimental achievement of the 1D gas in the deep Tonks-Girardeau regime has been made by Paredes et al. [117]. In this very experiment, the correlation functions of the system such as the momentum distribution function have been measured directly and the data confirm the "fermionized" theory (see also the work of Kinoshita et al. [84]).

¹Remember that BEC is a phase transition which appears in the 3D case even in the absence of any interaction.

1.2 Fermions and Bose-Fermi mixtures

New correlation effects appear when the particles considered have internal degrees of freedom like fermions with spin. Extensive theoretical studies exist for 1D Fermi gases due to their equivalence with TL liquids [64, 41]. Remarkably, the δ -interacting fermion gas is also exactly solvable [47, 60, 138], but one has to work harder to account for the spin degrees of freedom. The attractive case is particularly interesting because bound fermion pairs can be created. For strong attraction, the bound states behave like tightly bound molecular dimers (condensation-like behaviour), but in the weakly attractive regime, the system is described by Cooper-like pairs (superconductivity behaviour). The attractive fermi gas is thus a playground for investigating the famous BEC-BCS transition.

Given the ongoing experimental progresses in the trapping of fermions in low dimensions, the 1D interacting fermion model may soon be experimentally realized. Then the door is open to realize even more exotic systems. For example, in cold gases containing different constituent atoms Bose-Fermi mixtures can be realized [110, 96]. In fact, a Bose-Fermi mixture in a three-dimensional optical lattice has recently been realised [72].

Chapter 2

The one-dimensional δ -Bose gas

For the first part of this thesis dealing with critical properties of one-dimensional gases, an explicit Bethe Ansatz solution is sufficient to understand what we need. In the second part, when dealing with correlated electrons models and integrable impurities, a more general and powerful (and also more mathematically involved) framework will be introduced: The Quantum Inverse Scattering Method (QISM). This technique is an algebraic version of the traditional Bethe Ansatz. But first let us see through a simple example the ideas behind the coordinate Bethe Ansatz method (as opposed to the algebraic one).

2.1 Construction of exact eigenstates

The model introduced by Lieb and Liniger [99] is given by the following Hamiltonian

$$H = - \sum_{i=1}^N \frac{\partial^2}{\partial x_i^2} + 2c \sum_{i < j} \delta(x_i - x_j) , \quad (2.1.1)$$

or, in second quantization,

$$H = \int dx \{ \partial_x \Psi^\dagger \partial_x \Psi + c \Psi^\dagger \Psi^\dagger \Psi \Psi \} \quad (2.1.2)$$

where the field Ψ is a scalar bosonic field obeying the usual commutation relation

$$[\Psi(x), \Psi^\dagger(y)] = \delta(x - y). \quad (2.1.3)$$

This model describes a system of bosons on a line scattering via contact (δ) interactions. The interaction strength is controlled by the parameter c that can be positive in the case of repulsive bosons or negative, attractive bosons. The first thing to notice is that the Hamiltonian (2.1.2) commutes with the number operator $N = \int \Psi^\dagger \Psi$. Thus every sector a the Hilbert space of the

theory can be classified by their occupation number. This provides us with a natural vacuum $|0\rangle$ of the underlying Fock space.

In the first paragraphs of this section we will consider the case of attractive interaction among the bosons meaning that we will choose $c > 0$. In the last paragraph we will comment briefly on how to treat the repulsive case, namely $c < 0$.

2.1.1 2-particle scattering

Let us start by considering the simple case of two interacting bosons. The free eigenstates of the system are simply constructed by acting with the creation operator $a_k^\dagger = \int dx e^{ikx} \Psi^\dagger(x)$ on the Fock vacuum, i.e.

$$|\psi^{(0)}(k_1, k_2)\rangle = \int dx_1 dx_2 e^{i(k_1 x_1 + k_2 x_2)} \Psi^\dagger(x_1) \Psi^\dagger(x_2) |0\rangle . \quad (2.1.4)$$

To first correction to the free two-boson state can be written, in perturbation theory, as

$$\begin{aligned} |\psi^{(1)}(k_1, k_2)\rangle &= \int \frac{dp_1}{2\pi} \frac{dp_2}{2\pi} \frac{4c(2\pi)\delta(k_1 + k_2 - p_1 - p_2)}{k_1^2 + k_2^2 - p_1^2 - p_2^2 + i\epsilon} a_{p_1}^\dagger a_{p_2}^\dagger |0\rangle \\ &= \frac{2ic}{k_1 - k_2} \int dx_1 dx_2 \theta(x_1 - x_2) e^{i(k_1 x_1 + k_2 x_2)} \Psi^\dagger(x_1) \Psi^\dagger(x_2) |0\rangle , \end{aligned} \quad (2.1.5)$$

with the choice $k_1 < k_2$. For the model (2.1.2) the full diagrammatic expansion of the two-body scattering (see Fig. 2.1) can be re-summed explicitly as a geometric series:

$$1 + 2 \left(\frac{ic}{k_1 - k_2} \right) + 2 \left(\frac{ic}{k_1 - k_2} \right)^2 + \dots = \frac{k_2 - k_1 - ic}{k_2 - k_1 + ic} \equiv e^{i\Delta(k_2 - k_1)} \quad (2.1.6)$$

with

$$\Delta(k) = -i \ln \left(\frac{k - ic}{k + ic} \right) . \quad (2.1.7)$$

From Eq. (2.1.6) one can deduce the relation between the in and out states

$$|\psi(k_1, k_2)\rangle_{\text{in}} = e^{i\Delta(k_1 - k_2)} |\psi(k_1, k_2)\rangle_{\text{out}} . \quad (2.1.8)$$

Here we recognize the two-body S -matrix to be $e^{i\Delta}$. Notice that the states $|\psi(k_1, k_2)\rangle$ we just constructed are perfectly well normalized states. For convenience, it is sometimes useful to introduce an alternative normalization, and consider the state

$$\begin{aligned} |\Phi(k_1, k_2)\rangle &= \left(1 + \frac{ic}{k_2 - k_1} \right) |\psi(k_1, k_2)\rangle_{\text{in}} \\ &= \int dx_1 dx_2 \left(1 + \frac{ic}{k_2 - k_1} \right) \epsilon(x_1 - x_2) e^{i(k_1 x_1 + k_2 x_2)} \Psi^\dagger(x_1) \Psi^\dagger(x_2) |0\rangle , \end{aligned} \quad (2.1.9)$$

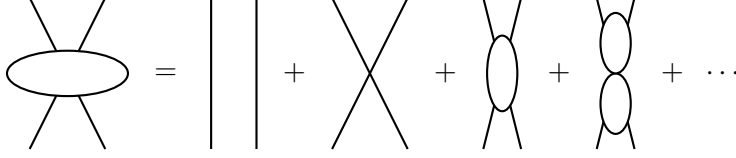


Figure 2.1: The sum of Feynmann graphs appearing in the two-body scattering amplitude.

which is also an eigenstate of the Hamiltonian (2.1.2). The Schrödinger equation satisfied by $|\Phi(k_1, k_2)\rangle$ gives us the energy of the two-body state:

$$H|\Phi(k_1, k_2)\rangle = (k_1^2 + k_2^2)|\Phi(k_1, k_2)\rangle . \quad (2.1.10)$$

2.1.2 N -particle scattering

So far, the two-particle eigenfunctions were easily constructed. The power of the Bethe Ansatz comes from the fact that the N -particle states can be constructed as a rather natural generalization of the two-body case. Using the unnormalized version, the Bethe Ansatz reads

$$|\Phi(k_1, \dots, k_N)\rangle = \int \left(\prod_{i=1}^N e^{ik_i x_i} dx_i \right) \prod_{i < j \leq N} \left(1 - \frac{ic}{k_i - k_j} \epsilon(x_i - x_j) \right) \times \\ \times \Psi^\dagger(x_1) \dots \Psi^\dagger(x_N) |0\rangle \quad (2.1.11)$$

and one can verify that this is indeed an eigenstate of H through

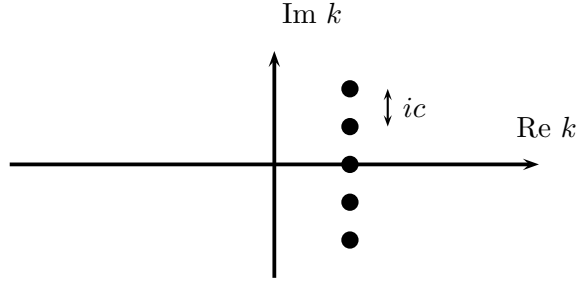
$$H|\Phi(k_1, \dots, k_N)\rangle = \left(\sum_{i=1}^N k_i^2 \right) |\Phi(k_1, \dots, k_N)\rangle \quad (2.1.12)$$

for $c > 0$ (repulsive interaction).

2.1.3 The case of attractive interaction

For attractive interaction, i.e. $c < 0$, it sounds physically plausible that bound states can be formed and are energetically stable. Within the Bethe Ansatz description, such bound states may be constructed by letting the k_i become complex¹. To obtain a N -body bound state we keep the total momentum

¹This statement is in fact quite general and will come back in part II of this thesis in the context of open chains of correlated electrons.

Figure 2.2: Illustration of the N -string configuration.

$K = \sum_{i=1}^N k_i$ real and arrange the k_i to be spaced by ic on the imaginary axis (see Fig. 2.2):

$$\begin{aligned} k_1 &= \frac{K}{N} + \frac{1}{2}(N-1)ic \\ k_2 &= \frac{K}{N} + \frac{1}{2}(N-3)ic \\ &\vdots \\ k_N &= \frac{K}{N} - \frac{1}{2}(N-1)ic . \end{aligned} \quad (2.1.13)$$

Such a mode configuration is called in the literature an N -string. Taking (2.1.13) into consideration in Eq. (2.1.11) leads to the following N -particle bound state wave function:

$$\psi_{BS}(x_1, \dots, x_N) = \exp\left(\frac{1}{2}c \sum_{i < j \leq N} |x_i - x_j|\right) . \quad (2.1.14)$$

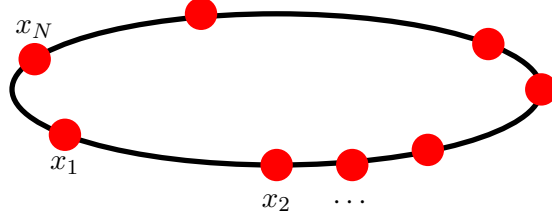
The energy of this bound state is

$$E = \sum_{i=1}^N k_i^2 = \frac{1}{N}K^2 - \frac{N(N^2-1)}{12}c^2 . \quad (2.1.15)$$

2.2 The many-body ground state

In this section, we should go back to our analysis of repulsive interactions and set $c > 0$. We will, from now on, impose Periodic Boundary Conditions (PBC) to the system, meaning that we will consider a finite particle density arranged on a ring of length L (see Fig. 2.3). The consequent (spatial) periodicity of the many-body wave-function

$$\Psi(-L/2, x_2, \dots, x_N) = \Psi(L/2, x_2, \dots, x_N) \quad (2.2.16)$$

Figure 2.3: Bosons arranged on a ring of length L .

restricts the possible values of the k_i . In fact, the set of $\{k_i\}_{i=1,\dots,N}$ entering (2.1.11) and compatible with the PBC must satisfy the so-called Bethe Ansatz Equations (BAE)

$$\exp\left(-ik_i\frac{L}{2}\right) \prod_{j \neq i} \left(1 + \frac{ic}{k_i - k_j}\right) = \exp\left(ik_j\frac{L}{2}\right) \prod_{j \neq i} \left(1 - \frac{ic}{k_i - k_j}\right) \quad (2.2.17)$$

or, written in a more compact form,

$$\exp(ik_i L) = \prod_{j \neq i} \exp(i\Delta(k_i - k_j)) . \quad (2.2.18)$$

At this point, a very useful and standard procedure consists in taking the logarithm of the BAE (2.2.18). This gives

$$k_i L = \sum_{j \neq i} \Delta(k_j - k_i) + 2\pi n_i , \quad (2.2.19)$$

where n_i is integer (resp. half-integer) for N odd (resp. even).

NB: In order to take the log of Eq. (2.2.18) one needs to specify a branch cut for the log appearing in the definition of $\Delta(k)$ (2.1.7). Actually, a change in the branch is equivalent to a redefinition of the n_i . We will adopt the convention that $\Delta(k) \rightarrow 0$ as $k \rightarrow \infty$ such that $\Delta(k)$ is a smooth function defined on the real axis.

The logarithmic BAE (2.2.19) provide us with a suitable description of the spectrum. Remarkably, this description, in terms of the quantum numbers n_i , is of fermionic nature. This may seem in contradiction with the fact that our original basis was the Fock basis of free bosons, not fermions. To see how this "fermionization" arises, let us consider the simple example of two particles in a box. The two equations (2.2.19) may be added and subtracted to give the condition that the total momentum $k_1 + k_2$ must be $2\pi/L$ times an integer, while the relative value $k_{12} \equiv k_1 - k_2$ must satisfy

$$\begin{aligned} k_{12} L &= \Delta(-k_{12}) - \Delta(k_{12}) + 2\pi(n_1 - n_2) \\ &= -4 \arctan\left(\frac{k_{12}}{c}\right) + 2\pi(n_1 - n_2) , \end{aligned} \quad (2.2.20)$$

where $-\pi/2 < \arctan < \pi/2$. Eq. (2.2.20) has a solution k_{12} for each choice of $(n_1 - n_2)$. But for $n_1 = n_2$, the solution is $k_{12} = 0$ and the corresponding state (2.1.11) vanishes identically. Thus the state $n_1 = n_2$ is excluded as it is for free fermions. In fact, taking the limit $c \rightarrow \infty$ (the so-called hard-core or impenetrable bosons limit) in Eq. (2.2.20) shows that the spectrum is identical to that of free fermions. A generalisation to N -body states holds. To conclude on this point, we can say that the hard-core repulsive interaction has the same effect on the density of states as the Pauli exclusion principle has in a system of fermions. Thus the ground state has the structure of a "Fermi sea" which is realised by choosing the n_i as closely spaced as possible, i.e. $n_{i+1} = n_i + 1$.

In the thermodynamic limit, $L \rightarrow \infty$ while N/L being finite, the Bethe roots become dense and we can introduce a so-called counting function $x(k)$ defined on \mathbb{R} which interpolates the numbers n_i/L . The logarithmic BAE can be rewritten

$$Lk(x) + \sum_j \Delta(k(x) - k_j) = 2\pi Lx . \quad (2.2.21)$$

Differentiating (2.2.21) with respect to the now continuous variable k , we obtain

$$1 + \frac{1}{L} \sum_j K(k(x) - k_j) = 2\pi\rho(k(x)) \quad (2.2.22)$$

where

$$\rho(k(x)) = \frac{dx(k)}{dk} \quad (2.2.23)$$

is the root density. Taking $L \rightarrow \infty$, all the modes will fill the volume $k \in [-k_F, k_F]$ where $k_F = \lim \lambda_N$ is the "Fermi momentum". Under this condition, Eq. (2.2.22) becomes an integral equation

$$2\pi\rho(k) = 1 + \int_{-k_F}^{k_F} dk' K(k - k')\rho(k') \quad (2.2.24)$$

for the distribution of k_i

$$\rho(k_i) = \frac{1}{L(k_{i+1} - k_i)} . \quad (2.2.25)$$

The kernel entering Eq. (2.2.24) is defined by

$$K(k) \equiv \Delta'(k) = \frac{2c}{k^2 + c^2} . \quad (2.2.26)$$

The density of particle D and the ground state energy per site are then expressed as integrals over $\rho(k)$:

$$D \equiv \frac{N}{L} = \int_{-k_F}^{k_F} dk \rho(k) \quad (2.2.27)$$

$$\epsilon_0 \equiv \frac{E_0}{L} = \int_{-k_F}^{k_F} dk k^2 \rho(k) \quad (2.2.28)$$

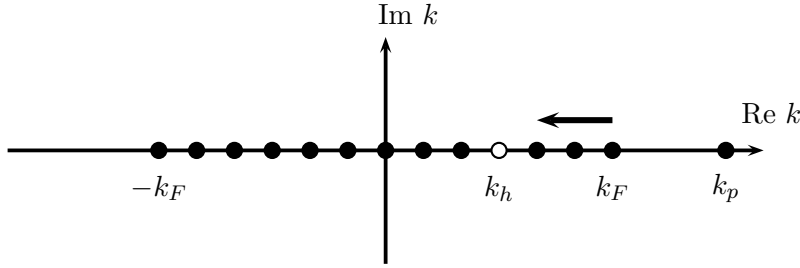


Figure 2.4: Particle-hole excitation above the pseudo-Fermi sea in the attractive 1D Bose gas. The hole created in the Fermi sea has momentum k_h and the particle has momentum $k_p > k_F$. In reaction, the Fermi sea will rearrange itself leading to a backflow of the momentum above the hole (arrow).

2.3 Elementary excitations

The excitations above the ground state consist of quasi-particles which are filled above the "Fermi" surface and quasi-holes which are empty modes below the Fermi level. Let us evaluate, as an illustration, the energy of a single particle-hole excitation formed by removing a mode from below the Fermi surface, at $k = k_h$, and placing it above the Fermi level, at $k = k_p$ (see Fig. 2.4). In response to this excitation, the Fermi sea will rearrange itself. This effect will be reflected in a slight modification of the PBC: each mode in the sea shifts only by an amount of order $1/L$, but since the number of modes is of order L , the shift or "backflow" of the sea makes a finite contribution to the excitation energy. Denoting the sea modes of the excited state by k'_i , we obtain the modified PBC:

$$k'_i L = \sum_{j \neq i} \Delta(k'_j - k'_i) + \Delta(k_p - k'_i) - \Delta(k_h - k'_i) + 2\pi n_i. \quad (2.3.29)$$

Subtracting Eq. (2.3.29) from the corresponding ground-state PBC gives

$$(k'_i - k_i)L = \sum_j [\Delta(k'_j - k'_i) - \Delta(k_j - k_i)] + \Delta(k_p - k'_i) - \Delta(k_h - k'_i). \quad (2.3.30)$$

As $L \rightarrow \infty$, the left-hand side of Eq. (2.3.30) becomes a continuous function which we denote $w(k)$. In this limit, Eq. (2.3.30) reduces to an integral equation

$$w(k) = \int_{-k_F}^{k_F} dk' K(k - k') [w(k') - w(k)] \rho(k') + \Delta(k_p - k) - \Delta(k_h - k). \quad (2.3.31)$$

Using (2.2.24) and defining $w(k)\rho(k) \equiv F(k)$, Eq. (2.3.31) simplifies to

$$2\pi F(k) = \int_{-k_F}^{k_F} dk' K(k - k') F(k') + \Delta(k_p - k) - \Delta(k_h - k). \quad (2.3.32)$$

Finally, the excitation energy $E - E_0 \equiv E_1$ is found by subtracting eigenvalues,

$$\begin{aligned} E_1 &= k_p^2 - k_h^2 + \sum_{k \in \text{sea}} (k_i'^2 - k_i^2) \\ &= k_p^2 - k_h^2 + 2 \int_{-k_F}^{k_F} dk k F(k). \end{aligned} \quad (2.3.33)$$

Thus, the excitation energy may be regarded as the sum of the bare energy of the particle and hole and a backflow energy of the sea, the latter being expressed by the integral over the function $F(k)$ in Eq. (2.3.33).

This concludes our summary of the results initially derived in [99, 98]. The key-steps of the solution of the Lieb-Liniger model (2.1.2) have been presented, and the elementary excitations have been identified. We should make use of this basic knowledge to understand the finite-size spectrum of the system (Chap. 3), and to tackle more complicated situation involving internal degrees of freedom (Chap. 4).

Chapter 3

Finite-size scaling and conformal field theory

It is well known that 1+1 dimensional quantum systems can be described, at criticality, by a two-dimensional Conformal Field Theory [24]. In the case of one-dimensional exactly solvable models, there is a one-to-one correspondence between the spectrum of low-lying excitations, computed with arbitrary precision from the Bethe ansatz, and the universality class of the theory describing the system at a large scale. Therefore, the analysis of the finite-size spectrum of a Bethe ansatz solvable model can provide us with some precious information regarding the asymptotic behaviour of correlation functions within the CFT.

3.1 Universality and finite-size spectrum

For periodic boundary conditions, the finite-size scaling behaviour of a 1+1 dimensional quantum model has been proved to be [2, 26]:

$$E_0 - L\epsilon_0 = -\frac{\pi}{6L}v\mathbf{c} + o(1/L) \quad (3.1.1)$$

where v is the velocity of light of the theory (more generally the speed of the massless mode) and \mathbf{c} is the notorious central charge of the underlying CFT that gives the universality class. For the case of open boundary conditions, notice the factor 1/4 in the prefactor in front of the \mathbf{c} -term:

$$E_0 - L\epsilon_0 - f_0 = -\frac{\pi}{24L}v\mathbf{c} + o(1/L) . \quad (3.1.2)$$

To be precise, in Eq. (3.1.1) and (3.1.2), E_0 is the ground state energy of the finite system, ϵ_0 is the energy density of the ground state of the infinite system and f_0 is the surface energy of the system with open boundaries.

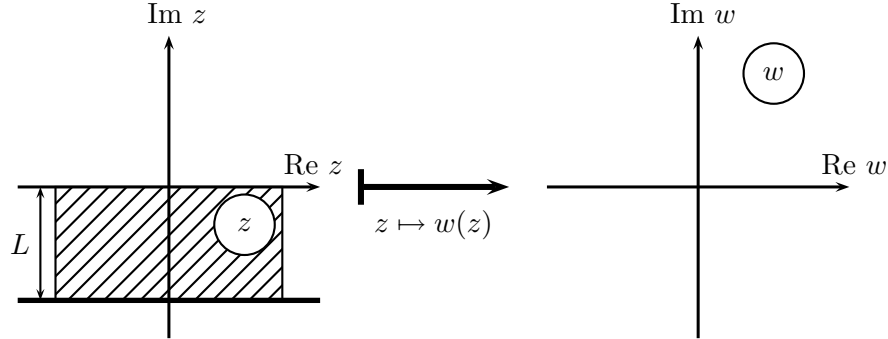


Figure 3.1: Conformal mapping $z \mapsto w(z) = \exp(2\pi z/L)$ from the strip $-L < \text{Im } z \leq 0$ onto the full complex plane.

3.2 Correlation functions

At criticality, i.e. where the theory becomes conformal invariant, a power-law decay of the two-point functions is expected,

$$\langle \mathcal{O}^\dagger(z_1, \bar{z}_1) \mathcal{O}(z_2, \bar{z}_2) \rangle = \frac{C}{(z_1 - z_2)^{2\Delta^-} (\bar{z}_1 - \bar{z}_2)^{2\Delta^+}}. \quad (3.2.3)$$

This fact is characteristic of a massless theory. The presence of any internal scale, such as a gap for the excitations modes, will lead, instead, to having correlation functions decaying exponentially fast. Notice that the two-point function (3.2.3) is the product of an holomorphic and anti-holomorphic part.

For simplicity, let us consider only the holomorphic part. Under a conformal mapping¹ $z \mapsto w = w(z)$, the (holomorphic part of the) two-point function changes to

$$\langle \mathcal{O}^\dagger(z_1) \mathcal{O}(z_2) \rangle \rightarrow \frac{1}{(w(z_1) - w(z_2))^{2\Delta^-}} \left(\frac{\partial w}{\partial z_1} \frac{\partial w}{\partial z_2} \right)^{\Delta^-}. \quad (3.2.4)$$

A particularly useful conformal mapping is given by $w(z) = \exp(2\pi z/L)$. This maps the strip $-L < \text{Im } z \leq 0$ onto the full complex plane (see Fig. 3.1). This way, one can compute the correlation functions of finite quantum chains of length L or finite temperature correlators defining $T = i/L$ from the

¹In 2D, the group of conformal transformations is infinite-dimensional and is represented by all analytic functions in the complex plane.

infinite system or zero temperature formula:

$$\langle \mathcal{O}^\dagger(z_1)\mathcal{O}(z_2) \rangle = \left[\frac{\pi}{L \sinh(\frac{\pi}{L}(z_1 - z_2))} \right]^{2\Delta^-}. \quad (3.2.5)$$

For a chain of length L ,

$$z = \tau - ix, \quad -\infty < \tau < \infty, \quad -L < x \leq 0, \quad (3.2.6)$$

we can expand (3.2.5) in the asymptotic limit $\tau_{12} = \tau_1 - \tau_2 \ll 1$. One obtains

$$\begin{aligned} \langle \mathcal{O}^\dagger(z_1, \bar{z}_1)\mathcal{O}(z_2, \bar{z}_2) \rangle &\rightarrow \left(\frac{2\pi}{L}\right)^{2d} \sum_{n,m} c_{n,m} \exp\left(-\frac{2\pi v}{L}(d+n)\tau_{12}\right) \times \\ &\exp\left(-\frac{2\pi i}{L}(s+m)x_{12}\right) \end{aligned} \quad (3.2.7)$$

where we have introduced the scaling dimension $d = \Delta^+ + \Delta^-$ and the conformal spin $s = \Delta^- - \Delta^+$. Alternatively a similar expression for the two-point function can be derived from a transfer matrix formalism,

$$\begin{aligned} \langle \Omega | \mathcal{O}^\dagger(z_1, \bar{z}_1)\mathcal{O}(z_2, \bar{z}_2) | \Omega \rangle &= \sum_q \langle \Omega | \mathcal{O}^\dagger(\tau_1, x_1) | q \rangle \mathcal{O}(\tau_2, x_2) | \Omega \rangle \\ &= \sum_q \exp(-E_q \tau_{12} - iP_q x_{12}) |\langle q | \mathcal{O}(0) | \Omega \rangle|^2, \end{aligned} \quad (3.2.8)$$

where $|\Omega\rangle$ is the ground state of the Hamiltonian (PBC) and $|q\rangle$ are eigenstates with energy E_q and momentum P_q . Comparing (3.2.7) with (3.2.8) we can read off the key relations between the scaling dimensions and spin of the CFT on one hand, and the finite-size corrections of the spectrum (taking into account the low-lying states) on the other hand:

$$\begin{aligned} E_{\Delta^\pm}^{N^+, N^-} - E_0 &= \frac{2\pi v}{L}(d + N^+ + N^-) + o(1/L), \\ P_{\Delta^\pm}^{N^+, N^-} - P_0 &= \frac{2\pi}{L}(s + N^+ - N^-) + 2Dk_F. \end{aligned} \quad (3.2.9)$$

Here N^+, N^- are non-negative integers and $2D$ is the macroscopic contribution to the momentum of the state $\mathcal{O}|\Omega\rangle$ in units of the ultra-violet cut-off k_F . Eqs. (3.2.9) capture a very important result: Every operator within the CFT is in one to one correspondence with a tower of excited states labelled by N^\pm . In particular, after identifying the lowest energy state of such a tower to be $N^\pm = 0$, one can extract the scaling limit of a primary field ϕ correlator to be

$$\begin{aligned} \langle \phi_{\Delta^\pm}(x, \tau)\phi_{\Delta^\pm}(0, 0) \rangle &= \frac{\exp(2iDk_F x)}{(v\tau + ix)^{2\Delta^+}(v\tau - ix)^{2\Delta^-}} \\ &= \frac{\exp(2iDk_F x)}{(v^2\tau^2 + x^2)^d} \left(\frac{v\tau - ix}{v\tau + ix}\right)^s. \end{aligned} \quad (3.2.10)$$

3.3 Example: correlation functions for the Bose gas

3.3.1 Finite-size corrections

In Chap. 2, we have studied the one dimensional Bose gas with δ -interaction. We have presented the results of Lieb and Liniger and their main achievement was the derivation of the exact ground state of the model as well as the classification of the low-lying excitations in the system. At least for the case of zero-temperature, we were able to evaluate physical quantities such as the density of particles, the energy and the total momentum in the thermodynamic limit when $L \rightarrow \infty$. In this paragraph we will include finite-size corrections to the energy and momentum.

Let us start with the evaluation of the finite-size corrections to the ground state energy. Following this purpose, we shall include a chemical potential to the original Hamiltonian

$$H_\mu = \int dx \{ \partial_x \Psi^\dagger \partial_x \Psi + c \Psi^\dagger \Psi^\dagger \Psi \Psi - \mu \Psi^\dagger \Psi \} . \quad (3.3.11)$$

The total energy is then shifted due to the presence of the chemical potential μ

$$E = \sum_j \epsilon_0(k_j) \quad \text{with} \quad \epsilon_0(k_j) = k_j^2 - \mu \quad (3.3.12)$$

and the momentum is still

$$P = \sum_j p_0(k_j) \quad \text{with} \quad p_0(k_j) = k_j . \quad (3.3.13)$$

Using the Euler-Maclaurin formula the equation for the density is

$$\begin{aligned} \rho_L(k) = & \frac{1}{2\pi} \int_{-k_F}^{k_F} dk' K(k - k') \rho_L(k') \\ & + \frac{1}{2\pi} \left[p'_0(k) + \frac{1}{24L^2 \rho(k_F)} (K'(k - k_F) - K'(k + k_F)) \right] . \end{aligned} \quad (3.3.14)$$

The function $\rho_L(k)$ should be used when changing the summation into an integral in Eq. (3.3.12). This gives

$$\begin{aligned} E = & L \int_{-k_F}^{k_F} dk \epsilon_0(k) \rho(k) \\ & + \frac{1}{48\pi L \rho(k_F)} \int_{-k_F}^{k_F} dk \epsilon(k) (K'(k - k_F) - K'(k + k_F)) - \frac{\epsilon'_0(k_F)}{12L \rho(k_F)} . \end{aligned} \quad (3.3.15)$$

3.3. EXAMPLE: CORRELATION FUNCTIONS FOR THE BOSE GAS 37

Introducing

$$\epsilon'(k_F) = \epsilon'_0(k_F) + \frac{1}{2\pi} \int_{-k_F}^{k_F} dk K'(k - k_F) \epsilon(k) , \quad (3.3.16)$$

we can rewrite Eq. (3.3.15) as

$$E = L \int_{-k_F}^{k_F} dk \epsilon_0(k) \rho(k) - \frac{\pi}{6L} v_F + \dots \quad (3.3.17)$$

where v_F is the "Fermi velocity",

$$v_F = \frac{1}{2\pi\rho(k_F)} \left. \frac{\partial \epsilon}{\partial k} \right|_{k=k_F} . \quad (3.3.18)$$

Comparing Eq. (3.3.17) with (3.1.1) allows to identify an underlying $\mathbf{c} = 1$ CFT.

Now, considering low-lying excitations of the type described in Chap. 2, we can distinguish three physical processes: (1) The integer n_j in (2.2.19) corresponding to the particle on the Fermi surface will be changed by a finite amount N^+ (at $k = k_F$) and N^- (at $-k_F$). (2) The number of particles can vary of ΔN . (3) A certain number of particles (d) can undergo a backscattering process under which they jump from one Fermi point ($-k_F$) to the other ($+k_F$). It can be proved (cf [88]) that the changes in energy and momentum corresponding to these processes are

$$\begin{aligned} \Delta E &= \frac{2\pi v_F}{L} \left[\left(\frac{\Delta N}{2\mathcal{Z}} \right)^2 + (\mathcal{Z}d)^2 + N^+ + N^- \right] \\ \Delta P &= 2k_F d + \frac{2\pi}{L} (N^+ - N^- + \Delta N d) \end{aligned} \quad (3.3.19)$$

where \mathcal{Z} is the value of the dressed charge,

$$Z(k) = 1 + \frac{1}{2\pi} \int_{-k_F}^{k_F} dk' K(k - k') Z(k') , \quad (3.3.20)$$

on the Fermi surface ($\mathcal{Z} \equiv Z(\pm k_F)$). It will be convenient to introduce $\theta = 2\mathcal{Z}^2$. The parameter θ can be expressed in terms of the density D and the Fermi velocity as

$$\theta = \frac{4\pi D}{v_F} . \quad (3.3.21)$$

Remember that for the one-dimensional Bose gas $D = k_F/\pi$. Comparing Eq. (3.3.19) with (3.2.9) we can infer that the conformal dimensions of the one-dimensional Bose gas theory are given by

$$2\Delta^\pm = 2N^\pm + \left(\frac{\Delta N}{2\mathcal{Z}} \pm \mathcal{Z}d \right)^2 . \quad (3.3.22)$$

3.3.2 Boson Green's function

First, let us consider the asymptotic behaviour of the boson Green's function defined as

$$G(x, \tau) = \langle \Psi(x, \tau) \Psi^\dagger(0, 0) \rangle . \quad (3.3.23)$$

$G(x, \tau)$ can be interpreted as the response of the system to adding a particle at the origin. Thus, we have $\Delta N = 1$ in this case. Using (3.2.7), the asymptotic limit of the boson Green's function is then given by

$$G(x, \tau) = \sum_{d, N^\pm} \frac{A(d, N^\pm) e^{-2idk_F x}}{(v\tau + ix)^{2\Delta^+} (v\tau - ix)^{2\Delta^-}} , \quad (3.3.24)$$

where Δ^\pm are defined by Eq. (3.3.22), d and N^\pm being integers. The leading contribution to the asymptotics corresponds to the slowest decaying term in (3.3.24), i.e. the minimum value of Δ^\pm ; the other terms are corrections. The leading term is obtained by setting $N^\pm = d = 0$, giving

$$G(x, \tau) \rightarrow A |v\tau - ix|^{-1/\theta} . \quad (3.3.25)$$

3.3.3 Density correlations

Another quantity which of relevance experimentally is the density-density correlator $\langle n(x, \tau) n(0, 0) \rangle$ where $n(x, \tau) \equiv \Psi^\dagger(x, \tau) \Psi(x, \tau)$. Since the operator $n(x, \tau)$ conserves the number of particles in the system, we should set $\Delta N = 0$ in the formula 3.3.22. We obtain

$$\begin{aligned} \langle :n(x, \tau) n(0, 0): \rangle &= \langle n(x, \tau) n(0, 0) \rangle - \langle n(0, 0) \rangle^2 \\ &\rightarrow \frac{A}{(v\tau - ix)^2} + \frac{A}{(v\tau + ix)^2} + \frac{A_3 \cos 2k_F x}{|v\tau - ix|^\theta} . \end{aligned} \quad (3.3.26)$$

The first term corresponds to $d = 0, N^+ = 0, N^- = 1$, the second term to $d = 0, N^+ = 1, N^- = 0$ and the last term has quantum numbers $d = \pm 1, N^+ = N^- = 0$. At finite coupling constant, $c < \infty$, the last term has $\theta > 2$ and therefore decays faster than the other ones.

NB: The results (3.3.24) and (3.3.26) obtained from this CFT approach coincide with the results coming from the Tomonaga-Luttinger (TL) liquid description of the one-dimensional Bose gas [73]. In the latter approach, the large-distance behaviour of the boson Green's function is controlled by the TL parameter K_b characterizing the theory. More precisely, we have

$$G(x) \sim |x|^{-1/2K_b} . \quad (3.3.27)$$

3.3.4 Finite temperature

The finite-temperature correlation functions can be obtained with the help of the conformal mapping we have introduced above (3.2.5). Doing so, the asymptotics of the Green's function and the density correlator are

$$\langle \Psi(x, \tau) \Psi(0, 0) \rangle_T = B_1 \left| \frac{\frac{\pi T}{v}}{\sinh \frac{\pi T}{v}(x + iv\tau)} \right|^{1/\theta} + \dots \quad (3.3.28)$$

and

$$\begin{aligned} \langle :n(x, \tau)n(0, 0): \rangle &= \text{Re } B_2 \left(\frac{\frac{\pi T}{v}}{\sinh \frac{\pi T}{v}(x + iv\tau)} \right)^2 \\ &+ B_3 \left| \frac{\frac{\pi T}{v}}{\sinh \frac{\pi T}{v}(x + iv\tau)} \right|^\theta \cos(2k_F x) + \dots \end{aligned} \quad (3.3.29)$$

3.3.5 Experimental considerations

To conclude, we would like to emphasize that the calculation of correlation functions within the Lieb-Liniger model is not simply a piece of mathematical physics but has some experimental relevance. A quantity like the Green's function, or more precisely its Fourier transform, the momentum distribution, can be measured directly in time-of-flight experiments or using Bragg spectroscopy [117, 44]. Another setup for the measurement of various density correlation functions has been recently proposed for the identification of dominant correlations in the atomic gas [8, 106]. In Fig. 3.2, we show the results of the experiment of Paredes et al. [117], where the momentum distribution of a 1D Bose gas in the Tonks-Girardeau (TG) regime of dominant interactions has been measured. In the TG regime, $K_b = 1$, and, according to Eq. (3.3.27), the low- p behaviour of the density should be $p^{-1/2}$. This feature is observed in Fig 3.2.a where the slope of 1/2 line fits the data for small p in the log-log plot. This is in the absence of any confinement trap in the axis of the atomic tube. In Fig. 3.2.b–f, the depth of the axial trap is increased. The trap has the effect of breaking the integrability of the original Lieb-Liniger model and deviation from the scaling prediction starts to be observed. Nevertheless, if the axial harmonic trap would vary smoothly along the tube, the universality class of the model with the harmonic term taken into account should not differ from the one of the Lieb-Liniger. For long enough tubes and large numbers of particles, universal results should be recovered. For the case of small samples, ab-initio theories including the trap and finite-size effects are useful to compare with current data.

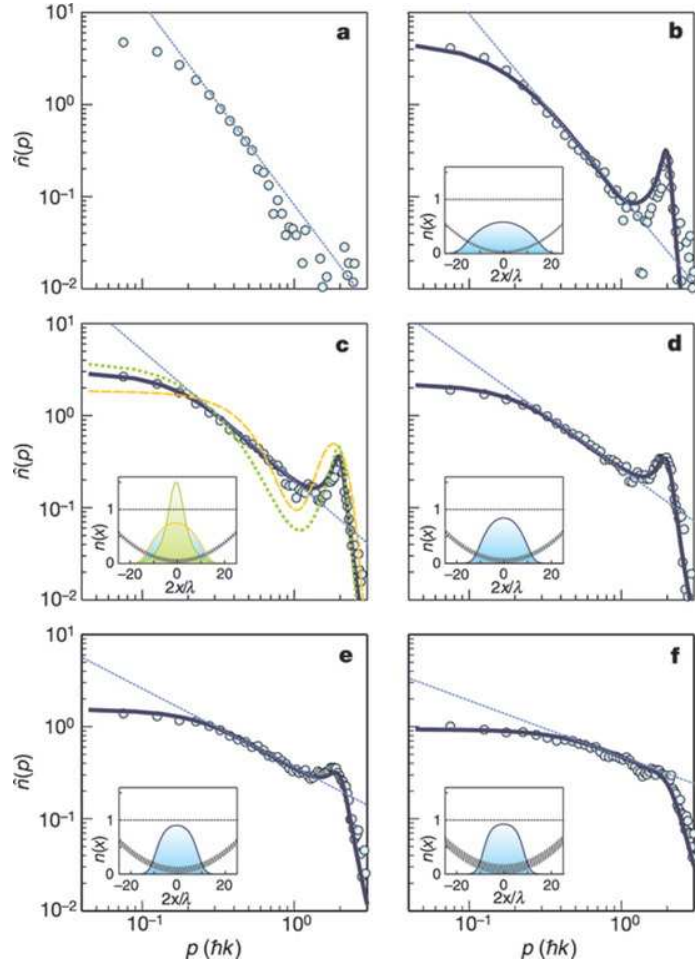


Figure 3.2: Momentum profiles of the 1D quantum Bose gas for different axial lattice depths V_{ax} . From (a) $V_{\text{ax}} = 0$ to (f) $V_{\text{ax}} = 18.5$ in units of the recoil energy. Extracted from [117] ©2004 Nature Publishing Group

Chapter 4

Critical one-dimensional Bose-Fermi mixtures

Theoretical studies of correlation functions in cold atomic gases have been performed both using analytical methods, e.g. bosonization [64] combined with exact results from integrable models such as the Bose-gas with repulsive δ -function interaction (see [99, 98] and Chap. 3), and numerically. Only recently, theoretical investigations have been extended to Bose-Fermi mixtures: some correlation functions have been calculated numerically in the strong coupling limit [30, 76] where the problem simplifies due to the factorization of the many-particle wave function (see e.g. [114]). For analytical results on these systems one has to go beyond mean-field approximations and use methods which can capture the strong quantum fluctuations in 1D systems. The phase diagram and certain correlation functions of atomic mixtures have been studied in the Luttinger liquid picture [29, 107]. Without further input, however, these results are limited to the weakly interacting regime since the TL parameters which determine the low-energy theory cannot easily be related to the microscopic parameters describing the underlying gas. Therefore, instabilities predicted within this approach may not appear in a specific realizations [92, 76, 17].

In this chapter, we establish the relation between the TL and the microscopic parameters for an integrable Bose-Fermi mixture [92]. We employ methods from conformal field theory (CFT) introduced in Chap. 3 to determine the asymptotic (long distance, low-energy) behaviour of correlation functions in the model from a finite size scaling analysis of the exact spectrum obtained by means of the Bethe ansatz. This approach gives the complete set of critical exponents of the model as a function of the parameters in the microscopic Hamiltonian (see e.g. [49, 50, 82, 41] for applications to 1D correlated electrons). As an application we compute the momentum distribution function of bosons and fermions in the atomic mixture as a function of their respective densities and the effective coupling constant. It should be emphasized

that our results can be expected to describe the generic (universal) low-energy behaviour of atomic mixtures. Additional interactions – as long as they do not lead to a phase transition – will merely change the anomalous exponents but not the qualitative behaviour of the correlation functions.

4.1 Description of the model

The 1D Bose-Fermi mixture of $N = M_f + M_b$ particles with repulsive interaction ($c > 0$) on a line of length L subject to periodic boundary conditions is described by the integrable Hamiltonian [92]

$$H = - \sum_{i=1}^N \frac{\partial^2}{\partial x_i^2} + 2c \sum_{i<j} \delta(x_i - x_j) . \quad (4.1.1)$$

Here $M_f = M_{\uparrow} + M_{\downarrow}$ of the particles are fermions carrying spin $\sigma = \uparrow, \downarrow$ and M_b of them are bosons. In second quantization, the Hamiltonian looks like

$$H = \int_0^L dx (\partial_x \Psi_b^\dagger \partial_x \Psi_b + \partial_x \Psi_f^\dagger \partial_x \Psi_f) + c \int_0^L dx (\Psi_b^\dagger \Psi_b^\dagger \Psi_b \Psi_b + \sum_{\sigma=\uparrow,\downarrow} \Psi_b^\dagger \Psi_{f,\sigma}^\dagger \Psi_{f,\sigma} \Psi_b) . \quad (4.1.2)$$

where Ψ_b^\dagger creates a boson while Ψ_f^\dagger creates a fermion. Ψ_b^\dagger (resp. Ψ_f^\dagger) obey the standard commutation (resp. anti-commutation) relations. NB: For the model (4.1.1) to be integrable, the masses of all particles should be the same as well as the boson-boson and boson-fermion interaction strengths. Although those conditions seem somewhat restrictive, the exactly solvable model is relevant to current experiments and can be used to check the validity of different approximate approaches.

The many-particle eigenstates of (4.1.1) are parametrized by the solutions of the Bethe ansatz equations (BAE) [92]

$$\begin{aligned} \exp(iq_j^{(0)} L) &= \prod_{k=1}^{M_1} e_c(q_j^{(0)} - q_k^{(1)}) \\ \prod_{j=1}^{M_0} e_c(q_k^{(1)} - q_j^{(0)}) \prod_{\ell=1}^{M_2} e_c(q_k^{(1)} - q_\ell^{(2)}) &= \prod_{k' \neq k}^{M_1} e_{2c}(q_k^{(1)} - q_{k'}^{(1)}) \\ \prod_{k=1}^{M_1} e_c(q_\ell^{(2)} - q_k^{(1)}) &= 1 \end{aligned} \quad (4.1.3)$$

where $e_a(x) = (x + ia/2)/(x - ia/2)$ and $M_0 = N$, $M_1 = N - M_\uparrow$, $M_2 = M_b$. The corresponding eigenvalue of (4.1.1) is

$$E = \sum_{j=1}^N (q_j^{(0)})^2 . \quad (4.1.4)$$

In the thermodynamic limit $L \rightarrow \infty$ with M_i/L kept fixed, the root configurations $\{q^{(i)}\}$ of Eqs. (7.2.7) can be described by distribution functions ρ_i (cf Chap. 2) which, as a consequence of (7.2.7) are solutions to [92]

$$\begin{pmatrix} \rho_0(k) \\ \rho_1(\lambda) \\ \rho_2(\mu) \end{pmatrix} = \begin{pmatrix} \frac{c}{2\pi} \\ 0 \\ 0 \end{pmatrix} + \begin{pmatrix} 0 & \int_1 a_1 & 0 \\ \int_0 a_1 & -\int_1 a_2 & \int_2 a_1 \\ 0 & \int_1 a_1 & 0 \end{pmatrix} * \begin{pmatrix} \rho_0(k) \\ \rho_1(\lambda) \\ \rho_2(\mu) \end{pmatrix} . \quad (4.1.5)$$

Here we used the notation

$$\int_j k * f(x) \equiv \int_{-Q_j}^{Q_j} dy k(x-y)f(y) \quad (4.1.6)$$

and the functions entering the matrix kernel in (4.1.5) are defined by $2\pi a_n(x) = 4n/(4x^2 + n^2)$. Just like for the case of the simple Bose gas in one-dimension (Chap. 2), the densities of the different species in the mixture are expressed by an integral over the ρ_i

$$\begin{aligned} \frac{N}{L} &= \int_{-Q_0}^{Q_0} dk \rho^{(0)}(k) \\ \frac{M_\uparrow + M_b}{L} &= \int_{-Q_1}^{Q_1} d\lambda \rho^{(1)}(\lambda) \\ \frac{M_b}{L} &= \int_{-Q_2}^{Q_2} d\mu \rho^{(2)}(\mu) \end{aligned} \quad (4.1.7)$$

as well as the energy

$$\frac{E}{L} = \int_{-Q_0}^{Q_0} dk k^2 \rho^{(0)}(k) . \quad (4.1.8)$$

Note that the relations (4.1.7) determine the boundaries Q_i of the above integral equations (4.1.5). The dimensionless coupling strength $\gamma = Lc/N$ controls the various interacting regimes of the system, from $\gamma = 0$, the free fermions and bosons case to $\gamma \gg 1$, the strongly interacting regime. For later, use we shall also introduce the fraction of bosons in the system, $\alpha = M_b/N$.

4.2 Finite-size spectrum

Generically, there are three modes of collective elementary excitations, one for each specie constituting the Bose-Fermi mixture, above the many-particle

ground state of (4.1.1). Their dispersion relation $\epsilon_i(k)$ is linear at low energies with different sound velocities $v_i = \partial\epsilon_i/\partial k$, $i = 0, 1, 2$ [17]. As we have seen in Chap. 3, these quantities determine the finite-size scaling behaviour of the ground state energy

$$E_0 - L\epsilon_\infty = -\frac{\pi}{6L} \sum_i v_i + o\left(\frac{1}{L}\right). \quad (4.2.9)$$

The physical excitations of the system are combinations of the elementary ones. Due to the interacting nature of the system, the different modes are coupled and excitations in one of the modes shift the energies in the other ones. In general, this effect can be described in terms of generalized susceptibilities which may be determined in an experiment or numerically from studies of small systems [41]. It is possible to describe the coupling of the modes through the dressed charge that we already encountered in Chap. 2 in the calculation of the finite-size spectrum of the 1D Bose gas. In the case of the Bose-Fermi mixture, and in general for models with internal degrees of freedom (e.g. models of correlated electrons [49, 50, 82]), the dressed charge takes the form of a matrix satisfying

$$Z(X) = \mathbb{1} + \begin{pmatrix} 0 & \int_1 a_1 & 0 \\ \int_0 a_1 & -\int_1 a_2 & \int_2 a_1 \\ 0 & \int_1 a_1 & 0 \end{pmatrix} * Z(X), \quad (4.2.10)$$

where $X = (k, \lambda, \mu)$. We should from now on introduce the matrix \mathcal{Z} which is the dressed charge matrix evaluated at the generalised Fermi surface:

$$\mathcal{Z}_{ij} = Z_{ij}(Q_i), \quad (4.2.11)$$

In the followong we will often make an abuse of language and call the matrix \mathcal{Z} simply the dressed charge matrix. For the Bethe ansatz solvable model, \mathcal{Z} determines the general form of the finite size corrections to the energies of low-lying excitations

$$\begin{aligned} \Delta E(\Delta\mathbf{M}, \mathbf{D}) &= \frac{2\pi}{L} \left(\frac{1}{4} \Delta\mathbf{M}^\top (\mathcal{Z}^\top)^{-1} V \mathcal{Z}^{-1} \Delta\mathbf{M} \right. \\ &\left. + \mathbf{D}^\top \mathcal{Z} V \mathcal{Z}^\top \mathbf{D} + \sum_k v_k (N_k^+ + N_k^-) \right) + o\left(\frac{1}{L}\right). \end{aligned} \quad (4.2.12)$$

Here, $V = \text{diag}(v_0, v_1, v_2)$ is a 3×3 matrix of the sound velocities, N_k^\pm are non-negative integers, $\Delta\mathbf{M}$ is a vector of integers denoting the change of M_i with respect to the ground state for charged excitations. The D_i are integers or half-odd integers according to

$$\begin{aligned} D_0 &\sim (\Delta M_0 + \Delta M_1)/2 = \Delta M_\uparrow/2 \pmod{1} \\ D_1 &\sim (\Delta M_0 + \Delta M_2)/2 = \Delta M_f/2 \pmod{1} \\ D_2 &\sim (\Delta M_1 + \Delta M_2)/2 = \Delta M_\downarrow/2 \pmod{1} \end{aligned} \quad (4.2.13)$$

and enumerate finite momentum transfer processes:

$$\begin{aligned} \Delta P(\Delta \mathbf{M}, \mathbf{D}) = & \frac{2\pi}{L} \left(\Delta \mathbf{M}^\top \cdot \mathbf{D} + \sum_k (N_k^+ - N_k^-) \right) \\ & + 2k_{F,\uparrow} D_0 + 2k_{F,\downarrow} (D_0 + D_1) + 2k_B \sum_j D_j . \end{aligned} \quad (4.2.14)$$

Here $k_{F,\sigma} = \pi M_\sigma / L$ are the Fermi momenta of the fermion components, $k_B = \pi M_b / L$ is the corresponding quantity for the interacting bosons. Note that Eqs. (4.2.12) and (4.2.14) are generalization of the Eqs. (3.3.19) we obtained for the Bose gas to the case of three degrees of freedom.

4.3 Asymptotics of correlation functions

In the framework of CFT, the finite size spectrum (4.2.9), (4.2.12) can be understood as that of a critical theory based on the product of three Virasoro algebras each having central charge $\mathbf{c} = 1$ [49, 50, 41]. Correlation functions of a general operator in the theory – characterized by the quantum numbers ΔM_i and D_i – will contain contributions from these three sectors. The simplest ones, analogues of primary fields in the CFT, have correlation functions (in Euclidean time τ)

$$\langle \phi_\Delta(x, \tau) \phi_\Delta(0, 0) \rangle = \frac{\exp \left(2i D_0 k_{F,\uparrow} x + 2i (D_0 + D_1) k_{F,\downarrow} x + 2i \left(\sum_j D_j \right) k_B x \right)}{\prod_k (v_k \tau + ix)^{2\Delta_k^+} (v_k \tau - ix)^{2\Delta_k^-}} . \quad (4.3.15)$$

The operators ϕ_Δ are characterized by their scaling dimensions Δ_k^\pm in the chiral (left- and right moving) components of all three constituent theories. The latter are uniquely determined from the finite size energies (4.2.12) and momenta (4.2.14) and form towers starting at

$$2\Delta_k^\pm = \left(\sum_j \mathcal{Z}_{kj} D_j \pm \frac{1}{2} \sum_j \Delta M_j (\mathcal{Z}^{-1})_{jk} \right)^2 . \quad (4.3.16)$$

The asymptotic exponential decay of correlation functions in a large but finite system or at finite temperature T can be obtained from (4.3.15) by conformal invariance. For example, at $T > 0$ the denominators in (4.3.15) have to be replaced by $(v_k \tau \pm ix)^{2\Delta_k^\pm} \rightarrow (\pi T / v_k \sinh \pi T (\tau \pm ix / v_k))^{2\Delta_k^\pm}$ (cf Chap. 3).

With (4.3.16) the critical exponents which determine the long-distance asymptotics of *any* correlation function are known as soon as we have computed the dressed charge matrix (4.2.11). To calculate the correlation functions of a given local operator \mathcal{O} in the microscopic theory (4.1.1) one needs to know its expansion in terms of the fields ϕ_Δ of the CFT. Usually, this

expansion is not known but \mathcal{O} and ϕ_Δ have to generate the same set of selection rules in calculating the correlation function. This drastically reduces the number of possible terms in the expansion.

4.3.1 Boson Green's function

As an example, let us consider the bosonic Green's function

$$G_b(x, \tau) = \langle \Psi_b(x, \tau) \Psi_b^\dagger(0, 0) \rangle . \quad (4.3.17)$$

Clearly Ψ_b^\dagger generates a state with $\Delta M_b = 1$ which implies $\Delta M_j \equiv 1$ in (4.3.16). By (4.2.13) the quantum numbers D_j are further restricted to integers: the uniform part of the Green's function (3.3.23) is described by the operator with $D_j \equiv 0$ which allows to identify the TL parameter K_b [73] from (4.3.16),

$$G_b(x) \sim |x|^{-1/2K_b} . \quad (4.3.18)$$

The interactions lead to additional contributions to G_b oscillating with wave numbers $k_0 = 2k_{F\sigma}, 2k_B, \dots$

For a comparison with experimental data one is often interested in Fourier transforms of the two-point correlation functions given above. The large distance behaviour of (4.3.15) determines the singularities of spectral functions near $\omega \approx \pm v_k(k - k_0)$ (see e.g. [41]). Quantities accessible in experiments with cold gases [117, 44] are the momentum distribution functions of the constituent particles. For the bosons this is the Fourier transform of the equal time Green's function $G_b(x)$. From (4.3.15) its singularities at wave numbers $k \approx k_0$ are then

$$n_b(k) \sim |k - k_0|^{\nu_b} . \quad (4.3.19)$$

The exponent ν_b is the minimal value of $2(\sum_k \Delta_k^+ + \Delta_k^-) - 1$ compatible with the quantum numbers ΔM and the selection rules for the D for the given k_0 . For example,

$$1/2K_b = \nu_b + 1 = \frac{1}{4} \sum_k \left(\sum_j (\mathcal{Z}_{jk}^{-1}) \right)^2 \quad \text{for } k_0 = 0 . \quad (4.3.20)$$

4.3.2 Fermion Green's function

Using the same procedure for the fermionic Green's functions,

$$G_\sigma(x, \tau) = \langle \Psi_\sigma(x, \tau) \Psi_\sigma^\dagger(0, 0) \rangle , \quad (4.3.21)$$

we find that their asymptotic behaviour is determined by the conformal fields with $\Delta M_0 = 1, \Delta M_1 = \Delta M_2 = 0$, half-odd integers D_0, D_1 and integer D_2 for G_\uparrow and $\Delta M_0 = 1 = \Delta M_1, \Delta M_2 = 0$, half-odd integers D_1, D_2 and integer D_0

| | ΔM_0 | ΔM_1 | ΔM_2 | D_0 | D_1 | D_2 |
|-------------------------------|--------------|--------------|--------------|--------------------|--------------------|--------------------|
| Ψ_b^\dagger | 1 | 1 | 1 | \mathbb{Z} | \mathbb{Z} | \mathbb{Z} |
| $\Psi_{f,\uparrow}^\dagger$ | 1 | 0 | 0 | $\mathbb{Z} + 1/2$ | $\mathbb{Z} + 1/2$ | \mathbb{Z} |
| $\Psi_{f,\downarrow}^\dagger$ | 1 | 1 | 0 | \mathbb{Z} | $\mathbb{Z} + 1/2$ | $\mathbb{Z} + 1/2$ |

Table 4.1: The conformal fields and their associated quantum numbers corresponding to the leading singularity in the Bose and Fermi Green's functions.

for G_\downarrow . Again, the singularities of the fermions' distribution functions $n_\sigma(k)$ follow from (4.3.15). We find singularities of the form

$$n_\sigma(k) \sim \text{sign}(k - k_0)|k - k_0|^{\nu_f} \quad (4.3.22)$$

near $k_0 - k_{F\sigma} = 0, \pm 2k_B, \pm 2k_F, \dots$. The corresponding critical exponent, ν_f , is related to the dimensions (4.3.16) for the quantum numbers ΔM and D just as ν_b above. Notice that the Fermi distribution of non-interacting particles is recovered for $\nu_f(k_{F\sigma}) = 0$, but in general the presence of interacting among the bosons and the fermions lead to additional singularities in the density distribution like the one at $k_F + 2k_B$ for instance.

NB: The various quantum numbers associated to the Bose and Fermi Green's functions are compiled in Tab. 4.1.

4.4 Experimentally relevant examples

In the following we consider two cases of particular relevance [92, 107, 17], namely (i) the unpolarized case where $M_\uparrow = M_\downarrow = M_f/2$ and the ground state of the system is invariant under rotations in the spin index of the fermions and (ii) the fully polarized case where there is only one spin component of the fermions.

4.4.1 The unpolarized gas

For $Q_1 = \infty$ one obtains $M_\uparrow = M_\downarrow$ from (4.1.5), i.e. with vanishing net magnetization. In this case the dressed charge matrix (4.2.11), evaluated at the generalised Fermi surface, takes the form

$$\mathcal{Z} = \frac{1}{2} \begin{pmatrix} 2\zeta_{00} & (\zeta_{00} + \zeta_{01}) & 2\zeta_{01} \\ 0 & \sqrt{2} & 0 \\ 2\zeta_{10} & (\zeta_{10} + \zeta_{11}) & 2\zeta_{11} \end{pmatrix}. \quad (4.4.23)$$

Here the Wiener-Hopf method (see App. C for details) has been used to determine $\mathcal{Z}_{11} = 1/\sqrt{2}$ and $\zeta_{0j} = \zeta_{0j}(Q_0)$, $\zeta_{1j} = \zeta_{1j}(Q_2)$. The functions $\zeta_{ij}(x)$ are given by

$$\zeta_{ij}(x) = \delta_{ij} + \int_0^x R(x-y)\zeta_{0j}(y) + \int_2^x R(x-y)\zeta_{1j}(y) \quad (4.4.24)$$

with

$$R(x) = \frac{1}{\pi} \int_0^\infty d\omega e^{-|\omega|/2} \frac{\cos(\omega x)}{\cosh(\omega/2)} . \quad (4.4.25)$$

Using (4.4.23), the scaling dimensions Δ_1^\pm in (4.3.16) are independent on the remaining system parameters, i.e. the effective coupling γ and the bosonic fraction α . This a consequence of the $SU(2)$ invariance of the system in this case. The mode $\epsilon_1(k)$ is the spinon mode of the unpolarized system, the CFT describing its low-energy properties is an $[SU(2)]_1$ Wess-Zumino-Witten model.

Additional simplifications arise in the strong coupling limit $\gamma \rightarrow \infty$ (i.e. $Q_0 \rightarrow 0$) where

$$\begin{aligned} \zeta_{00} &= 1 , \\ \zeta_{10} &= 0 , \\ \zeta_{01} &= \zeta_{11}(0) - 1 = \alpha , \end{aligned} \quad (4.4.26)$$

$$\text{and } \zeta_{11}(x) = 1 + \alpha \int_{-Q_0}^{Q_0} dy R(x-y) + \int_{-Q_2}^{Q_2} dy R(x-y) \zeta_{11}(y) .$$

In Fig. 4.1 we present results obtained from the numerical solution of these integral equations for the exponents which determine the singularities of the momentum distribution functions for bosons at $k = 0$ and fermions at $k = k_F$ as a function of the bosonic fraction α for various values of γ . The exponents $\nu_{b,f}$ at the other wave numbers are always larger than 1. Note that the system is in a different universality class for $\alpha = 0$ or 1. At $\alpha = 0$, all particles are fermionic and the critical exponents are those of the 1D Fermi gas [41]. Here the exponent ν_f for the singularity at the Fermi point varies between 0 and 1/8 as a function of γ . On the other hand, the limit of ν_b as $\alpha \rightarrow 1$ gives exactly the exponent of the 1D Bose gas with δ -interaction [73].

4.4.2 The spin-polarized gas

Setting $Q_2 = \infty$ in (4.1.5) corresponds to $M_\downarrow = 0$. This case has been discussed recently in Ref. [76] where some correlation functions have been computed numerically in the strong coupling limit. Integrating out the 2-components the integral equations for the distribution function and the 2×2 dressed charge reduce to coupled pairs with kernel

$$\hat{K} = \begin{pmatrix} 0 & \int_1 a_1(x-y) \cdot \\ \int_0 a_1(x-y) \cdot & 0 \end{pmatrix} \quad (4.4.27)$$

In this case, the finite-size spectrum and the scaling dimensions are determined by two gapless modes. Again, the equations simplify in the strong coupling limit ($\gamma \rightarrow \infty$) where all exponents can be given as a function of α directly.

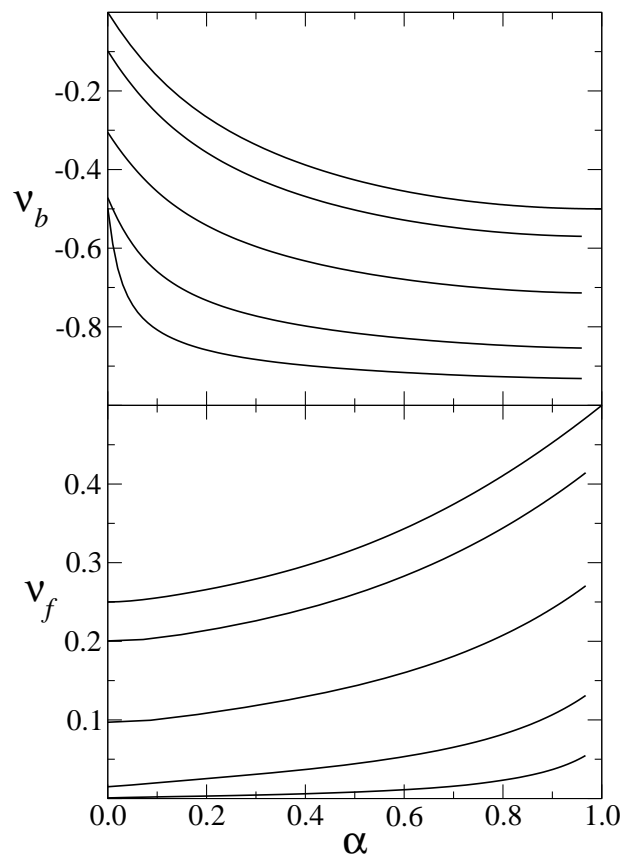


Figure 4.1: Exponents characterizing the singularities in the bosonic (upper panel) and fermionic (lower panel) momentum distribution function for the unpolarized gas at $k = 0$ and k_F , respectively, as a function of the bosonic fraction α in the mixture for $\gamma = 0.2, 1.0, 5.0, 25.0, \infty$ (bottom to top).

In fact, the dressed charge matrix in this case is simply

$$\mathcal{Z} = \begin{pmatrix} 1 & \alpha \\ 0 & 1 \end{pmatrix}. \quad (4.4.28)$$

From Eq. (4.4.28) one can deduce the dominant singularities of the bosonic and fermionic momentum distribution functions. We obtain

$$\nu_b(0) = \alpha^2/2 - \alpha \quad (4.4.29)$$

for the singularity of the bosonic function close to $k \approx 0$ and

$$\nu_f(k_F) = \alpha^2 - \alpha + 1/2. \quad (4.4.30)$$

for the fermionic distribution at $k \approx k_F$. In Fig. 4.2, we present plots of the critical exponents ν_b, ν_f in function of the boson ratio for different values of γ . We notice that while the dependence of ν_b on α is similar to the one found in the unpolarized case, the strong coupling behaviour of ν_f at small bosonic fraction is seen to be very different. Note that the singularity at $k_F + 2k_B$ (corresponding to $D_0 = D_1 = 1/2$) becomes very pronounced for sufficiently small α . We find

$$\nu_f(k_F + 2k_B) = \alpha^2 + \alpha + 1/2 \quad (4.4.31)$$

at strong coupling. In this regime, we give a comparison of the exponents $\nu_f(k_F)$ and $\nu_f(k_F + 2k_B)$ in Fig. 4.3 which shows the emergence of the $k_F + 2k_B$ contribution at low concentration of bosons. This result that we first predicted in [51] has been confirmed in the meantime by a numerical calculation of the correlation function based on the exact eigenstates. The results of this approach [77] are shown in Figs. 4.4–4.6 for different boson fractions. In Fig. 4.4 the densities of bosons and fermions are almost equal. The Fermi step at $k = k_F$ of the well-known Fermi gas here gets smeared out by the interactions, but the relative change in the occupation number as k_F is crossed is significant. Reducing the fraction of bosons in the system, the discontinuity at $k_F + 2k_B$ appears and becomes enhanced as α decreases (see Figs. 4.5–4.6). One should note, that the singularity in the fermion distribution function at $k_F + 2k_B$ is a direct signature of the interactions and should be observable in experiments.

4.5 Summary

In summary we have used predictions from CFT on the finite size scaling of the low-energy spectrum to compute the critical properties of a 1D Bose-Fermi mixture for the integrable model (4.1.1). In the generic case there are three linearly dispersing modes which determine the low-energy effective theory and the asymptotic behaviour of the correlation functions. Within this formalism we have related the critical exponents directly to the parameters describing the microscopic Hamiltonian, i.e. the coupling strength, the fraction of bosons

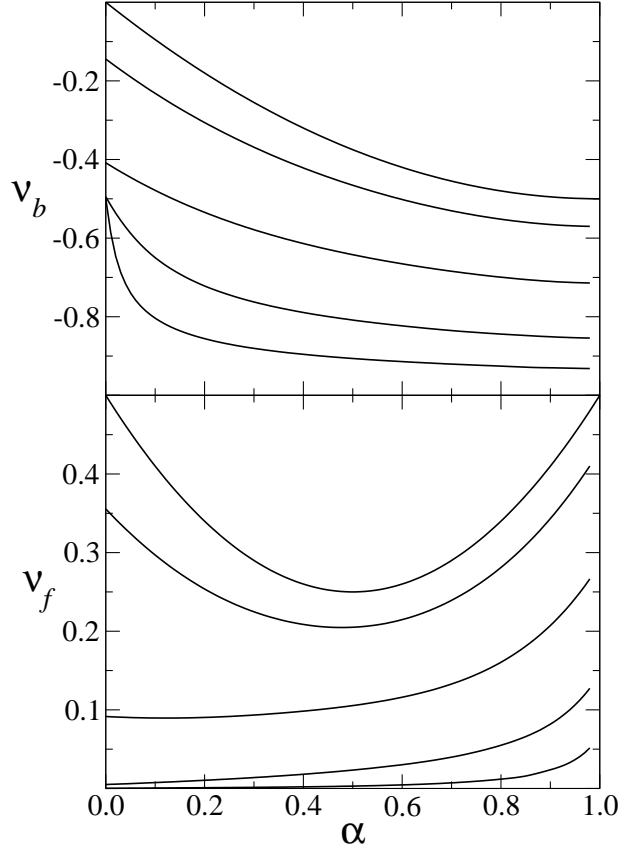


Figure 4.2: Same as Fig. 4.1 for a mixture with polarized fermions.

and polarization of the fermions. At zero temperature, the boson momentum distribution has a singularity at $k \approx 0$ reminiscent of BEC in higher dimensions, and its strength is controlled by the TL parameter K_b which depends only on boson fraction for strong interactions. For polarized fermions, the momentum distribution has a lot of interesting features. In addition to the standard $k \approx k_F$ discontinuity, $n_f(k)$ develops an extra singularity at $k_F + 2k_B$, and the strength of this singularity is higher for small boson fractions. These results on the distribution function of the gas can be extended to finite temperature via a conformal mapping (cf Chap.3). It should be possible to verify experimentally the existence of the predicted singularities. One would need to work with systems of constant densities along the x -direction. Such constant density can be achieved in experiments with micro traps [74, 115, 71, 43, 14],

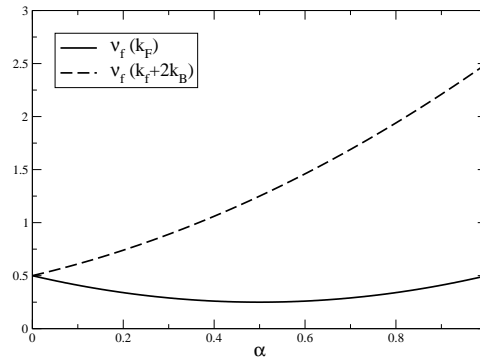


Figure 4.3: Comparison of the exponents $\nu_f(k_F)$ and $\nu_f(k_F + 2k_B)$ in the polarized case and in the strong coupling limit in function of α . We see that, if the $k \approx k_F$ is always the leading singularity (smallest exponent), the singularity close to $k_F + 2k_B$ becomes more pronounced for small values of α .

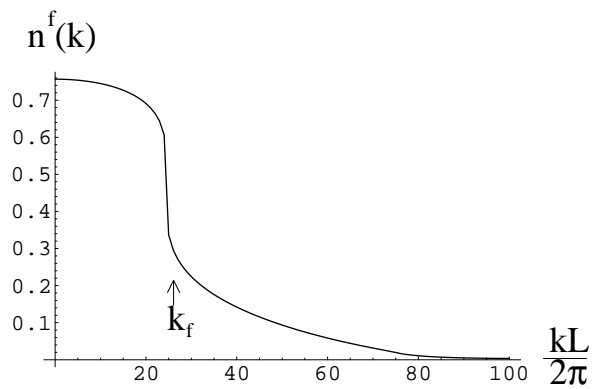


Figure 4.4: Fourier transform of the Fermi-Fermi correlation function for $\alpha = 51\%$. The Fermi step at k_F gets smeared out by interactions. Taken from [77]

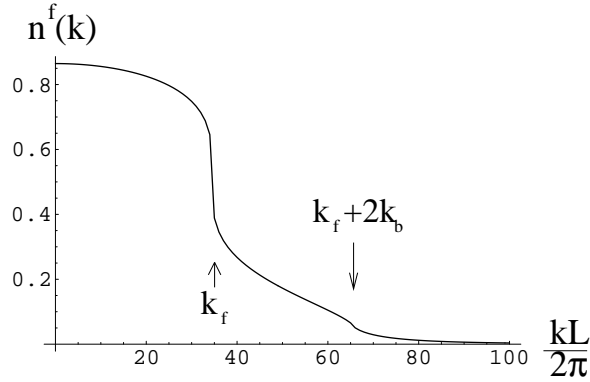


Figure 4.5: Fourier transform of the Fermi-Fermi correlation function for $\alpha = 31\%$. In addition to the Fermi step at k_F , another discontinuity appears at $k_F + 2k_B$. Taken from [77]

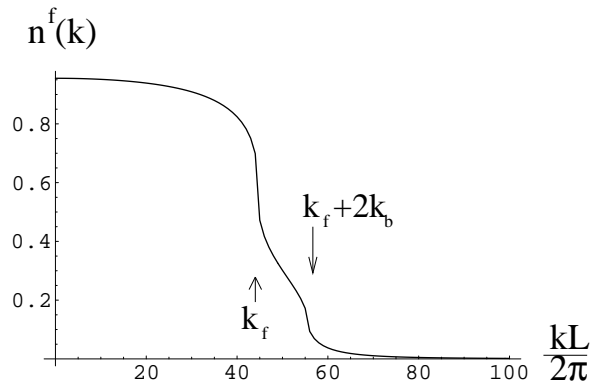


Figure 4.6: Fourier transform of the Fermi-Fermi correlation function for $\alpha = 11\%$. The Discontinuity at $k_F + 2k_B$ gets stronger as α decreases. Taken from [77]

or in 2D arrays of tubes, if one makes a very shallow harmonic confinement, and creates strong box-like impenetrable potential at the sides of the tubes with the help of additional lasers. If the system is in harmonic trap, lots of the features of correlations themselves (i.e. singularity at $k_F + 2k_B$) may get washed out due to averaging over inhomogeneous density profile [61]. Finally, let us mention that the approach that we developed here can be used to investigate the phase diagram of the 1D mixture by identifying the order parameter with the slowest long-distance decay of its correlation functions (smallest exponent) [29, 107]. Within the integrable model there is no instability leading to a phase transition [92, 17]. This reason for this is that an effect such as the demixing predicted in [33] relies on a mean-field theory which fails at strong interactions. The general expression (4.3.16), however, allows to obtain esti-

mates on the exponents in a more general system based on numerical data on the spectrum of finite systems.

Part II

Boundaries/Impurities in correlated electrons models

Chapter 5

Quantum impurities and Kondo effect

A quantum impurity is, by definition, a local scatterer carrying internal degrees of freedom like a quantum spin or local orbitals for example. When embedded into a many-body system, quantum impurities lead to a variety of phenomena which are non-perturbative in nature. The most prominent example is the so-called Kondo effect which occurs when the system contains magnetic impurities. The coupling between the localised spin of the impurity and the conduction electrons of the host change dramatically the low-temperature (low-energy in general) physics of the system. In the 1930's it was found in many dilute magnetic alloys that the resistivity as a function of the temperature shows a minimum and increases at low temperature [34, 35]. This was in contradiction with the accepted theoretical prediction that impurities give a constant contribution at zero temperature (see Fig. 5.1 for comparison between the case with and without magnetic impurities). In fact, Kondo found the following expression for the resistivity:

$$\rho(T) = \rho_0 + aT^2 + c_m \ln \frac{\mu}{T} + bT^5.$$

ρ_0 is the residual resistance, aT^2 shows the contribution from the Fermi liquid properties, and the term bT^5 is from the phonons. But the log-term which diverges at $T \rightarrow 0$ was derived by Kondo thanks to a higher order perturbative calculation. It is important to say right now that this calculation is correct only for temperatures larger than the so-called Kondo temperature T_K which is the threshold of validity of the perturbation theory in this case as we will see in next section. A special feature of the strong local electronic correlations is the “Kondo-resonance” in the impurity spectral function which influences various measurable properties. Recently, a novel application of such “quantum impurity systems” to describe the electronic transport through artificial “quantum dots” has emerged, as such quantum dots can be modeled by single or multi-impurity systems.

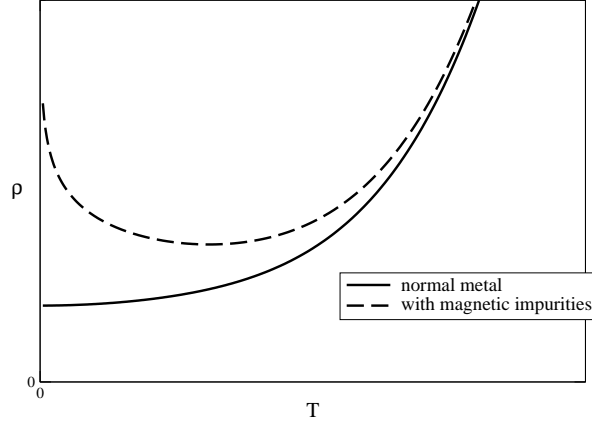


Figure 5.1: Resistivity ρ as a function of the temperature T for a sample without (solid) and with magnetic impurities (dashed).

5.1 Conventional Kondo effect

The first step towards a theoretical understanding of the resistance minimum emerged when Kondo proposed in 1964 a model in which the magnetic impurity is modeled by a localized spin coupled to the spin density of the metallic host at the impurity site, which is assumed to consist of noninteracting electrons. The phenomenological Hamiltonian (a.k.a. the s - d model) which captures this physical situation reads

$$H_K = H_0 + J\mathbf{s}\cdot\mathbf{S} \quad (5.1.1)$$

where $H_0 = \sum_{k,s} \xi_k \psi_{k,s}^\dagger \psi_{k,s}$ describes the electron gas, $\mathbf{s} = \frac{1}{2} \sum_{kk's's'} \psi_{k,s}^\dagger \sigma_{ss'} \psi_{k's'}$ is the spin density of the conduction electrons at the impurity site (with $\sigma = (\sigma_x, \sigma_y, \sigma_z)$ being the Pauli matrices), and \mathbf{S} is a spin-1/2 operator representing the magnetic impurity.

From now on, let us consider only the non-trivial case of anti-ferromagnetic coupling ($J > 0$). Going beyond the Born approximation, Kondo obtained a logarithmic temperature dependence already in the third order in the exchange amplitude J [86],

$$\delta\rho \sim n_i(\nu J)^2 [1 + 2\nu J \ln(D/T)]. \quad (5.1.2)$$

Here ν is density of states (so that $\nu J \ll 1$ is a dimensionless parameter) and D is the bandwidth. This solved the problem of the resistance minimum in magnetic alloys. Soon after Kondo's paper, Abrikosov and Suhl found that logarithmically-divergent contributions appear in all orders of perturbation

theory, forming a geometric series [1, 126]

$$\delta\rho(T)/\delta\rho(0) \propto \left(\sum_{n=0}^{\infty} (\nu J)^n [\ln(D/T)]^{n-1} \right)^2 = \left(\frac{\nu J}{1 - \nu J \ln(D/T)} \right)^2. \quad (5.1.3)$$

This result can be also written as

$$\delta\rho(T)/\delta\rho(0) \propto \ln(T/T_K)^{-2}, \quad (5.1.4)$$

where T_K is the famous Kondo temperature given by

$$T_K = D e^{-1/(\nu J)}. \quad (5.1.5)$$

Obviously, Eq. (5.1.4) diverges when T approaches T_K . Similar untractable (and clearly unphysical) divergencies appear in thermodynamic quantities as well, indicating the failure of the perturbation theory. The problem of dealing with these divergencies became known as the *Kondo problem*, and its resolution came later with the advent of the powerful Renormalization Group (RG) ideas [10, 116, 136]. The RG- β function of the dimensionless coupling $\lambda = \nu J$ is given by

$$\beta(\lambda) = \frac{d\lambda}{d \ln D} \simeq -\lambda^2 + \dots \quad (5.1.6)$$

where the bandwidth D is here reinterpreted as an ultraviolet cutoff of the theory. Eq. (5.1.6) shows that at low temperature the coupling to the impurity is described by an effective (renormalised) coupling diverging for $T \ll T_K$,

$$\lambda_{\text{eff}} = \frac{\lambda_0}{1 - \lambda \ln(D_0/D)}. \quad (5.1.7)$$

This observation makes of the Kondo effect the very first example of asymptotic freedom in physics, in which the coupling becomes non-perturbatively strong at low temperatures/low energies. In the Kondo problem, this refers to the interaction between the localized magnetic impurities and the itinerant electrons. Another very important illustration of the asymptotic freedom's concept is met in quantum chromodynamics (QCD), the theory of the strong nuclear force. In QCD the quarks, the fundamental constituents of nuclear matter, interact weakly at high energies and strongly at low energies, preventing the unbinding of baryons or mesons composing the nucleus¹.

Let us try to understand the physics by hand. In perturbation theory one starts with the impurity decoupled from the electron gas ($J \rightarrow 0$). Since the spin-up and spin-down states of the impurity are degenerate, the ground state of the system in this limit is a doublet. Because electrons are freely moving in space, it is hard for the impurity to capture an electron and form a singlet. Yet,

¹For this discovery, Frank Wilczek, David Gross, and David Politzer shared the 2004 Nobel Prize in physics.

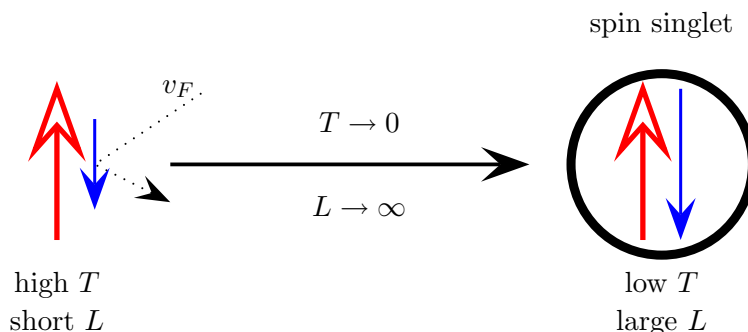


Figure 5.2: Schematic RG flow of the Kondo model. As the system goes to higher scales or lower energy, it flows from a free impurity spin to an infrared fixed point characterised by a singlet ground state. The impurity is said to be "screened" by the conduction electrons.

even an arbitrarily weak local antiferromagnetic exchange interaction suffices to form a singlet ground state which is the infrared fixed point of the theory (see Fig. 5.2). However, the characteristic energy for this singlet is given not by the exchange amplitude J , but by the Kondo temperature T_K , defined in Eq. (5.1.5). This lifting of the degeneracy of the ground state is the very essence of the Kondo effect. It is also the origin of the logarithmic divergences. Treating the strength of the exchange perturbatively is then justified only at temperatures that significantly exceed the singlet binding energy, i.e. at $T \gg T_K$. In the opposite limit $T \ll T_K$ Nozières used a perturbative approach [111] that explicitly takes into account the correct symmetry of the ground state right from the start yields

$$1 - \delta\rho(T)/\delta\rho(0) \propto (T/T_K)^2, \quad T \ll T_K. \quad (5.1.8)$$

Eqs. (5.1.4) and (5.1.8) are applicable, respectively, in the weak ($T \gg T_K$) and strong ($T \ll T_K$) coupling limits. Since the Kondo effect is a crossover phenomenon rather than a phase transition, the function $\delta\rho(T)/\delta\rho(0)$ varies smoothly with T in the crossover region $T \sim T_K$.

5.2 Kondo effect in nanostructures

Apparently the Kondo effect is a rather well established and well understood problem of condensed matter physics. Nevertheless, due to the recent progress in nanotechnology, we assist since the late 1990's to a real "revival of the Kondo effect" to use the expression of Kouwenhoven and Glazman [89]. The possibility to design pretty small and clean semiconductor devices in confined geometries allows to create in the laboratory fully controllable artificial impurities. In such systems the Kondo effect is playing a non-trivial role in the understanding of the transport properties as we will try to clarify in this section.

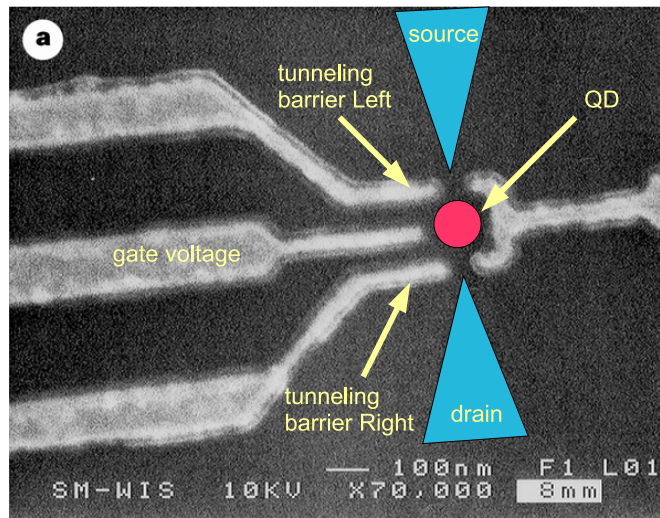


Figure 5.3: Electron microscopy image of a single electron transistor device extracted from Ref. [69]. The additional captions drawn on top on the original black and white picture are made to be explicit. QD stands for quantum dot. ©1998 Nature Publishing Group

One of the devices used for observing modern features of the Kondo effect consists of a quantum dot placed between two large metallic leads (called the source and the drain by the experts). A quantum dot is a tiny semiconductor island that can hold a small number of electrons. The first realization of this circuit is shown in Fig 5.3. It is an image of a quantum dot made by electronic microscopy extracted from the famous paper [69] of the M.I.T. team. A voltage applied to the gate electrode of the device controls the number of electrons N confined in the dot. If N is odd there is an effective spin $S = 1/2$ sitting on the quantum dot. This mimics the impurity-in-metal system which we have been discussed so far, where a localised spin is embedded into a metallic host. Therefore many features of Kondo physics are expected in the Single-Electron-Transistor (SET) devices. But it should be noted that the Kondo effect does not always manifest itself in the increase of the resistance. Indeed, the formation of the singlet ground state leads to an increase of the probability for an electron to scatter by the impurity. The closer the energy of the scattered electron is to the Fermi level, the higher is the scattering probability. If a magnetic impurity is imbedded in a bulk sample, the higher scattering probability translates to the increase of the resistivity. However, if the impurity resides in a tunneling barrier separating two conducting leads, the increase of the scattering probability leads to an enhanced probability for an electron to tunnel through the barrier, hence it is the differential conductance, rather than the resistance, that is enhanced with lowering the temperature or

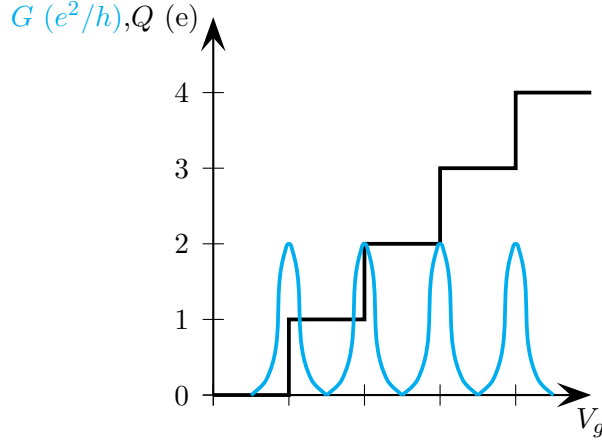


Figure 5.4: Diagram of the charge Q of the quantum dot (black) and the differential conductance G (cyan) as a function of the gate voltage V_g . The charge of the dot shows a staircase-like behaviour signature of the quantised nature of this quantity. The conductance features alternating Coulomb peaks synchronised with the variation by one unit of the charge and Coulomb blockade valleys at fixed Q .

the bias voltage.

Let us now sketch how this Kondo-assisted tunnelling works in the case of a quantum dot setup. At first sight the electronic transport through the dot is not easy. There are two reasons for that: First, due to the large Coulomb repulsion onto the dot, U , which has the tendency to prevent electrons to tunnel on and off the dot. This phenomenon is known as the *Coulomb blockade*. Second, the electron energy in the dot, ε_d , is in general off-resonance (i.e. away from the Fermi level). As a consequence of the large Coulomb interaction, the charge on the dot is quantised and shows a staircase-like behaviour when plotted as a function of the gate voltage V_g (see Fig. 5.4). The electrostatic energy of a state of N electrons in the dot is given by

$$E_C = \frac{Q^2}{2C} - V_g Q \quad (5.2.9)$$

with $Q = Ne$ is the total charge. The gate voltage V_g acts on the dot like a chemical potential. When the gate voltage is increased, ε_d is lifted up to the Fermi level. Then, the tunnelling of an electron from the lead is possible and the dot experiences a transition between the states of charge Ne and $(N+1)e$. The conductance naturally reaches a maximum at this point. When the system is in region of fixed charge, the probability to find an electron with energy E_C is proportional to $\exp(-E_C/T)$, and we expect the conductance to be exponentially suppressed (as long as $T \ll E_C$, which we assume since we will be interested mainly in the low- T physics in the following). These are the "Coulomb valleys" we can see on Fig 5.4. Consider now such a Coulomb

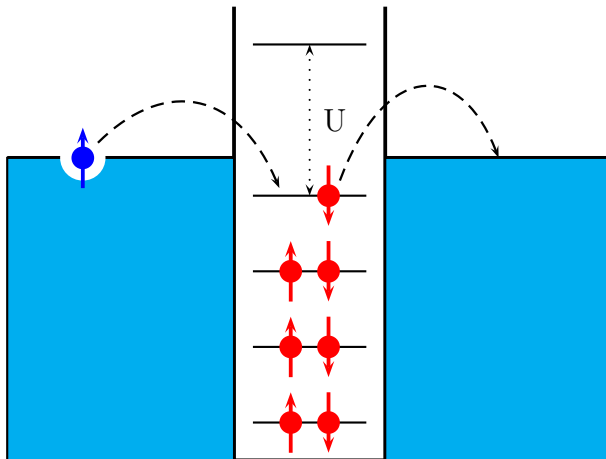


Figure 5.5: Tunneling process giving rise to the Kondo effect. If the number N of electrons on the dot is even, it would cost a large amount of energy (of the order of U) for an electron of the source to tunnel through the dot. At the contrary, if N is odd, a virtual process (similar to the super-exchange see Chap. 6) allows one electron from the source to hop onto the dot and the dot's electron to hop itself towards the drain. This process results in an effective spin-flip on the dot (Kondo effect) and favours tunnelling through the dot, energetically speaking.

blockade valley with an odd number of electrons in the dot. In the ground state, the top-most occupied level is filled with a single electron, which may be either in a spin-up or in a spin-down state. In other words, the dot has a spin $S = 1/2$ and its ground state is doubly degenerate. This singly-occupied level plays a special role in transport, as the elastic co-tunneling process involving this level may be accompanied by a flip of the transferred electrons spin with a simultaneous flip of the spin of the dot, see Fig. 5.5. This is precisely the kind of spin-flip process that gives rise to the Kondo effect in tunnelling. Accordingly, we expect the conductance to increase with the decrease of temperature. As a nice illustration of this phenomenon another realisation of the Kondo effect is presented in Fig. 5.6. This experimental curve extracted from [112] has been obtained by measurements of the conductance (G) on a setup consisted of a carbon nanotube suspended between two normal metallic leads. The nanowire acts in this case like an extended quantum dot. We clearly see a difference between the odd (O) and the even (E) regimes which are scrolled alternatively as the gate voltage is tuned on. When the temperature is lowered (arrows) the Kondo effect induces an increase of G as expected.

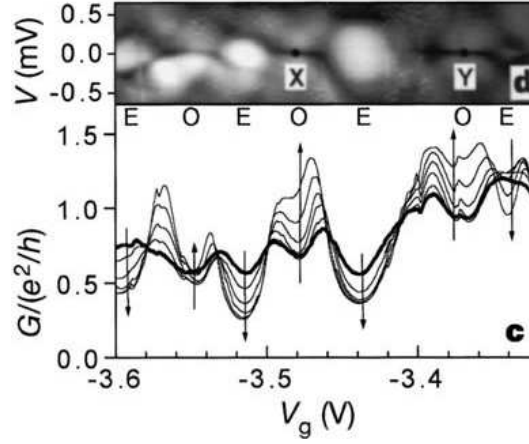


Figure 5.6: Signature of the Kondo effect in carbon nanotubes (extracted from [112]). Upper part shows the charging energy of the dot as the gate voltage is varied. One can see the alternation of region with even (E) number of electrons sitting on the dot and regions with odd (O) number of electrons. Lower part shows a plot of the differential conductance through the nanotube. One clearly sees the increase of the conductance as the temperature is decreased (arrows) for the odd regions (in opposition with the even ones) signalling the formation of a local magnetic moment. ©2000 Nature Publishing Group

5.3 Insight from exactly solvable models

5.3.1 The 1-lead Anderson model

So far we have only cited one theoretical model, namely the Kondo or s - d model, and commented on its physics. A more natural model for the quantum dot setup device is the Anderson model - which is equivalent in some limit to the Kondo model via the Schrieffer-Wolff transformation [75]. It involves an impurity with local orbitals instead of just a spin like in the Kondo model. It reads

$$H_A = \sum_{\sigma} \varepsilon_d n_{d,\sigma} + U n_{d,\uparrow} n_{d,\downarrow} + \sum_{k,\sigma} \varepsilon_k c_{k,\sigma}^{\dagger} c_{k,\sigma} + \sum_{k,\sigma} (V_k d_{\sigma}^{\dagger} c_{k,\sigma} + V_k^* c_{k,\sigma}^{\dagger} d_{\sigma}) \quad (5.3.10)$$

in its "one lead" original version ². The energy scales appearing in Eq. (5.3.10) are ε_d , the discrete energy of the artificial atom and U , the on-dot Coulomb repulsion, i.e. the cost in energy one should pay to have another electron sitting on the dot. This term is the one responsible for the Coulomb blockade mechanism which was discussed above. The term proportional to V_k is called the hybridisation. It describes the hopping of an electron from the Fermi sea

²The model describes a single Fermi sea coupled to an impurity. The word "lead" in the text is an abused expression referring to the Fermi sea.

onto the dot and vice versa. Here we have deliberately chosen to write the Hamiltonian (5.3.10) in one spatial dimension. The reason why this dimension reduction is appropriate goes as follows: If one wants to compute the effect of a localised impurity, standard scattering theory teaches us that we have to decompose the wave function into spherical harmonics (radial and angular variables). Doing so, one can convince himself that the main contribution to the scattering process comes from the s -wave term, which is invariant under rotation. Therefore, only remains the radial dependence of the wave function, and the scattering off the impurity can be essentially mapped onto a one-dimensional model.

After a long history of early approximate solutions, the Anderson single impurity model was solved “exactly” using the numerical renormalization group (NRG) and the Bethe ansatz method. In the early 80’s solutions for the s - d model were found independently by Andrei [11] and Wiegmann [134] followed by exact solutions for the Anderson model (Wiegmann [135], Kawakami and Okiji [81]). The solution is lengthy but extremely enlightening. Unfortunately we will not present it in full detail in this thesis. We refer to the original paper of Wiegmann for completeness. The remarkable thing is that the main ideas of the original Bethe-Ansatz technique, developed by Bethe in 1931 for solving the Heseinberg magnetic chain, has been adapted to solve the Anderson model which is a model of correlated electrons. The Wiegmann solution relies on two fundamental asumptions: First, that we have a linear (relativistic) dispersion for the conduction electrons and second, that there are only point-like interactions. The first assumption makes sense as long has we are interested in the low-lying excitations slightly above the Fermi energy. In that case, the free fermion dispersion relation can be linearised ³ around $k = k_F$, the ”Fermi surface”. The second assumption is a bit more restrictive. In essence it tells us to forget about the spatial extension of the impurity (or dot). So, taking these assumptions for granted, we can integrate out the lattice and rewrite the Hamiltonian (5.3.10) in the continuum limit as a field theory

$$H_A = \int dx \left\{ -i \sum_{\sigma} c_{\sigma}^{\dagger}(x) \partial_x c_{\sigma}(x) + V \delta(x) (c_{\sigma}^{\dagger}(x) d_{\sigma} + d_{\sigma}^{\dagger} c_{\sigma}(x)) \right\} + \sum_{\sigma} \varepsilon_d n_{d,\sigma} + U n_{d,\uparrow} n_{d,\downarrow}. \quad (5.3.11)$$

Note that the hybridisation V is now k -independent. Then, using Yang’s technique for the one-dimensional Fermi gas with δ -interaction [139], the spectrum of the Hamiltonian (5.3.11) is obtained by solving the following Bethe Ansatz

³It is actually the starting point of using the bosonisation technique.

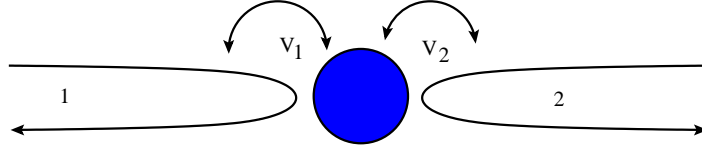


Figure 5.7: Diagram of the physical situation described by the 2-lead Anderson model. Electrons from lead 1 can tunnel through the dot towards lead 2 and vice-versa. The tunnelling barrier separated the leads from the dot are respectively V_1 and V_2 .

equations for the k 's momenta:

$$\begin{aligned} \exp(ik_j L) &= \prod_{\beta=1}^M \frac{iB(k_j) - i\Lambda_\beta - UV^2/2}{iB(k_j) - i\Lambda_\beta + UV^2/2} \frac{1 + iV^2/2(k_j - \varepsilon_d)}{1 - iV^2/2(k_j - \varepsilon_d)}, \quad j = 1, \dots, N \\ - \prod_{j=1}^N \frac{iB(k_j) - i\Lambda_\alpha + UV^2/2}{iB(k_j) - i\Lambda_\alpha - UV^2/2} &= \prod_{\beta=1}^M \frac{i\Lambda_\alpha - i\Lambda_\beta - UV^2}{i\Lambda_\alpha - i\Lambda_\beta + UV^2}, \quad \alpha = 1, \dots, M \end{aligned} \quad (5.3.12)$$

where $B(k) = k(k - U - 2\varepsilon_d)$. Solving the BAE (5.3.12) gives access quite easily to the full thermodynamics of the model. In particular, the magnetic properties of the system, such as the magnetisation and the magnetic susceptibility, can be calculated exactly. Signatures of Kondo physics are revealed by these quantities; for instance, the impurity magnetisation (at $T = 0$) as a function of the applied field H features a crossover from a linear H behaviour to a constant. The scale at which this crossover is observed is the Kondo temperature defined by $T_K \propto \exp[-(\pi/4)(U/V^2 - V^2/U)]$.

5.3.2 The 2-lead Anderson model

To make contact with any experimental realisation, it is necessary to consider a version of the Anderson model slightly more sophisticated, namely a theory with two leads coupled to the dot (see Fig. 5.7). The Hamiltonian is then

$$\begin{aligned} H_{A2} &= -t \sum_{i,\sigma} (c_{i,\sigma}^\dagger c_{i+1,\sigma} + \text{h.c.}) \\ &\quad + \sum_{\sigma} [V_1 (c_{-1,\sigma}^\dagger d_{\sigma} + \text{h.c.}) + V_2 (c_{1,\sigma}^\dagger d_{\sigma} + \text{h.c.})] \\ &\quad + \varepsilon_d (n_{d,\uparrow} + n_{d,\downarrow}) + U n_{d,\uparrow} n_{d,\downarrow} \end{aligned} \quad (5.3.13)$$

where we have now explicitly two Fermi seas (non-interacting leads). The conduction electrons can scatter on and off the dot passing from one lead to another via tunnelling. This electronic transport will induce a current through the dot. This current is actually the relevant quantity measured in the experiments. The microscopic parameters of the two-lead Anderson model

are related to the energy scales of the quantum dot setup. The charging energy is defined with the help of the dot's electric capacitance C and the energy level spacing $\Delta\varepsilon$, $U = \frac{e^2}{2C} + \Delta\varepsilon$. As usual, the gate voltage V_g acts like a chemical potential on the dot such that $\varepsilon_d \propto V_g$. As we already said, but it worths emphasising it again, the gate can drift the energy level closer or away from the Fermi level and therefore controls the number N of electrons sitting on the dot. In particular, by tuning V_g , one can reach the regime where N is odd and thus investigate phenomena associated to Kondo physics. V_1 and V_2 are the respective heights of the barriers leads-dot and $\Gamma = (V_1^2 + V_2^2)/2$ is width of the resonance (just like in quantum optics when a discrete level is coupled to continuum this induces a spreading of the spectral peaks). Once again a theoretical analysis of the two-lead Anderson model is facilitated by taking the continuum limit,

$$H_{A2} = \sum_{l,\sigma} \int dx \left\{ -ic_{l,\sigma}^\dagger(x) \partial_x c_{l,\sigma}(x) + V_l \delta(x) (c_{l\sigma}^\dagger(x) d_\sigma + d_\sigma^\dagger c_{l,\sigma}(x)) \right\} + \sum_{\sigma} \varepsilon_d n_{d,\sigma} + U n_{d,\uparrow} n_{d,\downarrow}, \quad (5.3.14)$$

where l labels the leads 1 and 2. It is remarkable to see that the two-lead problem can be mapped onto the one-lead model. To do so, let us introduce the even and odd fermion operators as:

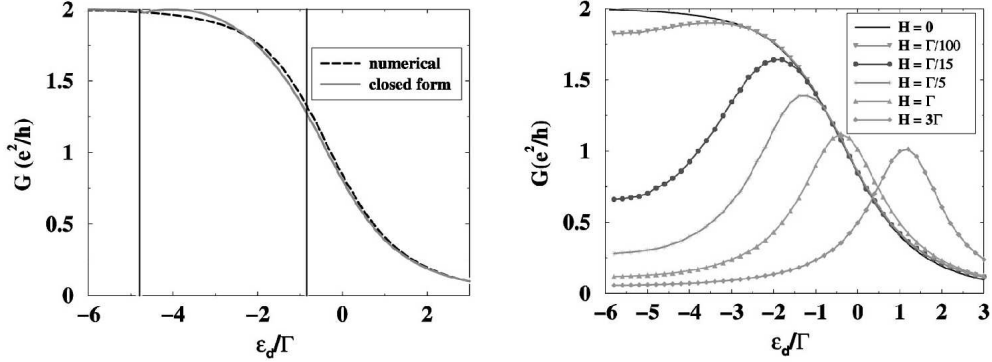
$$c_{e,o} = \frac{1}{\sqrt{V_1^2 + V_2^2}} (V_{1,2} c_1 \pm V_{2,1} c_2) \quad (5.3.15)$$

Injecting those new operators into Eq. (5.3.13) we end up with an effective Hamiltonian for the even electrons only and the solution for the one-lead Anderson model can be used. The Kondo temperature is now defined as $T_K \propto \exp \pi [\varepsilon_d(\varepsilon_d + U) - \Gamma^2] / (2\Gamma U)$

So long, one could ask the legitimate question: If the exact spectrum of the quantum dot problem can be inferred from results which are more than twenty years old, why should we continue studying those models anyway? Well in fact, the renewal of interest for the exact (thus non-perturbative) calculations within the Anderson model comes from the fact that transport properties like the conductance for instance can be calculated exactly, at least at low-energy and close to equilibrium. The idea is to work directly within the Bethe basis of quasi-particles (obeying a non-trivial statistics). In this language, the transmission of an excitation of energy ε is given by

$$T(\varepsilon) = \frac{V_1 V_2}{V_1^2 + V_2^2} (e^{i\delta(\varepsilon)} - 1) \quad (5.3.16)$$

where $\delta(\varepsilon)$ is the scattering phase shift. As far as we stay in the linear response regime, the Landauer-Büttiker formula gives us a suitable expression of the



(a) G at $T = 0$, $H = 0$ for $U = 0.75$ and $\Gamma = U/12$

(b) G at $T = 0$ for various H

Figure 5.8: Results of Konik et al. for the conductance in the 2-lead Anderson model (1)

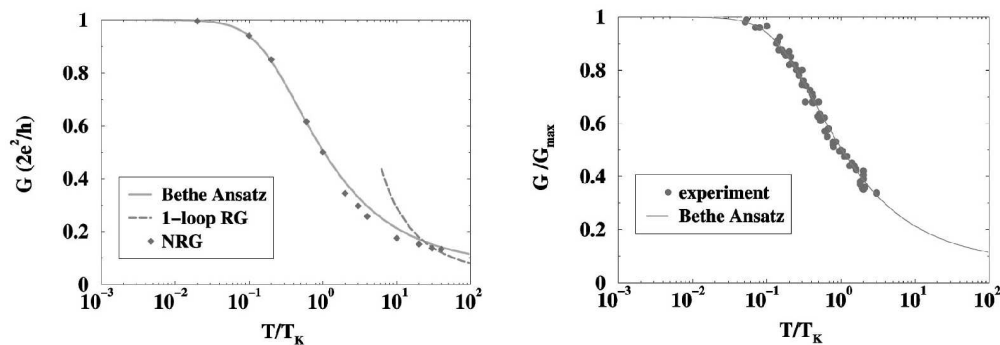
conductance,

$$G = \frac{e^2}{h} [|T_{\uparrow}(\varepsilon = 0)|^2 + |T_{\downarrow}(\varepsilon = 0)|^2]. \quad (5.3.17)$$

The key-point is that for the excitations close to Fermi energy or to the so-called symmetric point $\varepsilon_d = -U/2$ (where the Kondo effect is expected), the Friedel sum rule holds:

$$|T_{\sigma}|^2 = \sin^2 \left(\frac{\delta_{\sigma}(\varepsilon = 0)}{2} \right), \quad \delta_{\sigma} = 2\pi n_{d,\sigma}. \quad (5.3.18)$$

This formula is far from trivial since it relates the occupation of the dot, n_d , which is a thermodynamic quantity, to the transmission (via the dephasing δ) which is dynamic quantity. Konik, Saleur and Ludwig performed this kind of calculation using the Bethe Ansatz and we will show now some graphs extracted from [87]. In Fig. 5.8(a) the conductance G at zero temperature is depicted as a function of the gate voltage. G goes up to the unitary limit $2e^2/h$ which is the optimal conductance of a quantum wire where both spin channel can travel through. As the gate voltage is increased, a Coulomb valley develops and the conductance drops down to zero. In Fig. 5.8(b) the external magnetic field H is switched on. The maximum in the conductance curves is shifted. It is just the sign that maximum conductance is connected to the Kondo effect. Therefore the local magnetic moment feels to the magnetic field and is sensitive to Zeeman splitting. Fig. 5.9(a) and 5.9(b) are plots of the conductance at finite temperature. The conductance is enhanced as the temperature is lowered. The crossover appears around $T = T_K$. Fig. 5.9(b) compares the Bethe Ansatz calculation to the experimental data of Goldhaber-Gordon et al. [68] and the agreement is excellent (provided a rescaling of T_K to be precise [119]).



(a) $G(T/T_K)$ at the sym. point $\varepsilon_d = -U/2$ (b) comparison with exp. data of Goldhaber-Gordon et al. [68]

Figure 5.9: Results of Konik et al. for the conductance in the 2-lead Anderson model (2)

5.4 Open questions and new trends in quantum impurity problems

To summarise, we have seen that, despite its apparent simplicity, the question of a single impurity coupled to a bath of electrons is highly non-trivial and cannot be answered from a single particle point of view. This problem contains basically all the ingredients of modern physics like the phenomenon of asymptotic freedom that we have quickly discussed, the mechanism of mass generation, the ideas of scaling and renormalisation. And even though it is a rather old problem it is still up-to-date in the context of nanotechnology. The Kondo and the Anderson models, which are the starting point (microscopically) of the theoretical understanding of the Kondo physics, can be generalised in many ways. One think we haven't mentioned is the very important multi-channel Kondo model which has a non-Fermi liquid fixed point when the number of channels is bigger than twice the spin of the impurity. The proper understanding of this fixed point has required the use of very sophisticated tools borrowed from high-energy physics, namely conformal and boundary conformal field theory (CFT and BCFT). It is a very interesting issue that we will not comment any longer and we will refer to the series of papers by Affleck and Ludwig on the subject [3, 4, 5, 101, 6]. Still remain some fundamental issues, and we have in mind two of them in particular: 1) What are the effects of interactions among electrons (in the bulk)? 2) What can we say about non-equilibrium situations to make contact with concrete experimental scenarii?

5.4.1 Strong correlations

First, let us comment briefly on the effect of having strong correlations within the leads. It is in fact a natural question to ask if one consider for example the case of an impurity coupled to two (quasi)one-dimensional nanowires. As we have said in the introduction to the thesis, the leads will be a Tomonaga-Luttinger liquid (TLL) rather than a conventional Fermi liquid. In particular, the density of states will behave like a power-low $\rho(\omega) \propto \omega^\alpha$. This problem has been tackled first by Kane and Fisher [79, 80] who considered a perturbed link in the middle of a one-dimensional interacting electron gas. Their RG analysis gives a quite counter-intuitive result: For repulsive electron interactions, the electrons are completely reflected by even the smallest scatterer, leading to a truly insulating weak link, in striking contrast to that for noninteracting electrons. Whereas for attractive interactions, the Luttinger liquid is argued to be perfectly transmitted through even the largest of barriers. Another result we would like to mention is the work of Fröhlich and Johannesson [57, 58] who used BCFT to investigate the situation where a magnetic impurity is coupled to a TLL. They showed that there are only two types of scaling behaviours consistent with the symmetries of the problem: either a local Fermi liquid or a non-trivial strong-coupling fixed point. The latter non-Fermi liquid fixed point seems to govern the low-temperature physics of the system as conjectured by Lee and Toner [94], and Furusaki and Nagaosa [59].

Certainly these (conformal) field theory approaches give a lot of information regarding the large-distance or low-energy sector of the theory. In particular, the characterisation of the various fixed points can be made in very elegant and powerful way using the concept of conformal invariance. But in order to understand the complete flow, one has to work with a particular model which allows for the coupling constants to vary precisely within the range between the UV to the IR fixed point(s). And of course, the best way to get some knowledge is to take an integrable model. We have already seen that the Anderson model for example is exactly solvable by Bethe ansatz, and that calculating exactly the thermodynamics of the model one can indeed see the low-temperature and high temperature behaviour of, say, the susceptibility. But not only this, the exact solution gives you also the behaviour of the physical observables in the crossover regime. In the following chapters of this thesis, two exactly solvable models will be constructed and studied in detail. These models consider an impurity put at the edge of an interacting electron chain and we will see some Kondo-like physics.

5.4.2 Out-of-equilibrium situations

The second direction towards which Kondo physics is going is the non-equilibrium physics. A lot of actual experimental situations deal with the far from equilibrium regime. Questions like the time-dependence of correlation functions,

the phenomenon of relaxation and non-equilibrium transport properties are still unsolved for the case of quantum interacting systems. And even simple localised interactions like the one we encounter in impurity problems can lead to very rich dynamics. Clearly, usual perturbation theory (which goes under the name of the Keldysh formalism for non-equilibrium problems) will fail in the presence of strong interactions. To attack those problems there is, unfortunately (or fortunately?) no universal route to follow. A lot of clever numerical techniques are being investigated as we speak like dynamical version of DMRG [78], flow equation techniques [83], or new methods coming from the quantum information community [130, 131, 32]. From the perspective of analytical results we just want to mention what may appear to be a promising technique: A non-perturbative approach to calculate transport properties, the so-called Scattering Bethe Ansatz (SBA) developed by Mehta and Andrei [109, 108]. The idea is to work on a basis which is not the natural free electron basis but rather a basis for which the interaction behaves nicely. We won't say much more about this topic but we just want to precise that, up to our knowledge, the very first attempt to use this type of scattering theory goes back to Lesage, Saleur and Skorik [95] in the context of tunnelling between edge states in the fractional quantum Hall effect. And, to be honest, the previously cited paper [87] contains also a computation of the conductance in the two-lead Anderson model out of equilibrium, even though the authors use a basis of quasi-particles within the bulk which is far from obvious.

To conclude this chapter in one sentence, we would say that quantum impurity problems are still an active topic and that there are still a lot of both fundamental and applied issues to be addressed, certainly many more than just the two we pointed out above.

Chapter 6

Integrable lattice models of correlated electrons

In this chapter, we first want to introduce the one-dimensional Hubbard model and its descendants. Those models are widely used to understand the very peculiar physics which arises in the world of one-dimension. Second, we will give, without any proof or derivation, a couple of ideas and results regarding quantum integrability (on the lattice). There, the powerful tools of the so-called Quantum Inverse Scattering Method (QISM) and Algebraic Bethe Ansatz (ABA) will be presented.

6.1 Models of correlated electrons

One of the main challenge of modern condensed matter theory is to fully understand the properties of many-body systems (fermions or bosons) in the presence of strong interactions. As we have already discussed in the introduction, in 1+1 dimension, the quantum correlations between the particles of the system can neither be neglected nor treated perturbatively. Including the interactions into any reasonable model of correlated electrons would mean taking into account the Coulomb interaction between the electrons, the phonon-electron coupling, the particular band-structure of the material, etc. But this program is way beyond human or computer power. This is why physicists introduce some simplified models writing down Hamiltonians (or actions) containing only the "most relevant" terms. What "most relevant" means and in particular what are the limits of validity of such approximate models is really an important question to answer before drawing any physical conclusions from the result of a calculation. But "*models are to be used, not believed*"¹.

¹H. Theil - *Principles of Econometrics*

6.1.1 The Hubbard model

Certainly one of the most famous models of correlated electrons is the so-called Hubbard model. It is considered as the most simple model which cannot be reduced to a single electron theory. The Hubbard Hamiltonian, in one-dimension, reads

$$H_H = -t \sum_{j,\sigma} (c_{j,\sigma}^\dagger c_{j+1,\sigma} + c_{j+1,\sigma}^\dagger c_{j,\sigma}) + U \sum_j (n_{j,\uparrow} - 1/2)(n_{j,\downarrow} - 1/2). \quad (6.1.1)$$

The first term of the Hamiltonian is the kinetic part (tight-binding model). The particles can jump from site j to $j + 1$ with a tunnelling amplitude t . This process conserves the spin. The term proportional to U incorporates the short-range part of the Coulomb interaction while avoiding the high complexity of the long-range Coulomb force. The interaction is only on-site, and because of the Pauli principle it is sufficient to consider the local coupling between electrons of opposite spins. U can be positive, in that case we talk about the repulsive Hubbard model, or negative, which corresponds to the attractive Hubbard model. The symmetry of the model is a $U(1)$ group for the charge and $SU(2)$ for the spin sector. However, at half-filling (one electron per site in average), the model possesses a hidden charge $SU(2)$ symmetry. The total symmetry group is in that case $SU(2) \times SU(2) \simeq SO(4)$.

In one dimension, the model is exactly solvable via the Bethe Ansatz [100]. This solution has been extremely useful in understanding the critical properties of Hubbard chains [41]. Unfortunately, in higher dimensions, no such exact solution exists, and one must rely on approximate or numerical schemes. Even though apparently simple, the Hubbard model contains a lot of interesting physics, like the Mott transition and also quantum magnetism effects as we will see right now.

6.1.2 The Heisenberg model

The first non-trivial approximation one can make is to consider the large- U limit of the Hubbard model. By large, we mean large compared to the hopping, $U/t \gg 1$. Let us take $\langle n_i \equiv n_{i,\uparrow} + n_{i,\downarrow} \rangle = 1$, the half-filled band. In that case, the charge degrees of freedom are completely frozen since they are restricted by a huge gap of order U . Nevertheless, a second order process in t is allowed (cf Fig. 6.1 for an intuitive explanation) which effectively amounts to a spin-flip. This is the so-called "super-exchange" mechanism first discussed by Anderson [9] which is the origin of the coupling between the remaining spin degrees of freedom. The effective Hamiltonian for the Hubbard model in the strong- U limit at half-filling is then a pure spin Hamiltonian:

$$H = J \sum_j \left(\mathbf{S}_j \cdot \mathbf{S}_{j+1} - \frac{1}{4} \right), \quad J = \frac{4t^2}{U}. \quad (6.1.2)$$

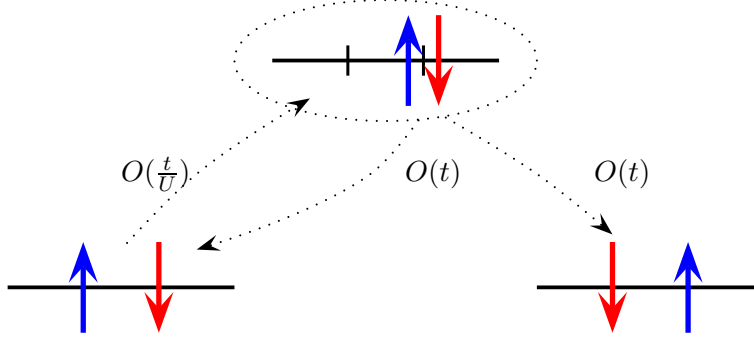


Figure 6.1: The mechanism of "super-exchange". If two neighbouring sites are occupied with electrons having their spins pointing in opposite direction, the first spin (blue) can hop onto the red site, a process of order $O(t/U)$. The virtual state created is unstable since it carries a huge U Hubbard repulsion. The system will prefer to "decay" into a more stable state: either it goes back to the original state (blue on the left, red on the right) or to the reverse configuration (i.e. red on the left, blue on the right). The whole process is equivalent to a spin-flip operation and is of order $O(t^2/U)$

This is the well known Heisenberg model. Note that if $U > 0$ then $J > 0$ such that an anti-ferromagnetic (AF) order will be favourable.

6.1.3 The t - J model

Away from half-filling, i.e. allowing doping on top of the spin model, electrons or holes can acquire a finite amount of kinetic energy. But the spectrum is still clearly split into different Hubbard sectors (characterised by a given number of doubly occupied sites) separated by a large gap U . The low-energy properties are then obtained by discarding the double occupancies. This can be achieved by a canonical transformation (see the book of Auerbach [15] for example), resulting in an effective Hamiltonian of the form:

$$H_{tJ} = -t\mathcal{P} \left(\sum_{j=1}^L \sum_{\sigma} c_{j,\sigma}^{\dagger} c_{j+1,\sigma} + c_{j+1,\sigma}^{\dagger} c_{j,\sigma} \right) \mathcal{P} + J \sum_{j=1}^L (\mathbf{S}_j \cdot \mathbf{S}_{j+1} - \frac{1}{4} n_j n_{j+1} + \frac{1}{2} (n_j + n_{j+1})), \quad (6.1.3)$$

where \mathcal{P} projects onto the lowest Hubbard sector ($\langle n_{\uparrow\downarrow} \rangle = 0$). It is important to notice that the t - J model is equivalent to the Hubbard model only for $J \ll t$. In the inverse limit, $J \gg t$, the model becomes unstable and exhibits a phase separation [113], the system having the tendency to have regions occupied with holes only and others with spins. This is also a very peculiar

signature of the spin-charge separation which is inherent to one-dimensional electronic systems. Despite this phase separation pathology, the model is of interest in its own right and no one prevents us from studying its physics even away from $J \ll t$. In particular, the t - J model seems to be relevant, in its two-dimensional version, for the study of CuO cuprates, an important family of high- T_c superconductors [118].

In the next section of this chapter we will present a general technique for solving a variety of one-dimensional lattice models and even for constructing some new ones. This technique goes under the name of QISM for Quantum Inverse Scattering Method.

6.2 Elements of Quantum Inverse Scattering Method

The coordinate Bethe Ansatz, which was developed historically to diagonalise the Heisenberg magnetic chain and which we have used in the first part of this thesis while dealing with one-dimensional gases, is about finding a clever basis of pseudo-momenta to rewrite the wave-function (Ansatz) easily. In contrast, the combined techniques QISM+ABA are based on a purely algebraic derivation of the Hamiltonian (which is integrable by construction). Both the coordinate and algebraic versions of the Bethe Ansatz are equally successful for finding the spectrum of the Heisenberg model for example. But the QISM and ABA techniques allow to go beyond this and to build new more sophisticated models keeping track of integrability at each step. What we want to emphasize in this chapter is that QISM provides a natural toolbox to build integrable Hamiltonians with many degrees of freedom (e.g. charge and spin), with impurities and/or non-trivial boundary conditions.

6.2.1 The main ideas behind QISM

In the framework of the quantum inverse scattering method, the construction of integrable Hamiltonians is based on vertex models obtained by combining \mathcal{L} -operators (called Lax operators) which satisfy

$$\mathcal{R}^{12}(\lambda - \mu) \overset{1}{\mathcal{L}}(\lambda) \overset{2}{\mathcal{L}}(\mu) = \overset{2}{\mathcal{L}}(\mu) \overset{1}{\mathcal{L}}(\lambda) \mathcal{R}^{12}(\lambda - \mu) \quad (6.2.4)$$

on the tensor product $V_1 \otimes V_2$, where we have defined $\overset{1}{\mathcal{L}} = \mathcal{L} \otimes I$ and $\overset{2}{\mathcal{L}} = I \otimes \mathcal{L}$. Eq. (6.2.4) is known as the intertwining relation. Models which are constructed in this approach are classified by a particular choice of the \mathcal{R} -matrix entering (6.2.4) which in turn has to solve the quantum Yang-Baxter equation (YBE):

$$\mathcal{R}^{12}(\lambda) \mathcal{R}^{13}(\lambda + \mu) \mathcal{R}^{23}(\mu) = \mathcal{R}^{23}(\mu) \mathcal{R}^{13}(\lambda + \mu) \mathcal{R}^{12}(\lambda). \quad (6.2.5)$$

(Superscripts denote the spaces in the tensor product $V_1 \otimes V_2 \otimes V_3$ in which \mathcal{R}^{ij} acts nontrivially). Different representations \mathcal{L} of the quadratic algebra τ_R defined by (6.2.4) for a given \mathcal{R} can be combined to construct integrable lattice models. It is sometimes useful to introduce another operator, $\check{\mathcal{R}}$, which acts directly on the tensor product of Lax matrices as

$$\check{\mathcal{R}}^{12}(\lambda - \mu) (\mathcal{L}(\lambda) \otimes \mathcal{L}(\mu)) = (\mathcal{L}(\mu) \otimes \mathcal{L}(\lambda)) \check{\mathcal{R}}^{12}(\lambda - \mu) . \quad (6.2.6)$$

Essentially $\check{\mathcal{R}}^{ij} = \Pi^{ij} \mathcal{R}^{ij}$, where Π^{ij} is a permutation operator on the space $V_i \otimes V_j$. A standard representation is realised by just choosing $\mathcal{L}_0^n(\lambda) = \mathcal{R}^{0n}(\lambda)$ which acts on the tensor product $V_0 \otimes V_n$. V_n is the quantum space corresponding to the physical sites $n = 1, \dots, L$ of a one-dimensional lattice while V_0 is the so-called "auxiliary space". Taking a product of \mathcal{L} operators in the auxiliary space V_0 , we define the so-called monodromy matrix T to be

$$T(\lambda) = \mathcal{L}_0^L(\lambda) \mathcal{L}_0^{L-1}(\lambda) \dots \mathcal{L}_0^1(\lambda) . \quad (6.2.7)$$

Of great physical interest is the object called the transfer matrix, $t(\lambda)$, which is given by the trace taken in the auxiliary space of the monodromy matrix:

$$t(\lambda) = \text{tr}_0 \left(\mathcal{L}_0^L(\lambda) \mathcal{L}_0^{L-1}(\lambda) \dots \mathcal{L}_0^1(\lambda) \right) . \quad (6.2.8)$$

It is easy to show that $t(\lambda)$ forms a family of commuting operators on the space $V_1 \otimes \dots \otimes V_L$, i.e.

$$[t(\lambda), t(\mu)] = 0 \quad \forall (\lambda, \mu) \in \mathbb{C}^2 \quad (6.2.9)$$

and thus will generate the integrals of motion of the underlying quantum system.

To summarise what are the key ingredients in the construction of an integrable quantum model: Given a solution $\mathcal{R}(\lambda)$ of the Yang-Baxter equation (6.2.5) one can define the quadratic algebra τ_R through Eq. (6.2.4). Given a representation of the algebra τ_R one obtains a quantum integrable system whose quantum space is the representation space of τ_R and the commutative integrals of motion are encoded in $t(\lambda)$. The main problem of QISM is to find their common spectrum and, possibly, correlators of some physically interesting operators. The standard program of QISM as proposed by Sklyanin [124] goes as follows:

1. Take a \mathcal{R} matrix.
2. Take a representation of τ_R .
3. Find the spectrum of $t(\lambda)$.
4. Find the correlators.

Of particular interest are models constructed from the ‘fundamental’ rational \mathcal{R} -matrices $\mathcal{R}^{ij}(\lambda) \propto (\lambda I + i\Pi^{ij})$. The fundamental rational models with nearest-neighbour interaction obtained within this approach are, among others, the spin $S = \frac{1}{2}$ Heisenberg chain and the one-dimensional supersymmetric t - J model with periodic boundary conditions. Since it is really *the* example of the method I cannot resist presenting very briefly how QISM works for the XXX Heisenberg magnetic chain. We will also give a few results regarding the t - J model, that will be used widely in the next chapters of the thesis.

6.2.2 Examples

The inevitable XXX spin chain

So let us recast the problem of interacting spins $S = 1/2$ on a chain. The simplest Hamiltonian one can imagine involves just nearest neighbours interaction between the spins. To simplify even more, let us focus on the case of isotropic interactions, i.e. the coupling is of the same strength in any directions of the spins. The resulting Hamiltonian

$$H = \sum_{n=1}^N \left[\left(\sum_{\alpha=x,y,z} S_n^\alpha S_{n+1}^\alpha \right) - \frac{1}{4} \right] \quad (6.2.10)$$

is the famous Heisenberg model that was derived from the large U limit of the Hubbard model at half-filling (see Sec. 6.1.2). Here we have set $J = 1$ for convenience. In addition, periodic boundary conditions are imposed. Let us now carry on the program of the QISM. We will go briefly through this and we apologise if it looks a bit like a catalogue. I refer to the excellent lecture notes of Faddeev, Sklyanin and the book of Korepin et al. [88] for details.

The \mathcal{L} -operator for this model is related to the rational \mathcal{R} matrix (as described above)

$$\mathcal{L}_0^n(\lambda) = \lambda I_0 \otimes I_n + i \sum_{\alpha} \sigma^\alpha \otimes S_n^\alpha = \begin{pmatrix} \lambda + iS_n^3 & iS_n^- \\ iS_n^+ & \lambda - iS_n^3 \end{pmatrix} \quad (6.2.11)$$

As we can see from Eq. (6.2.11), the structure of the \mathcal{L} -operator is quite clear in this particular example: it is a 2×2 matrix written in auxiliary space whose entries are the physical spin operators acting on site n . Written in this way, the \mathcal{L} -operator reflects the $SU(2)$ symmetry of the model. Introducing the form of the permutation operator P on $\mathbb{C}^2 \otimes \mathbb{C}^2$ (such that $Pa \otimes b = b \otimes a$)

$$P = \frac{1}{2}(I \otimes I + \sum_{\alpha} \sigma^\alpha \otimes \sigma^\alpha) \quad (6.2.12)$$

we can rewrite \mathcal{L} as

$$\mathcal{L}_0^n(\lambda) = (\lambda - \frac{i}{2})I_{0n} + iP_{0n}. \quad (6.2.13)$$

6.2. ELEMENTS OF QUANTUM INVERSE SCATTERING METHOD 79

The explicit \mathcal{R} matrix solution of the YBE is then quite simple²

$$\mathcal{R}_{12} = \lambda I_{12} + iP_{12} \quad (6.2.14)$$

where I_{12} and P_{12} are unity and permutation in $V_1 \otimes V_2$. The monodromy matrix $T(\lambda)$ is a 2×2 matrix given by

$$T(\lambda) = \mathcal{L}_N(\lambda) \cdots \mathcal{L}_2(\lambda) \mathcal{L}_1(\lambda) \equiv \begin{pmatrix} A(\lambda) & B(\lambda) \\ C(\lambda) & D(\lambda) \end{pmatrix}. \quad (6.2.15)$$

As already argued in the previous section, the transfer matrix,

$$t(\lambda) = \text{tr}_0 T(\lambda) = A(\lambda) + D(\lambda), \quad (6.2.16)$$

generates the integrals of motion, among them the Hamiltonian. It is in fact quite straightforward (playing with the properties of the permutation operators) to show that the Hamiltonian is obtained by taking the logarithmic derivative of the transfer matrix at the "special point", $\lambda = i/2$, where \mathcal{L} reduces to the permutation operator up to a factor i . We have,

$$\left. \frac{d \ln t(\lambda)}{d\lambda} \right|_{\lambda=i/2} = -i \sum_n P_{n,n+1} \quad (6.2.17)$$

such that

$$H = \frac{1}{2} \sum_n P_{n,n+1} - \frac{N}{2} = \frac{i}{2} \frac{d}{d\lambda} \ln t(\lambda) \Big|_{\lambda=i/2} - \frac{N}{2}. \quad (6.2.18)$$

The next move is to diagonalise $t(\lambda)$. Within the Algebraic Bethe Ansatz (ABA) the first key-step is to define a proper vacuum $|\Omega\rangle$ (highest weight vector) which is annihilated by the off-diagonal element $C(\lambda)$ of the monodromy matrix $T(\lambda)$. In addition, $|\Omega\rangle$ should be an eigenstate of T 's diagonal elements A and D ,

$$C(\lambda)|\Omega\rangle = 0, \quad (6.2.19)$$

$$A(\lambda)|\Omega\rangle = \alpha(\lambda)|\Omega\rangle, \quad (6.2.20)$$

$$D(\lambda)|\Omega\rangle = \delta(\lambda)|\Omega\rangle. \quad (6.2.21)$$

For the actual case of the XXX model, a "good" vacuum to start with is the ferromagnetic state where all spins are pointing up for example,

$$|\Omega\rangle = \bigotimes_n |\uparrow\rangle_n. \quad (6.2.22)$$

²Mathematically speaking: " \mathcal{R} is the simplest solution of the YBE corresponding to the Yangian $\mathcal{Y}[sl(2)]$ " - Sklyanin

Acting with \mathcal{L}_n on the pseudo-vacuum in the basis $\{| \uparrow \rangle = (1, 0)^\top, | \downarrow \rangle = (0, 1)^\top\}$ reduces to

$$\mathcal{L}_n | \uparrow \rangle_n = \begin{pmatrix} (\lambda + \frac{i}{2}) | \uparrow \rangle_n & \bullet \\ 0 & (\lambda - \frac{i}{2}) | \uparrow \rangle_n \end{pmatrix} \quad (6.2.23)$$

where \bullet is some function whose explicit expression doesn't really matter. Therefore we have $\alpha(\lambda) = (\lambda + \frac{i}{2})^N$ and $\delta(\lambda) = (\lambda - \frac{i}{2})^N$. $B(\lambda)$ acts on the pseudo-vacuum $|\Omega\rangle$ by flipping a spin. Of course, since we are dealing with a quantum chain, this excitation is not local and the flipped spin will propagate along the chain with rapidity λ . This type of excitation is called in the literature a magnon. In this picture, $B(\lambda)$ can be interpreted as the creation operator for the magnons. The idea is then to propose an ansatz for the eigenstates of the transfer matrix $t(u)$ of the form

$$|\lambda_1, \lambda_2, \dots, \lambda_M\rangle = \prod_{k=1}^M B(\lambda_k) |\Omega\rangle \quad (6.2.24)$$

where M will be the number of magnons on top the ferromagnetic vacuum. Making use of the fundamental commutation relations among the operators elements of T , the main result of this approach is that the problem of finding the eigenvalues $\tau(\lambda)$ of $t(\lambda)$,

$$t(\lambda) |\lambda_1, \lambda_2, \dots, \lambda_M\rangle = \tau(\lambda) |\lambda_1, \lambda_2, \dots, \lambda_M\rangle, \quad (6.2.25)$$

is equivalent to solving the following set of BAE

$$\left(\frac{\lambda_j + i/2}{\lambda_j - i/2} \right)^N = \prod_{\substack{k=1 \\ k \neq j}}^M \frac{\lambda_j - \lambda_k + i}{\lambda_j - \lambda_k - i}, \quad j = 1, \dots, M. \quad (6.2.26)$$

The energy of the system is just the sum of single magnons' dispersion,

$$E = \sum_{j=1}^M \epsilon(\lambda_j) = -\frac{1}{2} \sum_{j=1}^M \frac{1}{\lambda_j^2 + 1/4}, \quad (6.2.27)$$

which yields the spectrum of the Heisenberg model. Eq. (6.2.27) calls for a comment: if the spectrum of the XXX magnetic chain is complicated to understand in terms of the original interacting spins, it is easily apprehended in the collective excitation picture of (almost) free magnons. But the price to pay in return is that the Bethe states $B(\lambda_1) \dots B(\lambda_k) |\Omega\rangle$ are complicated objects in terms of the spin variables making the calculation of spin-spin correlation functions, for example, very difficult to handle in that representation. It is nevertheless tractable in some cases [85, 66]. Let us mention also that the thermodynamic quantities of the Heisenberg chain can be computed by an analysis of Eq. (6.2.27) in the $M \rightarrow \infty$ limit where the set of $\{\lambda_j\}_{j=1, \dots, M}$ becomes dense. We will not pursue this route right now but we will use this approach extensively later on when dealing with models with impurities.

The supersymmetric t - J model

After the spin chain we should analyse its charge-doped version which is the t - J model. In one spatial dimension and at the special point $J = 2t$ the model defined by Eq. (6.1.3) becomes supersymmetric (SUSY) and is integrable. For periodic boundary conditions, i.e. $c_{L+1} \equiv c_1$, the SUSY t - J model has been exactly diagonalised both by the coordinate Bethe Ansatz (see e.g. Bares et al. [16]) and by the algebraic Bethe Ansatz (Essler and Korepin [42]). The algebraic approach, we will concentrate on, is very interesting technically speaking because in the construction and solution of the model occur two subtleties: 1) the symmetry algebra underlying the SUSY t - J model is neither the $SU(2) \times SU(2)$ of the Hubbard model nor the simple $SU(2)$ algebra of the spin chain. It is the super-algebra $gl(2|1)$ meaning that grading has to be taken care of (for the tensor product of two such representations) when braiding two operators. The graded-algebra $gl(2|1)$ has a natural representation that contains two fermions and one boson. In the following we shall call this representation $\mathfrak{3}$ or $[1/2]_+$. 2) Since there are two inner degrees of freedom, spin and charge, it requires the nesting technique. A proper description of the Nested Bethe Ansatz (NBA) is beyond the ambition of this chapter, but let me describe how it works with hand-waving arguments. The idea is that we need two levels of parametrization of our Bethe states. One can write an ansatz of the form we made for the spin chain, Eq. (6.2.24). This fixes the spin part. But now, since the t - J Hamiltonian allows for a charge to hop from site to site, the latter ansatz is ambiguous. In order to fix completely all the coefficients of the Bethe states one needs to apply a second Bethe Ansatz. This is why it is called Nested Bethe Ansatz (one Ansatz to fix the coefficients of the other Ansatz). For details concerning the NBA approach to the SUSY t - J model, see Ref. [42].

To construct the SUSY t - J model by means of the QISM we first need to choose an \mathcal{R} (or $\check{\mathcal{R}}$) matrix. Because we will work directly with tensor products of Lax matrices let us consider the matrix

$$\check{\mathcal{R}}_{tJ} = \frac{\lambda}{\lambda + i} \Pi + \frac{i}{\lambda + i} I \quad (6.2.28)$$

with $\Pi_{a_2 b_2}^{a_1 b_1} = (-1)^{\epsilon_{b_1} \epsilon_{b_2}} \delta_{a_1 b_2} \delta_{a_2 b_1}$ being the graded permutation operator acting on $\mathfrak{3} \otimes \mathfrak{3}$. We choose the representation $\mathfrak{3}$ such that it is spanned by the three states $\{\uparrow, \downarrow, 0\}$ with the following grading convention: $\epsilon_\uparrow = \epsilon_\downarrow = 1$ and $\epsilon_0 = 0$. The \mathcal{L} -matrix is simply chosen to be $\mathcal{L}_{tJ} = \Pi \check{\mathcal{R}}_{tJ}$. It fulfils a graded intertwining relation

$$\check{\mathcal{R}}(\lambda - \mu)(\mathcal{L}(\lambda) \otimes \mathcal{L}(\mu)) = (\mathcal{L}(\mu) \otimes \mathcal{L}(\lambda)) \check{\mathcal{R}}(\lambda - \mu), \quad (6.2.29)$$

or, written explicitly in components,

$$\begin{aligned} \check{\mathcal{R}}(\lambda - \mu)_{a_2 c_2}^{a_1 c_1} \mathcal{L}(\lambda)_{\alpha \gamma}^{c_1 b_1} \mathcal{L}(\mu)_{\gamma \beta}^{c_2 b_2} (-1)^{\epsilon_{c_2}(\epsilon_{c_1} + \epsilon_{b_1})} \\ = \mathcal{L}(\mu)_{\alpha \gamma}^{a_1 c_1} \mathcal{L}(\lambda)_{\gamma \beta}^{a_2 c_2} (-1)^{\epsilon_{a_2}(\epsilon_{a_1} + \epsilon_{c_1})} \check{\mathcal{R}}_{c_2 b_2}^{c_1 b_1}(\lambda - \mu). \end{aligned} \quad (6.2.30)$$

Once again, one can construct the monodromy matrix,

$$T(\lambda)_{b\beta_1 \dots \beta_L}^{a\alpha_1 \dots \alpha_L} = \mathcal{L}(\lambda)_{\alpha_L \beta_L}^{a c_L} \mathcal{L}(\lambda)_{\alpha_{L-1} \beta_{L-1}}^{c_L c_{L-1}} \dots \mathcal{L}(\lambda)_{\alpha_1 \beta_1}^{c_2 b} (-1)^{\sum_{j=2}^L (\epsilon_{\alpha_j} + \epsilon_{\beta_j}) \sum_{i=1}^{j-1} \epsilon_{\alpha_i}}, \quad (6.2.31)$$

by simply multiplying a string of \mathcal{L} -matrices together, and from which we compute the transfer matrix:

$$t(\lambda) = \text{str } T(\lambda) \equiv \sum_{a=1}^3 (-1)^{\epsilon_a} T(\lambda)^{aa}. \quad (6.2.32)$$

The symbol **str** denotes a supertrace (the graded generalisation of the trace). The Hamiltonian is given by the logarithmic derivative of the transfer matrix at the 'special point' where \mathcal{L} is essentially the permutation, i.e. $\lambda = 0$ within the notations of Ref. [42]:

$$H_{tJ} = -i \frac{d}{d\lambda} \ln t(\lambda) \Big|_{\lambda=0} - 2N = - \sum_{k=1}^L (\Pi_{k,k+1} - 1) - 2N. \quad (6.2.33)$$

The similarity with the XXX spin chain is very striking when the Hamiltonian is written in terms of the (graded) permutation operator as in Eq. (6.2.33).

The next step of the program is to make the ABA to find the spectrum of $t(\lambda)$. The monodromy operator is this time a 3×3 matrix whose entries are the operators A_{ij} , B_i , C_i and D defined as follows:

$$T = \begin{pmatrix} A_{11} & A_{12} & B_1 \\ A_{21} & A_{22} & B_2 \\ C_1 & C_2 & D \end{pmatrix}. \quad (6.2.34)$$

The first question to ask is: What is a "good" pseudo-vacuum? There are three different choices of grading (1 boson out of three possible states) which implies three possible reference states to start from to build up the spectrum. One example is the so-called Lai vacuum [91], $\bigotimes_j |0\rangle_j$, which is the state with all sites empty. The eigenstates are constructed by application of the C_i operators onto the bosonic Lai vacuum:

$$|\lambda_1, \dots, \lambda_n; F\rangle = C_{a_1}(\lambda_1) \dots C_{a_n}(\lambda_n) |0\rangle F^{a_n \dots a_1}. \quad (6.2.35)$$

The values of the spectral parameters λ_i and the coefficients $F^{a_n \dots a_1}$, which are constructed by means of a nested algebraic Bethe ansatz (NABA), are

determined by requiring the cancellation of the so-called unwanted terms [42]. One obtains the following set of BAE

$$\begin{aligned} \left(\frac{\lambda_j - \frac{i}{2}}{\lambda_j + \frac{i}{2}} \right)^L &= \prod_{\alpha=1}^{N_\downarrow} \frac{\lambda_j - \lambda_\alpha^{(1)} - \frac{i}{2}}{\lambda_j - \lambda_\alpha^{(1)} + \frac{i}{2}}, \quad j = 1, \dots, N_e \\ \prod_{j=1}^{N_e} \frac{\lambda_\alpha^{(1)} - \lambda_j + \frac{i}{2}}{\lambda_\alpha^{(1)} - \lambda_j - \frac{i}{2}} &= - \prod_{\substack{\beta=1 \\ \alpha \neq \beta}}^{N_\downarrow} \frac{\lambda_\alpha^{(1)} - \lambda_\beta^{(1)} + i}{\lambda_\alpha^{(1)} - \lambda_\beta^{(1)} - i}, \quad \alpha = 1, \dots, N_\downarrow \end{aligned} \quad (6.2.36)$$

The energy of a Bethe state of the form (6.2.35) with spectral parameters $\{\lambda_j, j = 1, \dots, N_e\}$, $\{\lambda_\gamma^{(1)}, \gamma = 1, \dots, N_\downarrow\}$ is given by

$$E = \sum_{j=1}^{N_e} \frac{1}{\lambda_j^2 + \frac{1}{4}} - L. \quad (6.2.37)$$

Another ABA solution of the SUSY t - J model can be derived by starting from another pseudo-vacuum. The Sutherland vacuum [127], for instance, is a fermionic reference state with all spins pointing upwards (like in the spin chain case), $\bigotimes_j |\uparrow\rangle_j$. This time the B_i operators will be creating the excitations and, after some algebra, one ends up with a new but completely equivalent set of BAE to solve:

$$\begin{aligned} \left(\frac{\tilde{\lambda}_l + \frac{i}{2}}{\tilde{\lambda}_l - \frac{i}{2}} \right)^L &= \prod_{m=1, m \neq l}^{N_h + N_\downarrow} \frac{\tilde{\lambda}_l - \tilde{\lambda}_m + i}{\tilde{\lambda}_l - \tilde{\lambda}_m - i} \prod_{j=1}^{N_h} \frac{\tilde{\lambda}_l - \tilde{\lambda}_j^{(1)} - \frac{i}{2}}{\tilde{\lambda}_l - \tilde{\lambda}_j^{(1)} + \frac{i}{2}}, \quad l = 1, \dots, N_h + N_\downarrow \\ 1 &= \prod_{j=1}^{N_h + N_\downarrow} \frac{\tilde{\lambda}_j - \tilde{\lambda}_k^{(1)} - \frac{i}{2}}{\tilde{\lambda}_j - \tilde{\lambda}_k^{(1)} + \frac{i}{2}}, \quad k = 1, \dots, N_h. \end{aligned} \quad (6.2.38)$$

The energy computed in this Bethe basis is expressed by the following formula:

$$E = L - \sum_{j=1}^{N_h + N_\downarrow} \frac{1}{\tilde{\lambda}_j^2 + 1/4}. \quad (6.2.39)$$

The equivalence between the Lai and the Sutherland solutions relies on a particle-hole symmetry at the level of the BAE. We provide an explicit proof of this equivalence in App. E for the case of open boundary conditions.

This closes our quick overview of the algebraic Bethe ansatz. The examples we have used are the most simples ones: they are homogeneous systems with periodic boundary conditions. But even though the condition for integrability (YBE) may seem rather restrictive, QISM allows for some freedom. In particular, impurities and non-trivial boundary conditions can be added to the system without spoiling integrability. And for the aim of studying impurity problems, which is the focus of this part, having at hand integrable models is extremely useful.

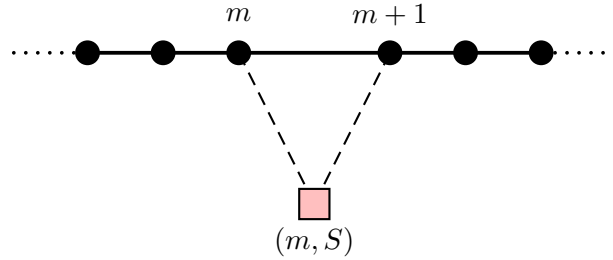


Figure 6.2: An isolated impurity (pink square) interacting with the Heisenberg chain (black) in the model proposed in Ref. [13]

6.2.3 Integrable impurities

Integrable inhomogeneities can be inserted into the system by replacing the \mathcal{L} -operator at one site of the lattice by a different solution \mathcal{L}_{imp} of the intertwining relation acting on $V_0 \otimes V_{\text{imp}}$ (see e.g. Refs. [13, 18, 19, 122]). In \mathcal{L}_{imp} the internal quantum degrees of freedom of the inhomogeneity are controlled by the choice of a specific representation of the underlying algebra, acting on the quantum space V_{imp} which may be different from the one used for the other (bulk) sites (i.e. $SU(2)$ for the Heisenberg chain, $gl(2|1)$ for the supersymmetric t - J model). In addition the coupling of the inhomogeneity site to the rest of the lattice can be varied by a shift of the argument, i.e. $\mathcal{L}_{\text{imp}}(\lambda) \rightarrow \mathcal{L}_{\text{imp}}(\lambda + t)$ which is consistent with relation (6.2.4). This construction has already been applied in the literature to our two favourite models: the XXX spin chain and the SUSY t - J model.

$SU(2)$

To our knowledge, the first successful attempt to construct an integrable spin chain with an impurity goes back to the paper of Andrei and Johannesson [13]. In this work, the authors are interested in a usual Heisenberg spin chain allowed to interact with an isolated spin- S impurity located at e.g. site m (see Fig. 6.2). The transfer matrix of the system is obtained in the standard way, by writing

$$t(\lambda) = \text{tr}_0 \mathcal{L}_0^{N,1/2}(\lambda) \cdots \mathcal{L}_0^{m+1,1/2}(\lambda) \mathcal{L}_0^{m,S}(\lambda) \mathcal{L}_0^{m,1/2}(\lambda) \cdots \mathcal{L}_0^{1,1/2}(\lambda) \quad (6.2.40)$$

with the following choice of Lax matrix:

$$\mathcal{L}_0^{(m,S)} = \frac{i\lambda + \frac{1}{2} + \boldsymbol{\sigma}_0 \otimes \mathbf{S}_m}{i\lambda + S + \frac{1}{2}}. \quad (6.2.41)$$

For $S = 1/2$, we recognise the \mathcal{L} -operator of the XXX spin chain (up to a trivial rescaling of the spectral parameter λ). For spin $S > 1/2$, the auxiliary

space V_0 is the 2-dimensional space of spin 1/2 while the operators acting on the physical space V_j belong to a $(2S+1)$ -dimensional representation of $SU(2)$. Within the geometry drawn in Fig. 6.2, Andrei and Johannesson derived from Eq. (6.2.40) the form of the bulk-impurity interaction:

$$H_{\text{int}} = \frac{4J}{(2S+1)^2} [\boldsymbol{\sigma}_m \cdot \mathbf{S} + \boldsymbol{\sigma}_{m+1} \cdot \mathbf{S} + \frac{1}{2} \{\boldsymbol{\sigma}_m \cdot \mathbf{S}, \boldsymbol{\sigma}_{m+1} \cdot \mathbf{S}\} - S(S+1) \boldsymbol{\sigma}_m \cdot \boldsymbol{\sigma}_{m+1}], \quad (6.2.42)$$

where $\{\cdot, \cdot\}$ denotes an anti-commutator. We see that this Hamiltonian is not as simple as one could have guessed. Despite the fact that it has some expected Heisenberg terms (just scalar products among the spins), it contains also some 4-spin interactions. This is, in general, the price to pay when we demand integrability.

$g(2|1)$

Following the work of Andrei and Johannesson, numerous generalisations have been accomplished, in particular some extensions to more complicated algebras like $gl(2|1)$ for instance. Let me mention two particular examples that we will encounter in the following chapters.

The first type of inhomogeneity in the t - J model I want to consider is an impurity of Hubbard type. Remember that the bulk sites of the usual SUSY t - J model "live" on a 3-dimensional representation of $gl(2|1)$ spanned by $\{\uparrow, \downarrow, 0\}$. A Hubbard impurity will be an isolated site in the chain where double occupancy is allowed. The quantum space of the impurity will be the 4-dimensional Hilbert space with local basis $\{\uparrow\downarrow, \uparrow, \downarrow, 0\}$, which is the basis of the Hubbard model. Fortunately, the representation theory of the superalgebra $gl(2|1)$ ([120, 105] and App. A) provides us with the so-called *typical* 4-dimensional representation $[b, \frac{1}{2}]$, with $\alpha \equiv b - \frac{1}{2} > 0$. Thus, we should be able to compute a transfer matrix of a lattice model taking a \mathcal{L} -operator based on $[b, \frac{1}{2}]$ to be attached to the impurity vertex. The corresponding solution of the intertwining relation (6.2.4) has been considered before [18, 19, 20]. Written as a matrix in auxiliary space, the \mathcal{L} -operator of the impurity reads:

$$\mathcal{L}_{\text{imp}}(\lambda) = \frac{\lambda - i(\frac{\alpha}{2} + 1)}{\lambda + i(\frac{\alpha}{2} + 1)} I + \frac{i}{\lambda + i(\frac{\alpha}{2} + 1)} \begin{pmatrix} 1 - n_{\uparrow} & -S^- & Q_{\uparrow} \\ -S^+ & 1 - n_{\downarrow} & Q_{\downarrow} \\ Q_{\uparrow}^{\dagger} & Q_{\downarrow}^{\dagger} & \alpha + 2 - n \end{pmatrix}. \quad (6.2.43)$$

Here $n = \sum_{\sigma=\uparrow, \downarrow} n_{\sigma} = \sum_{\sigma} c_{\sigma}^{\dagger} c_{\sigma}$ and $\vec{S} = \frac{1}{2} \sum_{\alpha\beta} c_{\alpha}^{\dagger} \vec{\sigma}_{\alpha\beta} c_{\beta}$ are the electron number and spin operators on the impurity site expressed in terms of canonical fermionic creation and annihilation operators. The Q_{σ} are the fermionic generators of $gl(2|1)$ in this representation which can be expressed in terms of projection operators (the so called 'Hubbard Operators') $\mathbf{X}^{ab} = |a\rangle\langle b|$ with $a, b = \uparrow, \downarrow, \uparrow\downarrow, 0$:

$$Q_{\sigma} = \sqrt{\alpha + 1} \mathbf{X}^{0\sigma} - 2\sigma \sqrt{\alpha} \mathbf{X}^{-\sigma 2} \quad (6.2.44)$$

with $\sigma = \pm\frac{1}{2}$ corresponding to $\sigma = \uparrow, \downarrow$.

The second type of inhomogeneity we want to evoke is the case of a Kondo-type impurity. The \mathcal{L} -operator of the impurity vertex is, in that case, based on a so-called *atypical* representation, $[s]_+$, of $gl(2|1)$ (see Refs. [120, 105] and App. A). This particular representation has already been used in constructing an integrable model of a doped spin- S Heisenberg chain [54, 48, 56]. In terms of the generators of $gl(2|1)$ the impurity \mathcal{L} -operator is given by [90]

$$\mathcal{L}_{\text{imp}}(\lambda) \equiv \mathcal{L}_s(\lambda) = \frac{\lambda - i(s + 1/2)}{\lambda + i(s + 1/2)} I + \frac{i}{\lambda + i(s + 1/2)} C_2^{(0s)}. \quad (6.2.45)$$

Here $C_2^{(0s)}$ is the quadratic Casimir operator (A.2.9) of $gl(2|1)$ on the tensor product $V_0 \otimes V_{\text{imp}}$ (the auxiliary space V_0 carries the three-dimensional fundamental representation $[1/2]_+$ of $gl(2|1)$).

6.2.4 Open boundary conditions

The last topic we would like to discuss briefly is the construction of open chains, eventually with boundary fields acting at the edge. Boundary conditions different from periodic (or twisted) ones can be treated within the QISM by extending the algebra defined by the intertwining relations through so-called reflection equations (RE) [31, 123]. The RE define two algebras \mathcal{T}_{\pm} whose representations allow for a classification of integrable boundary conditions. \mathcal{T}_+ and \mathcal{T}_- are related by an algebra automorphism, for \mathcal{T}_- the RE reads:

$$\mathcal{R}^{12}(\lambda - \mu) \overset{1}{\mathcal{T}}_-(\lambda) \mathcal{R}^{21}(\lambda + \mu) \overset{2}{\mathcal{T}}_-(\mu) = \overset{2}{\mathcal{T}}_-(\mu) \mathcal{R}^{12}(\lambda + \mu) \overset{1}{\mathcal{T}}_-(\lambda) \mathcal{R}^{21}(\lambda - \mu), \quad (6.2.46)$$

where \mathcal{R}^{12} is again a solution of the YBE (6.2.5) on the tensor product $V_1 \otimes V_2$ and $\overset{1}{\mathcal{T}}_- = \mathcal{T} \otimes I$, $\overset{2}{\mathcal{T}}_- = I \otimes \mathcal{T}$. The representations of \mathcal{T}_{\pm} determine the boundary terms in the Hamiltonian at the left (right) end of the chain.

Given these solutions to (6.2.4) and (6.2.46), the commuting integrals of motion of the system can be obtained from the transfer matrix

$$\begin{aligned} \tau_L(\lambda) = \text{tr}_0 \left(K_+(\lambda) \mathcal{L}_0^L(\lambda) \mathcal{L}_0^{L-1}(\lambda) \dots \mathcal{L}_0^1(\lambda) \times \right. \\ \left. \times K_-(\lambda) (\mathcal{L}_0^1(-\lambda))^{-1} (\mathcal{L}_0^2(-\lambda))^{-1} \dots (\mathcal{L}_0^L(-\lambda))^{-1} \right), \end{aligned} \quad (6.2.47)$$

where the matrix $K_+(\lambda)$ (resp. $K_-(\lambda)$) is an explicit realisation of the algebra \mathcal{T}_+ (resp. \mathcal{T}_-). In particular, the Hamiltonian is obtained by taking the derivative of τ_L at the ‘shift point’ $\lambda = 0$,

$$H = \sum_{n=1}^{N-1} h_{n,n+1} + \frac{1}{2} K'_-(0) + \frac{\text{tr}_0 [K_+^{\text{T}}(0) h_{N0}]}{\text{tr}_0 [K_+(0)]}, \quad (6.2.48)$$

with $\text{tr}_0 K_+(0) \neq 0$.

XXX spin chain

Let us start with the example of the XXX chain. For the spin chain, even with anisotropy, the classification of the K matrices solving Sklyanin's RE has been obtained by de Vega and González-Ruiz [36]. Here, let us just quote the result derived for the isotropic XXX magnetic chain. Taking the most general 2×2 boundary matrix,

$$K_{\pm}(\lambda) = \begin{pmatrix} \beta_{\pm}(\xi_{\pm} + \lambda) & \mu_{\pm}\lambda \\ \theta_{\pm}\lambda & \beta_{\pm}(\xi_{\pm} - \lambda) \end{pmatrix}, \quad (6.2.49)$$

and using the fundamental rational R matrix, the formula (6.2.48) leads to

$$H = \sum_{n=1}^{N-1} (\sigma_n^x \sigma_{n+1}^x + \sigma_n^y \sigma_{n+1}^y + \sigma_n^z \sigma_{n+1}^z) + b_- \sigma_1^z - b_+ \sigma_N^z + c_- \sigma_1^- - c_+ \sigma_N^- + d_- \sigma_1^+ - d_+ \sigma_N^+. \quad (6.2.50)$$

Here we recognise the bulk part of the Hamiltonian, the traditional XXX Hamiltonian, but with the sum running up to $N-1$, indicating open boundary conditions. The other terms are the most general boundary terms compatible with integrability of the open XXX chain. The "boundary fields" are expressed in terms of the parameters of the K -matrices as follows

$$b_{\pm} = \frac{1}{\xi_{\pm}} \quad (6.2.51)$$

$$c_{\pm} = \frac{\theta_{\pm}}{\beta_{\pm}\xi_{\pm}} \quad (6.2.52)$$

$$d_{\pm} = \frac{\mu_{\pm}}{\beta_{\pm}\xi_{\pm}} \quad (6.2.53)$$

where β_{\pm} and ξ_{\pm} are non-zero.

SUSY t - J model

In Ref. [70] González-Ruiz gave the K -matrices for the so-called trigonometric t - J . Here let us just quote a representation of the diagonal K -matrices at the rational point (SUSY point) that we will use in the following chapters:

$$K_-^p = \begin{pmatrix} 1 & 0 & 0 \\ 0 & 1 & 0 \\ 0 & 0 & -\frac{p\lambda+i}{p\lambda-i} \end{pmatrix}, \quad K_-^h = \begin{pmatrix} -\frac{h\lambda+i}{h\lambda-i} & 0 & 0 \\ 0 & 1 & 0 \\ 0 & 0 & 1 \end{pmatrix}. \quad (6.2.54)$$

They correspond respectively to a boundary chemical potential p and a boundary magnetic field h (in combination with a chemical potential) [39]. The

induced Hamiltonian is again the sum of a bulk part and a boundary part,

$$\begin{aligned}
 H_{tJ} = & -\mathcal{P}\left(\sum_{j=1}^{L-1} \sum_{\sigma} c_{j,\sigma}^{\dagger} c_{j+1,\sigma} + c_{j+1,\sigma}^{\dagger} c_{j,\sigma}\right)\mathcal{P} \\
 & + 2 \sum_{j=1}^L \left(\mathbf{S}_j \cdot \mathbf{S}_{j+1} - \frac{1}{4}n_j n_{j+1} + \frac{1}{2}(n_j + n_{j+1})\right) + H_{\alpha\beta}, \quad (6.2.55)
 \end{aligned}$$

where four possible choices of boundary Hamiltonians $H_{\alpha\beta}$ are compatible with integrability, the conservation of total spin in the z -direction and the particle number. Those four possible boundary terms are given by:

$$H_{aa} = p_1 n_1 + p_L n_L, \quad (6.2.56)$$

$$H_{ba} = p_1 n_1 + h_L \left(S_L^z - \frac{n_L^h}{2}\right), \quad (6.2.57)$$

$$H_{ab} = h_1 \left(S_1^z - \frac{n_1^h}{2}\right) + p_L n_L, \quad (6.2.58)$$

$$H_{bb} = h_1 \left(S_1^z - \frac{n_1^h}{2}\right) + h_L \left(S_L^z - \frac{n_L^h}{2}\right). \quad (6.2.59)$$

We have sketched how QISM works for constructing genuine models of correlated electrons, involving impurities, boundary fields, etc. Our main task, in the rest of this thesis, will be to study two particular examples of impurity problems within the SUSY t - J model.

Chapter 7

Anderson impurity in the SUSY t - J model

In Chap. 5, we caught a glimpse of how rich the physics of quantum impurity problems can be. Since those phenomena are non-perturbative, we argued that sophisticated tools such as exactly solvable model systems and powerful field theoretical methods are needed to gain insights into the properties of such systems (see e.g. Refs. [129, 12, 7, 64]). The recent advances in nanofabrication have led to new realizations of quantum impurities and Kondo physics has been observed, e.g., as Fano resonances in spectra from scanning tunneling microscopy of magnetic atoms on metallic surfaces or as zero-bias peak in the conductance of quantum dots occupied with an odd number of electrons [97, 103, 69]. The control over the parameters describing the impurity in these new devices such as their internal spectrum, the coupling to the many-body environment and the spectral properties, in particular the local density of states, of the latter poses new questions to be answered from theoretical investigations. For such studies specific models for a quantum impurity are needed which allow to cover the full range of experimentally available parameters on one hand and at the same time to make contact to the universal low-energy behaviour identified by the theoretical methods mentioned above. These requirements can be met by an approach based on integrable lattice models. In this chapter, we propose to study such a particular model describing an Anderson-like impurity embedded into a t - J chain.

7.1 Presentation of the model

There are at least two ways of dealing with impurities: one possibility is to alter the couplings precisely at the bonds where the impurity sits. Another possibility is to have the local Hilbert space of the impurity differing from the one in the bulk. We shall adopt, in the following, both points of view, and use the formalism of QISM, introduced in Chap. 6, to construct an in-

tegrable model of an impurity coupled to a chain of interacting electrons. To be specific, we consider a SUSY t - J model (which is based on the fundamental 3-dimensional representation of $gl(2|1)$) with one vertex replaced by an \mathcal{L} operator acting on a 4-dimensional quantum space. This preserves the supersymmetry of the model but at the same time lifts the restriction of no double occupancy present in the t - J model at the impurity site. The \mathcal{L} -operator of the impurity vertex is based on the *typical* representation $[b, \frac{1}{2}]$ of $gl(2|1)$ (see chapter 6). The first model derived from this construction was obtained by Bedürftig, Essler and Frahm in Refs. [18, 19] who investigated the situation in which the impurity is located in the middle of an usual, periodic, t - J chain. Their Hamiltonian is the sum of a standard t - J chain plus a term taking the coupling bulk-impurity into account. The latter local Hamiltonian depends essentially on one free (continuous) parameter, $\alpha \equiv b - \frac{1}{2} > 0$, associated with the 4-dimensional representation of the super-algebra, which controls the internal spectrum of the impurity. This makes the present model particularly interesting and relevant for the study of rather general situations since the impurity introduced here couples to both spin and charge degrees of freedom of the bulk Luttinger liquid.

7.1.1 The need for open boundaries

One of the only drawback of the model just cited, is the complete absence of backscattering at the inhomogeneity. And this is in fact a quite non-generic consequence of the embedding of a quantum impurity into an integrable lattice model. This pathology is somehow restricting because the renormalisation group studies [94, 59, 80] of the problem reveal that a backscattering potential acts as a relevant perturbation in the correlated host, driving the system to a fixed point which effectively breaks the chain at the site of the potential scatterer. Indeed, for a quantum impurity with internal degrees of freedom, studies based on bosonization and boundary conformal field theory imply that both forward and back scattering amplitudes have to be considered [57, 37]. This implies that in such a system, the properties of this fixed point have to be studied in lattice models subject to open boundary conditions. This can be achieved, within the integrable model, by combining the inhomogeneity, \mathcal{L}_{imp} , with a boundary matrix, K_{\pm} , satisfying the reflection equation (6.2.46) [20]. Furthermore, we will introduce a shift, t , of the spectral parameter at the impurity site, i.e. $\mathcal{L}_{\text{imp}}(\lambda + t)$, directly entering the coupling between the impurity and the host chain.

7.1.2 Derivation of the Hamiltonian

The situation we want to consider is depicted in Fig. 7.1 where we have placed the impurity vertex (6.2.43) at the boundary site 1. Thus, the expression

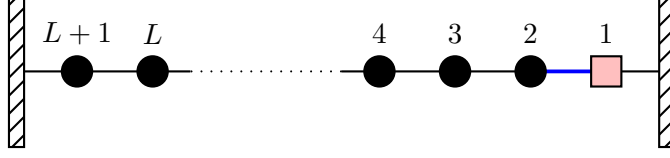


Figure 7.1: Diagram of the open t - J with an impurity (pink square) located at the boundary (site 1). Sites 2 to $L + 1$ are usual t - J sites (black circles). The boundaries (dashed zones) are chosen here to be perfectly reflecting.

$$\begin{aligned} \mathcal{T}_-(\lambda) &= \mathcal{L}_{L+1}(\lambda) \cdots \mathcal{L}_2(\lambda) \mathcal{L}_{\text{imp}}(\lambda + t) \\ &K_-(\lambda) (\mathcal{L}_{\text{imp}}(-\lambda + t))^{-1} (\mathcal{L}_2(-\lambda))^{-1} \cdots (\mathcal{L}_{L+1}(\lambda))^{-1} \end{aligned} \quad (7.1.1)$$

defines the integrable model with $L + 1$ sites through the transfer matrix

$$\tau(\lambda) = \text{str}_0 [K_+(\lambda) \mathcal{T}_-(\lambda)] . \quad (7.1.2)$$

$\text{str}_0(M) = \sum_a (-1)^{[a]} M_{aa}$ is the (graded) supertrace taken in auxiliary space. In this chapter we will focus on a chain with reflecting ends¹, i.e. $K_{\pm} \equiv \mathbb{1}$. Taking the derivative of the transfer matrix with respect to the spectral parameter,

$$\mathcal{H} \propto i \frac{\partial}{\partial \lambda} \tau(\lambda) \Big|_{\lambda=0} , \quad (7.1.3)$$

leads to the following Hamiltonian of the quantum chain,

$$\begin{aligned} \mathcal{H} &= -\mathcal{P} \left(\sum_{j=2}^L \sum_{\sigma} c_{j,\sigma}^{\dagger} c_{j+1,\sigma} + c_{j+1,\sigma}^{\dagger} c_{j,\sigma} \right) \mathcal{P} \\ &+ 2 \sum_{j=2}^L \left[\vec{S}_j \vec{S}_{j+1} - \frac{n_j n_{j+1}}{4} + \frac{1}{2} (n_j + n_{j+1}) \right] \\ &- HS^z - \mu N + \mathcal{H}_b , \end{aligned} \quad (7.1.4)$$

written in the grand-canonical ensemble. The bulk of the system is the supersymmetric t - J model: \mathcal{P} projects out double occupancies on sites $j = 2$ to $L + 1$ and \vec{S}_j and n_j are the electronic spin and number operators on site j .

¹A generalization describing, for the $gl(2|1)$ -symmetric t - J model, a boundary potential or boundary magnetic field is straightforward [39, 20] and will under consideration in chapter 8.

The external magnetic field H and chemical potential μ control magnetization and hole concentration $\delta = 1 - \sum_j n_j/L$ of the system.

The internal spectrum of the impurity at site 1 and its coupling to the bulk is determined by the boundary term [20] in (7.1.4)

$$\mathcal{H}_b = V_0 \left[\alpha n_2 + 2\vec{S}_1 \vec{S}_2 - \frac{n_1 n_2}{2} + n_1 + n_2 - \sum_{\sigma} (Q_{2,\sigma}^{\dagger} Q_{1,\sigma} + Q_{1,\sigma}^{\dagger} Q_{2,\sigma}) \right], \quad (7.1.5)$$

where

$$Q_{2,\sigma} = |0\rangle\langle\sigma|_2 \quad \text{and} \quad Q_{1,\sigma} = \sqrt{\alpha+1}|0\rangle\langle\sigma|_1 - 2\sigma\sqrt{\alpha}|\bar{\sigma}\rangle\langle 2|_1 \quad (7.1.6)$$

are generalised electron annihilation operators for the sites 1 and 2. The parameter α labels the four-dimensional representation of $gl(2|1)$ used in the construction of (7.1.5) and controls the internal spectrum of the impurity. The terms in (7.1.5) describe exchange and Coulomb interaction between the electrons on site 1 and those in the chain as well as a term allowing for the hopping of electrons between the bulk and the impurity. Comparing this model with that of the single-impurity Anderson model, $V_0 \equiv \frac{4}{4t^2 + (\alpha+2)^2}$ can be identified with an hybridization coupling. Since we consider an open chain, the parameter t can be either real positive or purely imaginary, thereby allowing to cover the entire range $-\infty < V_0 < \infty$ for this coupling between the bulk and the impurity site.

7.2 The Bethe Ansatz solution

The t - J model with a boundary impurity as given by Eqs. (7.1.4), (7.1.5) is solvable by means of the algebraic Bethe Ansatz. The pseudo-vacuum $|\Omega\rangle \equiv |\uparrow\uparrow \cdots \uparrow\rangle_{\text{bulk}} \otimes |\uparrow\downarrow\rangle_{\text{imp}}$ with maximal number of electrons and complete polarization of the bulk is a trivial eigenstate of the Hamiltonian. The $gl(2|1)$ highest weight eigenstates of (7.1.4) with $N_e = N_{\uparrow} + N_{\downarrow}$ electrons can be parametrized by $M_s = L + 1 - N_{\uparrow}$ roots λ_j and $M_c = L + 2 - N_e$ roots ϑ_{γ} of the Bethe Ansatz equations (BAE)

$$e_1^{2L}(\lambda_j)\Phi_s(\lambda_j) = \prod_{k \neq j}^{M_s} e_2(\lambda_j - \lambda_k)e_2(\lambda_j + \lambda_k) \times \prod_{\beta=1}^{M_c} e_{-1}(\lambda_j - \vartheta_{\beta})e_{-1}(\lambda_j + \vartheta_{\beta}), \quad j = 1, \dots, M_s, \quad (7.2.7)$$

$$\Phi_c(\vartheta_{\gamma}) = \prod_{k=1}^{M_s} e_{-1}(\vartheta_{\gamma} - \lambda_k)e_{-1}(\vartheta_{\gamma} + \lambda_k), \quad \gamma = 1, \dots, M_c,$$

with

$$\Phi_s(\lambda) \equiv 1, \quad \Phi_c(\vartheta) = e_{\alpha}(\vartheta + t)e_{\alpha}(\vartheta - t). \quad (7.2.8)$$

The spin (charge) rapidities λ_j (ϑ_γ) describe overturned spins (holes) added to $|\Omega\rangle$ and Φ_{cs} , depending on the parameters α and t , are the phase shifts due to the presence of the impurity in the system. The corresponding energy of the Bethe state is then given by the expression

$$E = V_0(\alpha+2) + 2(L-1) - \sum_{j=1}^{M_s} \frac{1}{\lambda_j^2 + \frac{1}{4}} + \left(\mu - \frac{H}{2} \right) M_c + H M_s - \mu(L+2) - \frac{H}{2} L. \quad (7.2.9)$$

7.2.1 Bound states formation

To begin, we should identify which root configurations solving the BAE (7.2.7) correspond to the ground state and to the low lying excitations of the system.² From the solution of the t - J model with periodic and reflecting open boundaries but without an impurity the ground state is known to be described by real spin and charge rapidities [121, 39]. This remains valid in the present case for impurities described by real t . As discussed in the previous section the combination of the impurity with open boundary conditions allows to choose purely imaginary $t = i\tau \in i\mathbb{R}^+$ and thereby extending the range covered by the hybridization V_0 . In the Bethe equations (7.2.7) this amounts to choosing

$$\Phi_c(\vartheta) = e_{\alpha+2\tau}(\vartheta_\gamma) e_{\alpha-2\tau}(\vartheta_\gamma). \quad (7.2.10)$$

In the Hamiltonian (7.1.5), choosing t imaginary corresponds to the regime of strong or negative hybridization V_0 . As a consequence one expects that it becomes energetically favourable for a hole to be bound to the impurity. On the level of the BAE with (7.2.10) the mechanism for bound state formation is similar to that discussed for the t - J model in the presence of boundary fields [40], where imaginary roots become stable solutions of the BAE. Let us illustrate how it works: Consider the second BAE (7.2.7) which involves explicitly the impurity phase shift $\Phi_c(\theta)$ now defined by (7.2.10). Suppose we have such a bound state solution (i.e. imaginary root) in the holon sector. Without loss of generality we can take this solution to be $\vartheta_{\gamma_0} \in i\mathbb{R}^+$. The right-hand side of the second BAE (7.2.7) now becomes

$$\prod_{k=1}^{M_s} \frac{i\text{Im } \vartheta_{\gamma_0} - \lambda_k - i/2}{i\text{Im } \vartheta_{\gamma_0} - \lambda_k + i/2} \frac{i\text{Im } \vartheta_{\gamma_0} + \lambda_k - i/2}{i\text{Im } \vartheta_{\gamma_0} + \lambda_k + i/2} = \prod_{k=1}^{M_s} \frac{\lambda_k^2 + (\text{Im } \vartheta_{\gamma_0} - 1/2)^2}{\lambda_k^2 + (\text{Im } \vartheta_{\gamma_0} + 1/2)^2} \rightarrow 0 \quad \text{as } M_s \rightarrow \infty. \quad (7.2.11)$$

thus vanishing in the thermodynamic limit. Therefore, the left-hand side of the second BAE (7.2.7) must also vanish which, in our case, is satisfied for $\tilde{\vartheta} = i(\tau - \alpha/2)$. Since the BAE (7.2.7) are coupled, the emergence of a

²We restrict ourselves to $T = 0$ to avoid the subtleties in dealing with open boundaries at finite temperatures [65].

bound state in the holon sector can induce a similar imaginary solution in the spinon sector. In fact, one can convince oneself that tuning τ across the thresholds $\tau_k = (\alpha + k)/2$, $k = 0, 1, 2$ will generate a sequence of poles (or zeroes) in the scattering phase shifts ($\vartheta_{\gamma_0} = i(\tau - \tau_0)$, $\lambda_{j_0} = i(\tau - \tau_1)$ and $\vartheta_{\gamma_1} = i(\tau - \tau_2)$ with exponential accuracy in the system size L) corresponding to bound states in the Bethe state configuration. A similar mechanism for the creation of bound states has been found to exist in integrable impurity problems (see e.g. [133, 67]), although it has not been studied systematically so far.

Explicitly taking into account those imaginary roots and rearranging the equations we end up with three different sets of BAE depending on the occupancy of the bound states:

Root configuration (I), $\tau > \tau_0$: $\vartheta_{\gamma_0} = i(\tau - \tau_0)$

$$\begin{aligned}\Phi_s(\lambda) &= e_{2\tau+1-\alpha}(\lambda)e_{1+\alpha-2\tau}(\lambda) \\ \Phi_c(\vartheta) &= e_{\alpha+2\tau}(\vartheta)e_{\alpha-2\tau}(\vartheta)\end{aligned}\tag{7.2.12}$$

The imaginary root ϑ_{γ_0} determines the impurity phase shifts Φ_{cs} . Therefore, in the products over the two-particle scattering phases on the right hand side of (7.2.7) only the remaining real rapidities enter, i.e. λ_j with $j = 1, \dots, M_s$ and ϑ_γ with $\gamma = 1, \dots, M_c - 1$.

Root configuration (II), $\tau > \tau_1$: ϑ_{γ_0} and $\lambda_{j_0} = i(\tau - \tau_1)$

$$\begin{aligned}\Phi_s(\lambda) &= e_{2\tau-\alpha-3}(\lambda)e_{1+\alpha-2\tau}(\lambda) \\ \Phi_c(\vartheta) &= e_{\alpha+2\tau}(\vartheta)e_{2+\alpha-2\tau}(\vartheta)\end{aligned}\tag{7.2.13}$$

In addition to ϑ_{γ_0} defined previously, the imaginary spin rapidity $\lambda_{j_0} = i(\tau - \tau_1)$ is also solution of the BAE. The real rapidities are now parametrized by λ_j with $j = 1, \dots, M_s - 1$ and ϑ_γ with $\gamma = 1, \dots, M_c - 1$. In Eq. (7.2.9), λ_{j_0} will give the following contribution to the energy: $E_{M_s} = [(\tau - \alpha/2)(1 - \tau + \alpha/2)]^{-1}$, that should be interpreted as the energy of the spinon bound state.

Root configuration (III), $\tau > \tau_2$: ϑ_{γ_0} , λ_{j_0} and $\vartheta_{\gamma_1} = i(\tau - \tau_2)$

$$\begin{aligned}\Phi_s(\lambda) &\equiv 1 \\ \Phi_c(\vartheta) &= e_{\alpha+2\tau}(\vartheta)e_{2+\alpha-2\tau}(\vartheta)\end{aligned}\tag{7.2.14}$$

The root configuration (III) is characterized by the emergence of a third imaginary solution of the BAE in the charge sector, $\vartheta_{\gamma_1} = i(\tau - \tau_2)$. The real rapidities are thus labeled λ_j with $j = 1, \dots, M_s - 1$ and ϑ_γ with $\gamma = 1, \dots, M_c - 2$.

N. B.: Increasing τ beyond $\alpha/2+1$ does not lead to additional bound states as expected for an impurity with a single orbital allowing for occupation of at most two charges. Therefore, we conclude that the maximum number of bound states allowed to develop themselves upon variation of the hybridization at the boundary impurity site is three - two holons and one spinon.

7.2.2 Continuum limit - Equations for the densities

The analysis of the BAE is simplified by doubling of the real roots of the BAE with positive and negative ones identified, i.e. $\lambda_{-j} = -\lambda_j$ and $\vartheta_{-\gamma} = -\vartheta_\gamma$. Doing so, we can show that, in the thermodynamic limit, the real roots $\{\lambda_j\}$ ($\{\vartheta_\gamma\}$) form continuous distributions which are conveniently described in terms of their densities $\rho_s(\lambda)$ ($\rho_c(\vartheta)$):

$$\begin{pmatrix} \rho_s(\lambda) \\ \rho_c(\vartheta) \end{pmatrix} = \begin{pmatrix} 2a_1(\lambda) \\ 0 \end{pmatrix} + \frac{1}{L} \begin{pmatrix} \hat{\rho}_s^{(R)}(\lambda) + \hat{\rho}_s^{(b)}(\lambda) \\ \hat{\rho}_c^{(R)}(\vartheta) + \hat{\rho}_c^{(b)}(\vartheta) \end{pmatrix} + \begin{pmatrix} -\int_{-A}^A a_2 & \int_{-B}^B a_1 \\ \int_{-A}^A a_1 & 0 \end{pmatrix} * \begin{pmatrix} \rho_s(\lambda) \\ \rho_c(\vartheta) \end{pmatrix}. \quad (7.2.15)$$

The detailed derivation of Eq. (7.2.15) are given in App. B. Here we have introduced $a_y(x) = \frac{1}{2\pi} \frac{y}{y^2/4+x^2}$ and $\int_{-k}^k f * g$ denotes the convolution $\int_{-k}^k dy f(x-y)g(y)$. The driving terms of the kernel-equation (7.2.15) correspond to the bulk (of order L^0) and impurity or boundary (of order L^{-1}) contributions to the densities. Within our notations, the impurity's driving terms carry a superscript (R) referring to the sector of bound states spectrum they correspond. The boundaries A and B for the spin and charge sector, respectively, are fixed by the conditions

$$\int_{-A}^A d\lambda \rho_s(\lambda) = \frac{2[M_s - \theta(\tau - \tau_1)] + 1}{L} \quad (7.2.16)$$

$$\int_{-B}^B d\vartheta \rho_c(\vartheta) = \frac{2[M_c - \theta(\tau - \tau_0) - \theta(\tau - \tau_2)] + 1}{L} \quad (7.2.17)$$

where $\theta(x)$ is the Heaviside step function and τ_k are the thresholds for the appearance of bound states identified above. Alternatively, the ground state, for given chemical potential μ and magnetic field H , is obtained by filling all the modes with negative dressed energies $\varepsilon_s(\lambda)$ and $\varepsilon_c(\vartheta)$ solving the integral equations

$$\begin{pmatrix} \varepsilon_s(\lambda) \\ \varepsilon_c(\vartheta) \end{pmatrix} = \begin{pmatrix} -2\pi a_1(\lambda) + H \\ \mu - \frac{H}{2} \end{pmatrix} + \begin{pmatrix} -\int_{-A}^A a_2 & \int_{-B}^B a_1 \\ \int_{-A}^A a_1 & 0 \end{pmatrix} * \begin{pmatrix} \varepsilon_s(\lambda) \\ \varepsilon_c(\vartheta) \end{pmatrix} \quad (7.2.18)$$

where A and B have to be chosen such that $\varepsilon_s(\pm A) = 0$ and $\varepsilon_c(\pm B) = 0$. In the dressed energies "language", the bulk parameters A (resp. B) can thus be interpreted as the pseudo-Fermi levels for the spin (resp. hole) band. A typical solution of the spinon and holon dispersion is shown in Fig. 7.2 for a given μ and H . Since (7.2.15) is a linear system of integral equations, the generic solution for both spin and charge densities is of the form

$$\rho = \rho_\infty + \frac{1}{L}(\rho_{\text{imp}} + \rho_b). \quad (7.2.19)$$

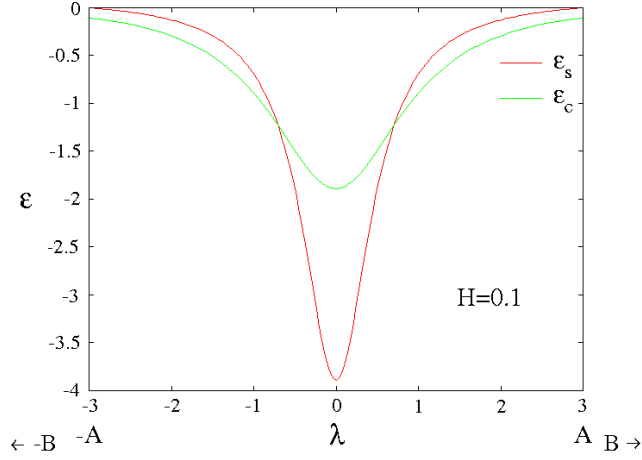


Figure 7.2: A typical solution of the dressed energies equations (7.2.18) for an arbitrary value of μ and H .

The first term in (7.2.19) is the bulk density obtained by solving (7.2.15) with $L = \infty$. The remaining two terms of order $1/L$ are the contribution due to the impurity site and the one due to the openness of the chain (boundaries). The imaginary roots which are treated separately from the continuum of real solutions give rise to various driving terms of the $1/L$ -corrections due to the impurity. From (7.2.10)–(7.2.14), we obtain:

$$\hat{\rho}_s^{(R)}(\lambda) = \begin{cases} 0 & t \in \mathbb{R}, R = 0 \\ a_{2\tau+1-\alpha}(\lambda) + a_{1+\alpha-2\tau}(\lambda) & R = I \\ -a_{3+\alpha-2\tau}(\lambda) - a_{2\tau-\alpha-1}(\lambda) & R = II \\ 0 & R = III \end{cases} \quad (7.2.20)$$

for the spin-sector and

$$\hat{\rho}_c^{(R)}(\vartheta) = \begin{cases} a_\alpha(\vartheta + t) + a_\alpha(\vartheta - t) & t \in \mathbb{R} \\ a_{\alpha+2\tau}(\vartheta) + a_{\alpha-2\tau}(\vartheta) & R = 0, I \\ a_{\alpha+2\tau}(\vartheta) + a_{2+\alpha-2\tau}(\vartheta) & R = II, III \end{cases} \quad (7.2.21)$$

for the charge-sector. The label R stands for the root configurations discussed above, $R = 0$ being the one without bound states solutions associated with the phase shifts (7.2.10). The $1/L$ contributions due to the boundaries have to be calculated with the driving terms $\hat{\rho}_s^{(b)}(\lambda) = a_2(\lambda)$ and $\hat{\rho}_c^{(b)}(\vartheta) = -a_1(\vartheta)$. Note that any thermodynamic quantity can also be split into parts corresponding to the bulk, the impurity and the boundaries. For instance, the ground state energy of the system is

$$E_0 = L\epsilon_\infty + (\epsilon_{\text{imp}} + \epsilon_b) + \dots \quad (7.2.22)$$

In the following, we will concentrate on the impurity's contributions to these quantities which are determined by the densities $\rho_{s/c}^{(R)}$. The effect of the boundaries, which is of purely geometric nature and therefore independent of the impurity's parameters, has been studied by Essler [39].

7.3 Characterization of the impurity

So far, four regions of the α - τ parameter space of the impurity have been identified which allow for different possible bound state configurations. Each of these configurations is described by a different set of BAE. Formally, the impurity's contribution to the energy expressed in terms of the densities is

$$\begin{aligned} \epsilon_{\text{imp}} = & V_0(\alpha + 2) - 2 - \pi \int_{-A}^A d\lambda \rho_s^{(R)}(\lambda) a_1(\lambda) \\ & + \left(\mu - \frac{H}{2} \right) \left(\frac{1}{2} \int_{-B}^B d\vartheta \rho_c^{(R)}(\vartheta) + \theta(\tau - \tau_0) + \theta(\tau - \tau_2) \right) \\ & + H \left(\frac{1}{2} \int_{-A}^A d\lambda \rho_s^{(R)}(\lambda) + \theta(\tau - \tau_1) \right) - 2\mu. \end{aligned} \quad (7.3.23)$$

In order to identify the true ground state of the system for given impurity parameters α and t (resp. τ), the expressions (7.3.23) have to be compared for the different allowed bound state configurations. In Fig. 7.3, we show a plot of $\epsilon_{\text{imp}}(V_0)$ for the simple case of $H = 0$. One can see that for positive hybridization V_0 , the maximum allowed number of bound states (in the configurations 0, I, II) has to be considered for the ground state [52]. For negative V_0 , $\tau > \tau_2 = \alpha/2 + 1$, however, the ground state is described by real rapidities alone (configuration (0)), i.e. the BAE (7.2.7) with the impurity phase shifts (7.2.10).

7.3.1 Zero field impurity susceptibility

With our parametrization of the BAE's roots, the impurity contribution to the magnetization is given by

$$\begin{aligned} - \frac{\partial \epsilon_{\text{imp}}}{\partial H} \equiv M_{\text{imp}} = & \frac{1}{4} \int_{-B}^B d\vartheta \rho_c^{(R)}(\vartheta) + \frac{1}{2}(\theta(\tau - \tau_0) + \theta(\tau - \tau_2)) \\ & - \frac{1}{2} \int_{-A}^A d\lambda \rho_s^{(R)}(\lambda) - \theta(\tau - \tau_1). \end{aligned} \quad (7.3.24)$$

Performing a Fourier transform of Eq. (7.2.15), we can rewrite this expression as an integral over the spin density only, in the low-field regime ($A \gg 1$, $A \gg B$):

$$M_{\text{imp}} = \frac{1}{2} \int_A^\infty d\lambda \rho_s^{(R)}(\lambda) - \theta(\tau - \tau_1) + \frac{1}{2}(\theta(\tau - \tau_0) + \theta(\tau - \tau_2)). \quad (7.3.25)$$

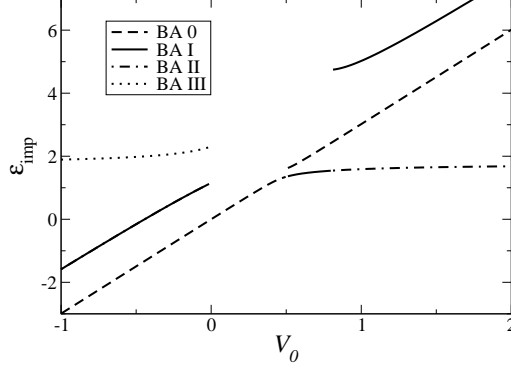


Figure 7.3: Impurity contribution to the ground state energy for different bound state configurations as a function of the hybridization V_0 for a bulk hole concentration of $\delta = 0.2$. The impurity parameter is fixed to $\alpha = 1$. Note that the Bethe ansatz for the configuration $R = I$ and $R = II$ gives identical results for ϵ_{imp} at negative V_0 .

This integral can be computed by means of a Wiener-Hopf (see App. C for details) analysis of the integral equations (7.2.15). Using the expression

$$\pi A = -\ln(H/H_0) + \frac{1}{4 \ln H}, \quad H_0 = \sqrt{2\pi/e}(2\pi - C) \quad (7.3.26)$$

connecting A and H in the large A (low H) limit, the resulting expression for the susceptibility of the impurity at zero field is then [52]:

$$\chi_{\text{imp}}(H = 0) = \frac{1}{2\pi(2\pi - C)} \left\{ \begin{array}{l} C_{\alpha,\tau}^{(0)} \\ C_{\alpha,\tau}^{(I)} + 2 \cos \pi(\tau - \tau_0) \\ C_{\alpha,\tau}^{(II)} + 2 \cos \pi(\tau - \tau_0) \\ C_{\alpha,\tau}^{(III)} \end{array} \right\} \begin{array}{l} R = 0 \\ R = I \\ R = II \\ R = III \end{array} \quad (7.3.27)$$

where we have defined $C_{\alpha,\tau}^{(R)} \equiv \int_{-B}^B d\vartheta e^{\pi\vartheta} \rho_c^{(R)}(\vartheta)$ and $C = \int_{-B}^B d\vartheta e^{\pi\vartheta} \varepsilon_c(\vartheta)$, ε_c being the solution of Eq. (7.2.18). We present in Fig. 7.4 some numerical computations of the zero field impurity' susceptibility for two different hole concentrations ($\delta = 20\%$ and 80%), as a function of V_0 and for various values of α [53]. Here we consider the configuration with all possible bound states occupied. Fig. 7.4 shows also the contribution of the impurity to the electronic density defined by

$$-\frac{\partial \epsilon_{\text{imp}}}{\partial \mu} \equiv D_{\text{imp}} = 2 - \frac{1}{2} \int_{-B}^B d\vartheta \rho_c^{(R)}(\vartheta) - \theta(\tau - \tau_0) - \theta(\tau - \tau_2). \quad (7.3.28)$$

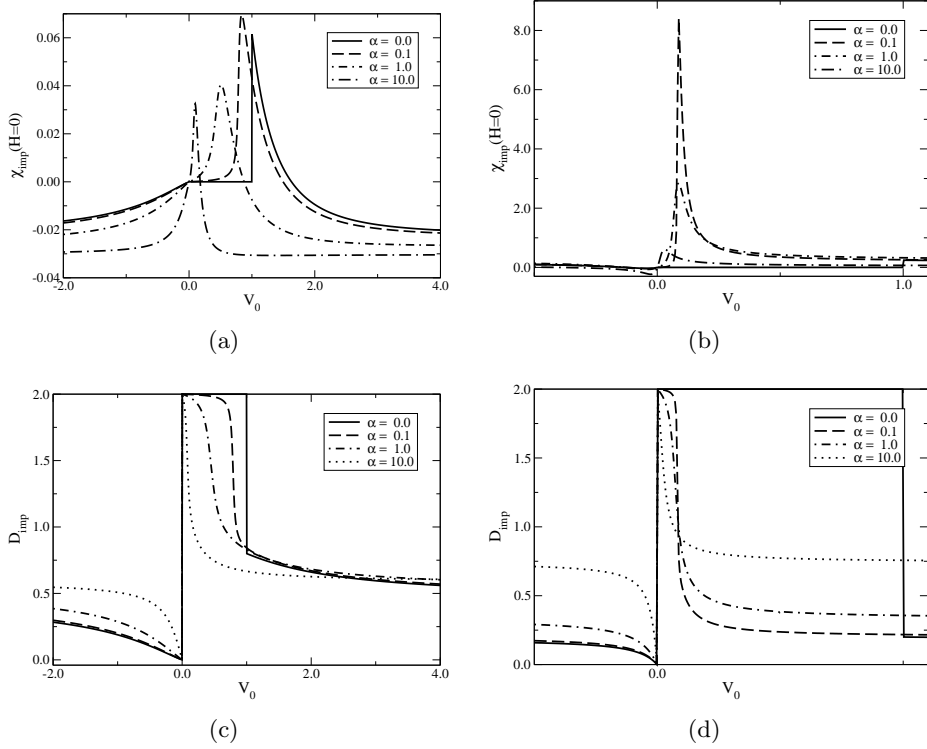


Figure 7.4: χ_{imp} and D_{imp} at zero magnetic field for hole concentration of 20% (left panel) and 80% (right panel)

First notice that for $\alpha = 0$ and $0 < V_0 < 1$, the impurity is doubly occupied, $D_{\text{imp}} \equiv 2$. Therefore the impurity does not contribute to the magnetic susceptibility of the system, i.e. $\chi_{\text{imp}} = 0$. For $V_0 > 1$ (configurations (I) and (II)) and $V_0 < 0$ (configuration (III)), the occupation is less than 2 due to the filled holon bound state and there is a small finite impurity contribution to the susceptibility. The resonance in the zero-field susceptibility is the response of the unpaired electron on the impurity site which appears when $D_{\text{imp}} \approx 1$. Although still limited by fluctuations in the impurity's occupation, the susceptibility at the resonance grows strongly with δ : while the maximum value of $\chi_{\text{imp}}(H = 0)$ approaches the bulk susceptibility as $\delta \rightarrow 0$ it diverges for $\delta \rightarrow 1$, i.e. vanishing bulk density of electrons. In this limit, the remaining electron on the impurity site is essentially an uncoupled local moment.

7.3.2 Magnetization of the impurity at finite magnetic field

Behaviour close to $H = 0$

As it has been shown in the previous section, in the zero-field limit and for a given set of impurity parameters (α and t), the susceptibility approaches

a non-universal constant (7.3.27). Hence, the leading low-field behavior of the impurity's magnetization is expected to be linear in H , up to subleading corrections. These corrections, that can be inferred from more accurate Wiener-Hopf analysis of Eq. (7.3.25), lead to the presence of a logarithmic singularity at zero field in the impurity's contribution to the susceptibility (see insert of Fig. 7.8). In the low-field limit where the relation (7.3.26) holds, we obtain

$$\chi_{\text{imp}}(H \rightarrow 0) = \chi_{\text{imp}}(0) \left[1 - \frac{1}{2} \left(\frac{1}{\ln H/H_0} - \frac{1}{(\ln H/H_0)^2} \right) \right]. \quad (7.3.29)$$

Such a feature is well known from the study of the magnetic response in isotropic one-dimensional antiferromagnets (see e.g. Ref. [38]).

Behaviour close to the saturation field

In the high-field limit, the impurity's magnetization saturates for the value $H = H^{\text{sat}} \equiv 4 \cos^2(\pi\delta/2)$ of the magnetic field above which the bulk system becomes completely polarised (see Fig. 7.5). As H approaches the saturation

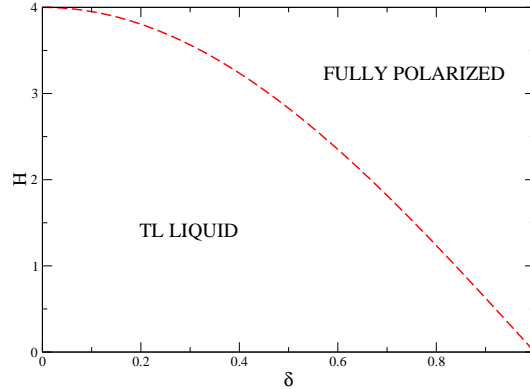


Figure 7.5: The saturation field $H^{\text{sat}} \equiv 4 \cos^2(\pi\delta/2)$ separates the (δ, H) plane into two phases: below H^{sat} the t - J chain behaves like a Tomonaga-Luttinger liquid, whereas for $H > H^{\text{sat}}$, the system is described by a fully polarised ground-state.

field, an analytical expression for the impurity's magnetization and susceptibility can be given. In the Bethe Ansatz integral equations this regime corresponds to $B \gg A$ with $B \rightarrow \infty$ for $H \rightarrow H^{\text{sat}}$

$$M_{\text{imp}} = M_{\text{imp}}^{\text{sat}} - \frac{1}{2} \left(\int_{-\infty}^{-B} + \int_B^{\infty} \right) d\vartheta \left[1 + \frac{2}{\pi} \arctan(2\vartheta - 2A) \right] \rho_c^{\text{imp}}(\vartheta). \quad (7.3.30)$$

Expanding the arctan for large arguments $\vartheta \gg 1$, one obtains the asymptotic behavior of the magnetization as a closed form

$$M_{\text{imp}} = \frac{1}{2} - \frac{1}{2\pi} \left(\arctan \frac{2(A_s - t)}{\alpha + 1} + \arctan \frac{2(A_s + t)}{\alpha + 1} \right) \cdot \left(1 + \frac{1}{\pi B_s} \right) - \frac{\alpha}{2\pi B_s}, \quad (7.3.31)$$

where A_s and B_s are the boundaries close to saturation. Their asymptotic behaviour near $H = H^{\text{sat}}$ is determined by

$$A_s \approx \frac{1}{2} \sqrt{4/H - 1}, \quad \delta = \left(1 - \frac{1}{\pi B_s} \right) \frac{2}{\pi} \arctan 2A_s. \quad (7.3.32)$$

Using this relation of the boundaries to the magnetic field and the doping δ one finds that the leading field dependence of the magnetization below $H = H^{\text{sat}}$ is a linear one, $\propto H^{\text{sat}} - H$. In Fig. 7.8 the expression (7.3.31) for the magnetization and the derived one for the impurity susceptibility are indicated by dotted lines.

Kondo regime

In between the two limits $H = 0$ and $H = H^{\text{sat}}$, the magnetic response of the system due to the presence of the impurity can become non trivial in the weak-hybridization regime which corresponds to real values of t . For $V_0 \ll 1$, a Kondo scale can be defined as a function of the parameter t as

$$H_K \sim H_0 \exp(-\pi t). \quad (7.3.33)$$

For the impurity to be visible in the magnetic response, both spin and charge sectors have to be coupled at the scale introduced by the hybridisation. This coupling is determined by the relative size of the impurity parameter t and that of the host parameters A and B . In Fig. 7.6 the profiles of the charge and spin densities are drawn. Due to the presence of the driving term $a_\alpha(\vartheta \pm t)$ in the equation for the charge density (7.2.15), we can say that $\rho_c(\vartheta)$ and $\rho_s(\lambda)$ have, roughly, two main Lorentzian contributions centered around $\vartheta, \lambda = \pm t$. As a consequence, two scenarii are possible: (i) For large t (corresponding to sufficiently weak hybridization) but such that $t = B > A$, the term $\int_{-A}^A a_1 * \rho_s$ in the equation for the charge densities is essentially zero (see Fig. 7.6 left). This means that the impurity is decoupled from the charge degrees of the host at the Kondo scale (7.3.33). The response of the impurity to an external field is governed by a magnetic scale H_B defined by the charge parameter, $t = B$. In this case, the impurity contribution χ_{imp} to the susceptibility will exhibit a resonance at $H = H_B > H_K$ while being suppressed below H_B , where the magnetic scale H_B is defined by $t = B$. In fact, if one computes the density D_{imp} of electrons sitting at the impurity, one clearly sees (cf Fig. 7.7) that below $H = H_B$, the impurity is doubly occupied implying that the impurity is already screened at the Kondo scale

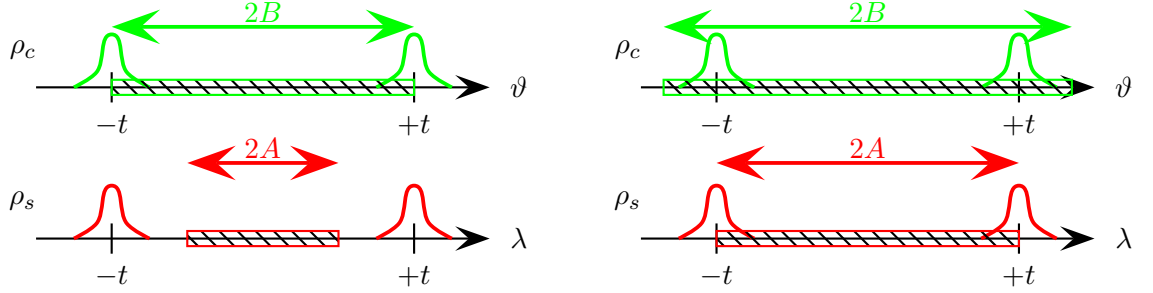


Figure 7.6: The two scenarii for the Kondo regime. Left: for $t = B > A$, the impurity spin density is completely decoupled from the charge degrees of the freedom of the host. Right: for $t = A < B$, both spin and charge densities are coupled at the Kondo scale determined by t . Kondo resonance is expected.

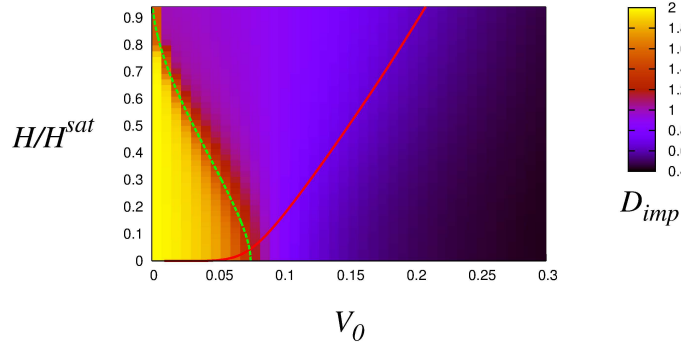


Figure 7.7: The occupation D_{imp} of the impurity as a function of the hybridization V_0 and magnetic field H for $\delta = 0.8$ and $\alpha = 1$. The phase boundaries defined by the scales H_B (green line) and H_K (red line) are superimposed. We clearly see the region of double occupancy below H_B where the impurity becomes decoupled from the bulk.

and effectively decouples from the host. (ii) If the impurity and the host are already coupled at the Kondo scale, i.e. $t = A < B$, Kondo physics can be seen in the magnetic response of the impurity. In Fig. 7.8 (b) the change in the dependence of the impurity magnetization on H from its low-field linear behaviour, $H < H_K$, to the high field behaviour is clearly observable. This Kondo regime is reached for t sufficiently large, i.e. $H_K \ll H^{\text{sat}}$. In Fig. 7.7, this regime corresponds to the average number of electrons on the impurity being close to one, signature of the formation of a local moment.

We can also compute the fluctuations in the densities via the impurity contribution to the magnetic susceptibility χ_{imp} and charge compressibility $\kappa_{\text{imp}} = \partial D_{\text{imp}} / \partial \mu$ of the system. Just as the corresponding bulk quantities

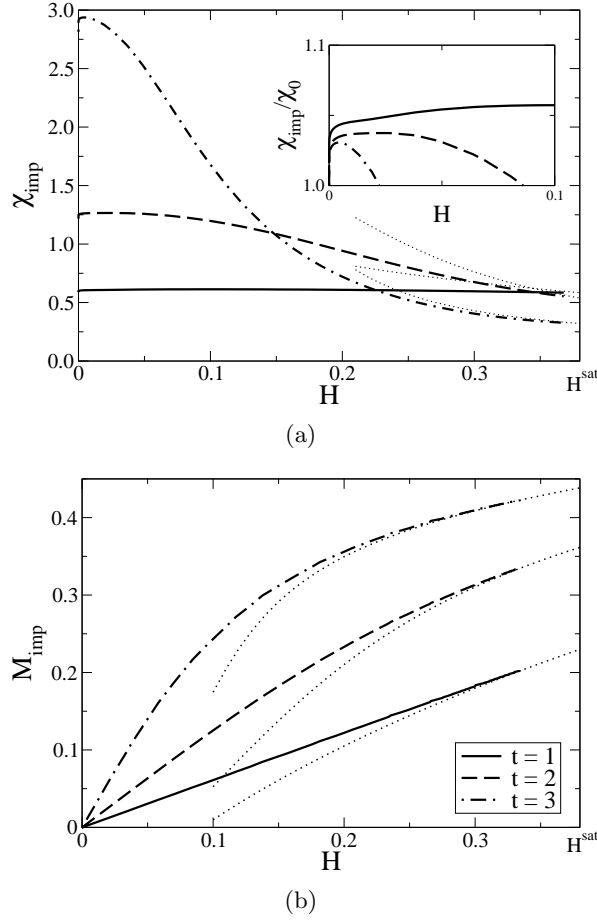


Figure 7.8: Susceptibility (a) and magnetization (b) of the impurity as a function of the external field for $t=1, 2$ and 3 , $\alpha = 1$ and $\delta = 0.8$ are fixed. The dotted curves show the behavior close to the saturated value (7.3.31). The insert in (a) focuses on the log-singularity (Eq. (7.3.29)) of χ_{imp} at zero field.

these thermodynamic coefficients are accessible through the coefficients of the dressed charge matrix [52]. In Fig. 7.9 we present some numerical results on these quantities (taken from [52]) as a function of the hybridization and the magnetic field are shown for hole concentration $\delta = 0.8$. For intermediate values of the hybridization $0.1 \lesssim V_0 \lesssim 0.2$ the coupling of the impurity to the holon excitations is effective. For small magnetic fields below the Kondo scale H_K the impurity contribution to the susceptibility takes a non-universal value χ_0 characteristic for the strong coupling regime of an Anderson impurity. Above H_K the field dependence is that of a local moment with logarithmic deviations from full polarization (see Figure 7.10). The emergence of universal Kondo like behaviour $\chi_{\text{imp}} = f(H/H_K)/2\pi H_K$ for smaller hybridization $V_0 \lesssim 0.1$ is suppressed by the decoupling of the impurity from the host. Here the

double occupancy of the impurity for small fields and the formation of a local moment with an impurity occupation close to 1 appears for fields $H \gtrsim H_B \gg H_K$ are clearly visible. In the vicinity of the transition between these regions the occupation and magnetization of the impurity fluctuate strongly, as shown by the resonances in the susceptibilities (Fig. 7.9). Finally, for larger values of $V_0 \gtrsim 0.2$, the occupation of the impurity decreases well below 1 and the susceptibilities are approximately constant over the entire range of the external field $0 < H < H^{\text{sat}}$.

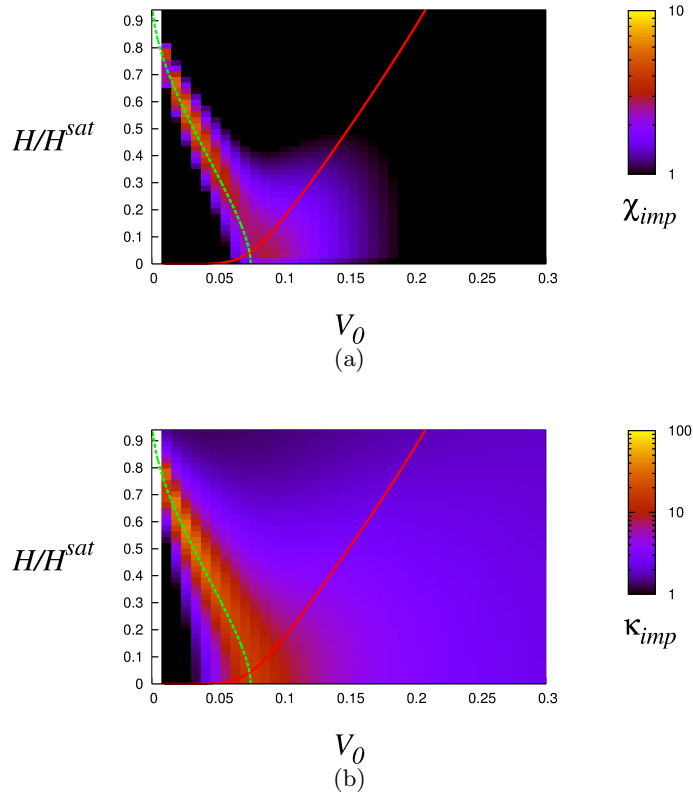


Figure 7.9: (a) Susceptibility χ_{imp} and (b) charge compressibility κ_{imp} (normalized to its bulk value) of the impurity as a function of the hybridization V_0 and magnetic field H for $\delta = 0.8$ and $\alpha = 1$. The phase boundaries defined by the scales H_B (green line) and H_K (red line) are superimposed. Note the logarithmic scale used for the shading of the susceptibilities.

7.4 Summary

In summary, we have constructed a one-dimensional lattice model for correlated electrons with an embedded Anderson-type impurity. Several parameters can be adjusted to fine-tune the properties of the impurity. Under variation

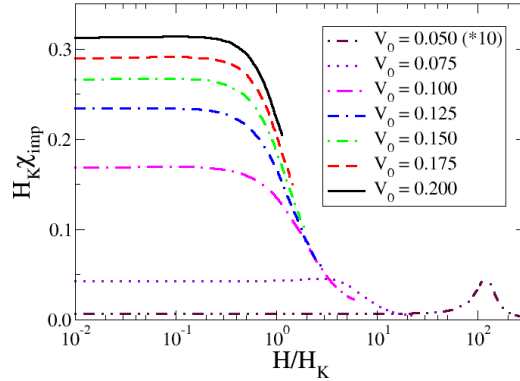


Figure 7.10: Magnetic field dependence of the impurity susceptibility for $\delta = 0.8$, $\alpha = 1$ and various values of the hybridization: for $V_0 \gtrsim 0.1$ the transition between the strong coupling behaviour for small fields and the formation of a local moment above $H \simeq H_K$ is clearly seen. At smaller values of V_0 the susceptibility is strongly suppressed due to the decoupling of the doubly occupied impurity from the host (data for $V_0 = 0.05$ are enhanced by a factor of 10).

of the hybridization the formation of a sequence of bound states is observed, similar to the situation observed in systems with open boundary conditions with static boundary potentials. By means of the Bethe Ansatz the spectrum of the model is obtained where contributions from the bulk, the boundaries and the impurity are easily identified. For weak hybridization the susceptibility of the impurity shows a strong Kondo-like resonance for low electron densities in the host system. Note that we have considered only contribution of the impurity to the systems response at order $1/L$. It is well known that the presence of the boundary leads to additional terms at this order diverging as $1/\chi_{\text{OBC}} \propto H(\ln H)^2$ as $H \rightarrow 0$ [39].

Chapter 8

Kondo impurity in the SUSY t - J model

We saw that boundary impurities can be obtained by combining a Lax operator satisfying the intertwining relation (6.2.4) with a boundary matrix, solution of the reflection equation (6.2.46). In Chap. 7, we used this approach to study a generalised Anderson model (impurity with local orbitals) and the boundary impurity was introduced in order to mimic the effects of backscattering within an integrable description of the problem. In the present chapter, we will construct and study a model describing a purely magnetic (Kondo) impurity in a t - J chain. This can be achieved by taking an integrable inhomogeneity acting on the particular representation of $gl(2|1)$, named $[s]_+$, which contains two well defined spin multiplets. Together with such a defect, we will add a boundary potential acting at the impurity site. Here the strength of this local potential appears as an additional parameter in the model and certain restrictions on the spectrum of the local scatterer can be relaxed. Synchronising the parameters of the impurity to the value of the boundary potential, it becomes possible to project out some of the local configurations of the impurity – similarly as in the Schrieffer-Wolff transformation allowing to go from the Anderson to the Kondo model.

8.1 Hamiltonian

We will attribute to the impurity vertex the following \mathcal{L} -operator

$$\mathcal{L}_{\text{imp}}(\lambda) \equiv \mathcal{L}_s(\lambda) = \frac{\lambda - i(s + 1/2)}{\lambda + i(s + 1/2)} I + \frac{i}{\lambda + i(s + 1/2)} C_2^{(0s)}$$

whose entries act on the physical space of the impurity, V_{imp} through the $[s]_+$ representation of $gl(2|1)$ (cf Chap. 6 and App. A). Here $C_2^{(0s)}$ is the quadratic Casimir of $gl(2|1)$ on the tensor product $V_0 \otimes V_{\text{imp}}$ (the auxiliary space V_0 carries the three-dimensional fundamental representation $[1/2]_+$ of

$gl(2|1)$). Additionally, we will impose a boundary chemical potential applied at the edge of the chain. Formally, the action of this local potential, we will denote by p , is encoded in the boundary matrix,

$$K_-^p(\lambda) = \text{diag} \left(1, 1, -\frac{p\lambda + i}{p\lambda - i} \right) \quad (8.1.1)$$

which is a c -number solution of the RE. Without loss of generality, we should also choose the left end of the chain to be purely reflecting $K_+ \equiv \mathbb{1}$. Thus the following transfer matrix,

$$\begin{aligned} \tau(\lambda) = \text{str}_0 & \left(\mathcal{L}_0^{L+1}(\lambda) \mathcal{L}_0^L(\lambda) \dots \mathcal{L}_s^1(\lambda + t) K_-^p(\lambda) \times \right. \\ & \left. \times (\mathcal{L}_s^1(-\lambda + t))^{-1} (\mathcal{L}_0^2(-\lambda))^{-1} \dots (\mathcal{L}_0^{L+1}(-\lambda))^{-1} \right), \end{aligned} \quad (8.1.2)$$

will then generate all the integrals of motion of the system. In particular, the Hamiltonian is obtained by taking the derivative of $\tau(\lambda)$ at the 'shift point', $\lambda = 0$, where the \mathcal{L} -operator of the bulk sites reduces to a permutation.

The Hamiltonian of the system described above is the sum of a usual (open) t - J chain,

$$\begin{aligned} \mathcal{H}_{tJ} = -\mathcal{P} & \left(\sum_{j=1}^{L-1} \sum_{\sigma} c_{j,\sigma}^\dagger c_{j+1,\sigma} + c_{j+1,\sigma}^\dagger c_{j,\sigma} \right) \mathcal{P} \\ & + 2 \sum_{j=1}^{L-1} \left[\vec{S}_j \cdot \vec{S}_{j+1} - \frac{n_j n_{j+1}}{4} + \frac{1}{2}(n_j + n_{j+1}) \right] \end{aligned} \quad (8.1.3)$$

plus a boundary Hamiltonian term including the boundary potential p and the impurity parameters, s and t ,

$$\begin{aligned} \mathcal{H}_{\text{bimp}} = -2p & \left(B_1 - \frac{1}{2} \right) - \frac{1}{t^2 + (s + 1/2)^2} \left((2s + 1)\mathbb{1} - C_2^{(s1)} \right) \\ & - \frac{2p}{t^2 + (s + 1/2)^2} \left(it[B_1, C_2^{(s1)}] - (s + \frac{1}{2})\{B_1, C_2^{(s1)}\} + C_2^{(s1)} B_1 C_2^{(s1)} \right). \end{aligned} \quad (8.1.4)$$

Here, $B_1 = 1 - \frac{1}{2}n_1$, n_1 counting the occupation at the bulk site "1", and $C_2^{(s1)}$ is the quadratic Casimir operator of $gl(2|1)$. Note that $C_2^{(s1)}$ acts on the quantum space $V_{\text{imp}} \otimes V_1$, where $V_{\text{imp}} = [s]_+$ is the space carrying the degrees of freedom of the impurity while $V_1 = [1/2]_+$ is the three-dimensional Hilbert space of the bulk site "1". Additionally, we want to be able to vary the magnetisation and the total number of electrons so we add a chemical

potential μ and a magnetic field H such that the full Hamiltonian of the system is

$$\mathcal{H} = \mathcal{H}_{tJ} + \mathcal{H}_{\text{bimp}} - \mu N - HS^z . \quad (8.1.5)$$

NB1: The Hamiltonian is hermitean for $(p, t) \in \mathbb{R}^+ \times \mathbb{R}$ and non-hermitean for $t \in i\mathbb{R}$.

NB2: Since the construction of the boundary Hamiltonian following our approach is non-standard, the key-steps of the derivation of (8.1.4) are compiled in App. D.

8.2 Spectrum and bound states

Both the boundary potential p and the presence of an impurity affect the nature of the spectrum of the chain. It is natural to expect that, for sufficiently strong p , boundary bound states (or anti-bound states) are formed at the end of the chain. This issue has been studied in the context of the X-ray edge singularity problem for one-dimensional lattice models of correlated electrons [40]. Similarly, an inhomogeneity can lead to the formation of bound states as its coupling to the bulk of the system is varied (cf Chap. 7 and Refs. [52, 53]). For the integrable model considered here, both scenarios can be discussed by the analysis of the Bethe ansatz equations (BAE).

8.2.1 Boundary bound states

Sutherland vacuum $|\uparrow \dots \uparrow\rangle_{\text{bulk}} \otimes |s\rangle_{\text{imp}}$

In this section, we shall restrict ourselves to the case of a repulsive boundary potential, $p > 0$. Starting from the fully polarized state which maximizes the number of particles (the Sutherland pseudo-vacuum [127]) the wave function of an eigenstate with N_h holes and N_\downarrow overturned spins is parametrized by the roots $\{\lambda_k\}$ and $\{\vartheta_\ell\}$ of the BAE [39]

$$(e_1(\lambda_k))^{2L} \eta_{\text{imp}(\lambda_k)} \eta_p(\lambda_k) = \prod_{\epsilon=\pm} \prod_{j \neq k}^{N_h+N_\downarrow} e_2(\lambda_k + \epsilon\lambda_j) \prod_{\ell=1}^{N_h} e_{-1}(\lambda_k + \epsilon\vartheta_\ell) \quad (8.2.6)$$

$$1 = \xi_{\text{imp}(\vartheta_\ell)} \xi_p(\vartheta_\ell) \prod_{\epsilon=\pm} \prod_{j=1}^{N_h+N_\downarrow} e_1(\vartheta_\ell + \epsilon\lambda_j)$$

where $e_y(x) = (x + iy/2)/(x - iy/2)$. The terms η_p and ξ_p are the phase factors related to the presence of a chemical potential acting on the boundary while η_{imp} and ξ_{imp} are the phase factors induced by the impurity. As we have already argued in Chap. 7, the presence of such phase factors will lead corrections of order L^0 to the thermodynamic quantities of the system. Let us here analyse the effect of the boundary potential and keep the discussion

of the influence of the impurity for the next section. First of all, for $p = 0$, i.e. without any boundary potential, it is known that the ground state of the system is given by the set of real spin $\{\lambda_j\}_{j=1, N_h + N_\uparrow}$ and hole rapidities $\{\vartheta_\ell\}_{\ell=1, N_h}$ solving the BAE. But when the boundary field is "switched on", purely imaginary solutions of the BAE may become energetically stable. Such imaginary BAE roots, that we will interpret as bound states in the spectrum of the system, appear step by step as p is increased. The series of boundary bound states (BBS) induced by p goes as follows:

(i) For $0 < p < 1$, no BBS is solution to the BAE. The boundary phase factors are the ones derived by Essler [39], i.e.

$$\eta_p(\lambda) \equiv 1, \quad \xi_p(\vartheta) = -e_{2/p-2}(\vartheta) \quad (8.2.7)$$

(ii) When $1 \leq p < 2$, the BAE allow for an imaginary solution (hole rapidity), $\vartheta_0 = i(1 - \frac{1}{p})$, with $\text{Im } \vartheta_0 \geq 0$). It can be checked that this solution is indeed a stable BBS. In consequence, the boundary phase factors have to be modified, taking into account the presence of the ϑ_0 BBS into the ground state configuration. The new phase factors are now given by

$$\eta_p(\lambda) = e_{3-2/p}(\lambda)e_{2/p-1}(\lambda), \quad \xi_p(\vartheta) = -e_{2/p-2}(\vartheta) \quad (8.2.8)$$

with $N_h - 1$ remaining real roots ϑ_ℓ .

(iii) For $p \geq 2$, an additional BBS solution (this time in the spin sector) arises in the thermodynamic limit: $\lambda_0 = i(\frac{1}{2} - \frac{1}{p})$ ($\text{Im } \lambda_0 \geq 0$). The effective boundary phase factors now become

$$\eta_p(\lambda) = e_{-1-2/p}(\lambda)e_{-1+2/p}(\lambda), \quad \xi_p(\vartheta) = -e_{2/p}(\vartheta) \quad (8.2.9)$$

with remaining $N_h - 1$ real hole rapidities ϑ and $N_h + N_\downarrow - 1$ real spin rapidities λ .

As a remark, we would like to mention that in the case of a t - J chain with boundary chemical potential and without impurity, the ground state for, $p > 0$, is obtained by including all possible BBS into the Bethe root configuration. We illustrate this result by showing a computation of the contribution of the physical boundary to the energy in Fig. 8.1.

Lai vacuum $|0\dots 0\rangle_{\text{bulk}} \otimes |s - 1/2\rangle_{\text{imp}}$

A different, but completely equivalent description of the spectrum of the open t - J model with boundary impurity can be obtained by starting from the Fock vacuum $|\Omega_L\rangle \equiv |0\rangle^{\otimes L} \otimes |s - \frac{1}{2}\rangle_{\text{imp}}$ (the so-called Lai pseudo-vacuum [91]). In this case the many-particle wave functions are parametrized by N_e charge

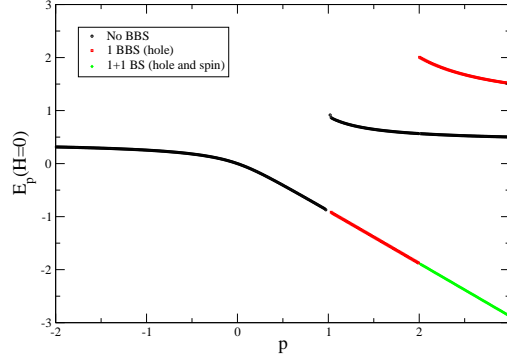


Figure 8.1: Contribution of the boundary potential term to the energy for $p > 0$ and $H = 0$. The ground state of the system with boundary chemical potential and without impurity is realised by populated all possible BS allowed.

rapidities w_k and N_\downarrow spin rapidities x_ℓ which solve the following set of BAE

$$\begin{aligned}
 (e_1(w_k))^{2L} \Phi_{\text{imp}}(w_k) \Phi_p(w_k) &= \prod_{\epsilon=\pm} \prod_{\ell=1}^{N_\downarrow} e_1(w_k + \epsilon x_\ell) \\
 \Xi_{\text{imp}}(x_\ell) \Xi_p(x_\ell) \prod_{\epsilon=\pm} \prod_{j=1}^{N_e} e_1(x_\ell + \epsilon w_j) &= \prod_{m \neq \ell}^{N_\downarrow} e_2(x_\ell + \epsilon x_m)
 \end{aligned} \tag{8.2.10}$$

As already mentioned in Chap. 6, the equivalence between the Lai and Sutherland description of the t - J model can be proved on the basis of particle-hole (p - h) transformation at the level of the BAE [137, 16, 42]. A detailed extension of this proof to the case of non-trivial open boundary conditions can be found in App. E. The main result of this transformation is that it fixes the relation among the isolated (we mean impurity and/or boundary) phase factors within the Lai (Φ , Ξ) and Sutherland (η , ξ) "language". Formally we have,

$$\eta(\lambda) \frac{\xi_+(\lambda + i/2)}{\xi_-(\lambda - i/2)} = \Phi(\lambda), \quad \xi^{-1}(x) = \Xi(x) \frac{\Phi_-(x + i/2)}{\Phi_+(x - i/2)} \tag{8.2.11}$$

where the subscripts $+/-$ stand for the polynomial numerator/denominator of the rational functions ξ and Φ . Starting from the 'bare' Sutherland equations (i.e. without occupied BBS) the p - h transformation (8.2.11) gives

$$\Phi_p(w) = -e_{2/p-1}(w), \quad \Xi_p(x) \equiv 1. \tag{8.2.12}$$

(i) The analysis of the Lai BAE in the thermodynamic limit shows that no BBS exist in this formulation for $p < 2$.

(ii) For $p \geq 2$, $w_0 = i(\frac{1}{2} - \frac{1}{p})$ is solution to the BAE (with $\text{Im } w_0 \geq 0$). It corresponds to a charge-like excitation in the Lai sector and therefore is not energetically stable for repulsive boundary potential ($p > 0$). The solution w_0 can nevertheless be including into the root configuration if the boundary phases are modified according to

$$\Phi_p(w) = -e_{2/p-1}(w), \quad \Xi_p(x) = e_{2/p}(x)e_{2-2/p}(x). \quad (8.2.13)$$

The number of charge rapidities should be lowered by one, $N_e \rightarrow N_e - 1$.

8.2.2 Impurity bound states

A similar sequence of bound states appears when the coupling to the impurity is varied by changing the parameter t in Eq. (8.1.2). Starting from the state with maximal polarization $|\Omega_S\rangle = |\uparrow\rangle^{\otimes L} \otimes |s\rangle$ the spectrum is determined by BAE of Sutherland type (8.2.6) with

$$\begin{aligned} \eta_{\text{imp}}(\lambda) &= e_{2s}(\lambda - t)e_{2s}(\lambda + t) \\ \xi_{\text{imp}}(\vartheta) &\equiv 1, \end{aligned} \quad (8.2.14)$$

while in the corresponding phase shifts in the Lai formulation of the BAE read

$$\begin{aligned} \Phi_{\text{imp}}(w) &= e_{2s}(w_k + t)e_{2s}(w_k - t) \\ \Xi_{\text{imp}}(x) &= e_{2s-1}(x_\ell + t)e_{2s-1}(x_\ell - t). \end{aligned} \quad (8.2.15)$$

The additional phases, e.g. η_{imp} from (8.2.14) in (8.2.6), allow for new imaginary solutions to the BAE which can be interpreted as impurity bound states (IBS) similar as in a continuum model related to the Kondo problem [67, 133] and for an Anderson-type impurity in the t - J model (see [52, 53] and Chap. 7). They appear for t being a pure imaginary number itself, $t = i\tau$ with $\tau \in \mathbb{R}^+$. A short analysis of the Eqs. (8.2.6) with (8.2.14) in the thermodynamic limit reveals that there are two absolute thresholds opening an IBS:

- (i) If $\tau \geq s$, $\lambda_0 = i(\tau - s)$ is a IBS solution with $\text{Im } \lambda_0 \geq 0$.
- (ii) For $\tau \geq s + 1/2$, a ϑ -IBS appears, $\vartheta_0 = i(\tau - s - 1/2)$ ($\text{Im } \vartheta_0 \geq 0$).

8.3 Reduction to a boundary Kondo problem

8.3.1 The projection method

As we have already foreseen in the introduction to this chapter, new integrable boundary Hamiltonians may be obtained after fine tuning of the parameters characterizing the boundary and impurity, respectively [55] by projection

onto an invariant subspace. An important application of this procedure is a Kondo spin coupled to the t - J model. To apply the projecting method, one has to start from an operator-valued solution of the RE obtained by 'dressing' a c -number boundary matrix with an inhomogeneity (cite Sklyanin): $\mathcal{K}_-(\lambda) = [\mathcal{L}_{\text{imp}}(\lambda+t)K^p(\lambda)(\mathcal{L}_{\text{imp}}(-\lambda+t))^{-1}]$. Such solutions are called 'regular'. Then, one should find a decomposition of the impurity Hilbert space $\mathbb{H} = \mathbb{H}_1 \oplus \mathbb{H}_2$ and fine tune the parameters in \mathcal{K}_- such that one of the following conditions is satisfied

$$\Pi_1 \mathcal{K}_-(\lambda) \Pi_2 = 0, \quad \text{or} \quad \Pi_2 \mathcal{K}_-(\lambda) \Pi_1 = 0 \quad (8.3.16)$$

where Π_1 (resp. Π_2) projects onto the subspace \mathbb{H}_1 (resp. \mathbb{H}_2).

The 'projected' boundary matrices resulting from this construction are called 'singular' in a sense that they cannot be derived from the standard dressing prescription. In the present case, the inhomogeneity is build upon the $[s]_+$ representation of $gl(2|1)$. This representation contains two spin multiplets thus providing a natural decomposition of the impurity Hilbert space as $\mathbb{H}_1 = \text{span}\{|s, s, m\rangle\}$ and $\mathbb{H}_2 = \text{span}\{|s + \frac{1}{2}, s - \frac{1}{2}, m\rangle\}$. With this decomposition one finds that $\Pi_1 \mathcal{K}_-(\lambda) \Pi_2$ vanishes for

$$t = i \left(-\frac{1}{p} - s + \frac{1}{2} \right) \equiv i\tilde{t} \quad (8.3.17)$$

while $\Pi_2 \mathcal{K}_-(\lambda) \Pi_1$ vanishes for $t = -i\tilde{t}$

NB: Both projections are actually equivalent and give rise to the same effective Hamiltonians within the two spin subsectors.

Enforcing the projection condition (8.3.17) implies that the two impurity subspaces \mathbb{H}_1 and \mathbb{H}_2 are decoupled. As a direct consequence, all the matrix elements of the boundary Hamiltonian (8.1.4) connecting \mathbb{H}_1 and \mathbb{H}_2 will vanish. This leads to an effective boundary Hamiltonian which has the following simple form

$$\begin{aligned} \mathcal{H}_{\text{bimp}}^s = & -2p(B_1 - \frac{1}{2}) + \frac{2ps}{-\tilde{t}^2 + (s + 1/2)^2} (2B_1 - 1) \\ & + \frac{2}{-\tilde{t}^2 + (s + 1/2)^2} (\mathbf{s} \cdot \mathbf{S}_1 - B_s B_1) \end{aligned} \quad (8.3.18)$$

for the spin s sector. Noticing that $B_s \equiv s$ in that case, we can rewrite the local Hamiltonian as the sum of a boundary potential contribution plus a purely Kondo coupling between the site 1 of the chain and the impurity spin s . This reads

$$\mathcal{H}^s = Vn_1 + J_K \mathbf{s} \cdot \mathbf{S}_1 \quad (8.3.19)$$

up to an irrelevant constant. In fact, the boundary Hamiltonian (8.3.19) is of the same form as the one derived in [132, 142, 141, 45] following a different path. The coupling constants in our cases are given as function of the

parameters p and s by

$$V = \frac{p^2 - sp^2 - p}{(p-1)(2sp+1)} \quad \text{and} \quad J_K = \frac{2p^2}{(p-1)(2sp+1)}. \quad (8.3.20)$$

8.3.2 The projected BAE

The question we want to address in this section is how the spectrum of the pure spin- s impurity system emerges from the original one and how the BAE have to be modified for the projected Kondo-type Hamiltonian. We first remark that after synchronizing the impurity and boundary parameters to the ‘projecting line’ Eq. (8.3.17), the sequences of BBS and IBS are no longer independent. Instead, one finds, that IBS’ thresholds now coincide with the BBS ones exactly, leaving only one sequence of bound states to take care of (see Fig. 8.2).

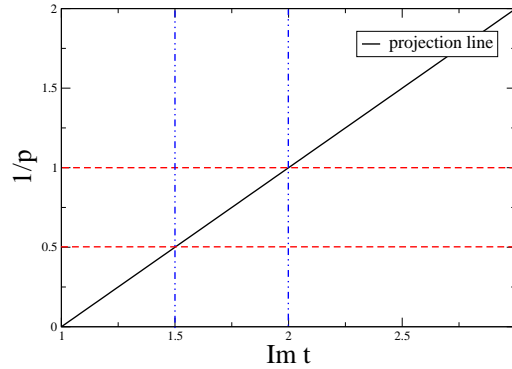


Figure 8.2: Intersection of the IBS (dash-dotted lines) and BBS thresholds (dashed lines) with the ‘projection line’ (solid line) (8.3.17) for $s = 3/2$ as an example.

Replacing $t = i\tilde{t}$ (8.3.17) into the ‘bare’ (i.e. without bound states) Sutherland BAE results in the following BAE:

$$(e_1(\lambda_k))^{2L} e_{1-2/p}(\lambda_k) e_{4s+2/p-1}(\lambda_k) = \prod_{\epsilon=\pm} \prod_{j \neq k}^{N_h+N_1} e_2(\lambda_k + \epsilon\lambda_j) \prod_{\ell=1}^{N_h} e_{-1}(\lambda_k + \epsilon\vartheta_\ell)$$

$$1 = -e_{2/p-2}(\vartheta_\ell) \prod_{\epsilon=\pm} \prod_{j=1}^{N_h+N_1} e_1(\vartheta_\ell + \epsilon\lambda_j) \quad (8.3.21)$$

Since the Sutherland BA starts from the fully polarized state, in particular the state $|s\rangle_{\text{imp}}$ for the impurity site, the solution to these equations will describe the spectrum of a Kondo spin s impurity in a correlated t - J chain.

Alternatively, a description of the spectrum of the spin s impurity sector should be possible starting from a Lai vacuum $|0 \dots 0\rangle_{\text{bulk}} \otimes |s - 1/2\rangle_{\text{imp}}$. The problem is that the reference state of the impurity in the Lai description, namely $|s - 1/2\rangle_{\text{imp}}$, does not belong to the subspace \mathbb{H}_1 . Let us apply blindly the p - h transformation to the BAE (8.3.21) to obtain a new set of BAE

$$\begin{aligned}
 -(e_1(w_k))^{2L} e_{4s+2/p-1}(w_k) &= \prod_{\epsilon=\pm} \prod_{\ell=1}^{N_\downarrow} e_1(w_k + \epsilon x_\ell) \\
 e_{2-2/p}(x_\ell) \prod_{\epsilon=\pm} \prod_{j=1}^{N_\epsilon} e_1(x_\ell + \epsilon w_j) &= e_{2-4s-2/p}(x_\ell) \prod_{m \neq \ell}^{N_\downarrow} e_2(x_\ell + \epsilon x_m).
 \end{aligned} \tag{8.3.22}$$

If we focus on the p and s dependent phase shifts, we can notice that Eqs. (8.3.22) are not the bare projected Lai BAE but instead are the equations one would obtain after populating the charge bound state w_0 explicitly. Therefore, the problem of working with a proper pseudo-vacuum in the Lai sector is overcome by enforcing the occupation of the bound state. In clear, both sets of BAE (8.3.21) and (8.3.22) can be used for studying the spin- s subspace \mathbb{H}_1 of the impurity, provided that the correct BS configuration is used.

We can follow the same reasoning concerning the spin- $(s - 1/2)$ impurity subspace and convince ourself that the spectrum of the system restricted to \mathbb{H}_2 can be obtained solving either the bare projected Lai equations or a set of Sutherland equations with both λ_0 and ϑ_0 BBS occupied. Those various equivalence of BAE before and after projection are summarised in Fig. 8.3.

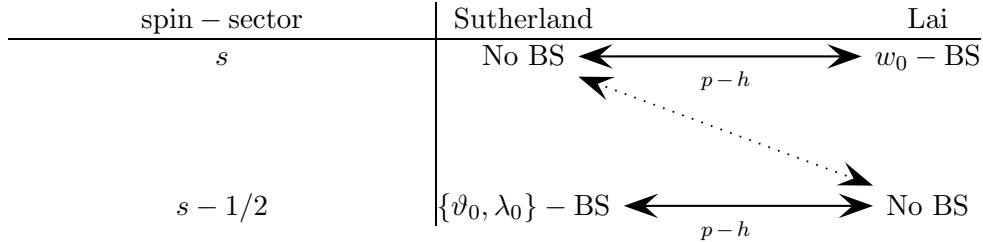


Figure 8.3: When the projection is enforced the link between the bare Sutherland and the bare Lai equations (dotted line) does not exist anymore as it would connect two states living in \mathbb{H}_1 and the other in \mathbb{H}_2 . Instead, BAE involving bound states solutions have to be considered to ensure the validity of a p - h transformation connecting the Sutherland and Lai sectors.

At this point we would like to make one more observation: due to the particular division of the impurity Hilbert space into a spin s and a spin $(s - 1/2)$ sector, the impurity spectrum has the structure of a "spin multiplets cascade". In particular, the construction of a pure spin- $(s - 1/2)$ impurity can be achieved by either starting from an inhomogeneity "living" in the $[s]_+$ representation or directly in the $[s - 1/2]_+$ (see Fig. 8.4).

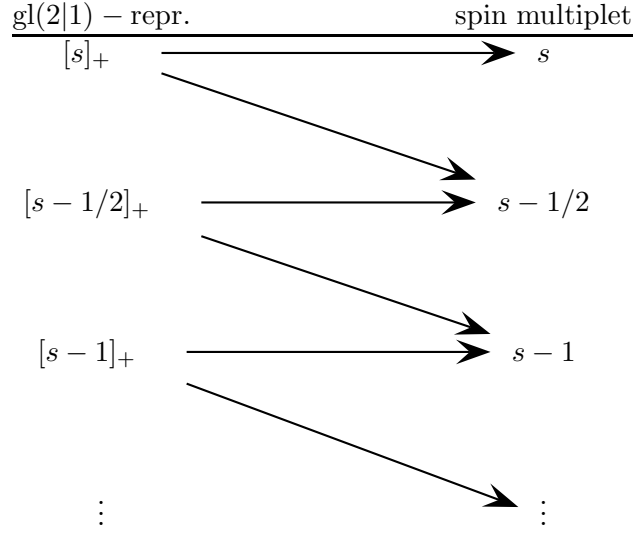


Figure 8.4: The "spin cascade" structure of the impurity Hilbert space.

8.4 Magnetic behaviour of the Kondo impurity

Now that we understand how to describe reliably the spectrum of a pure Kondo spin- s in the t - J model, we will solve the BAE we derived in the previous section to extract the thermodynamic contributions of the impurity. More specifically, we will focus on its magnetic behaviour.

8.4.1 Ground state configuration

First, we should exhibit the true ground state configuration that may differ depending on the values of p and s . Since the boundary impurity parameters enter directly into the potential V and the Kondo coupling J_K , it is likely that a series of bound states will be found while analysing the thermodynamic limit of the BAE. These bound states are in fact the BBS and IBS we discussed in the previous sections, but which are now synchronised. Indeed, in the Sutherland description, we can identify five different regimes, that we will eventually relate to the ground state configurations:

- (1) $\mathbf{p} < \mathbf{p}_0 \equiv \frac{2}{1-4s}$: No BS is present in the Bethe root configuration and the BAE are just the 'bare equations' obtained in Eq. (8.3.21). Using the same notation as in Eq. (8.2.6), the boundary impurity phase shifts are in this case:

$$\begin{aligned}
 \phi(\lambda_k) &= e_{1-2/p}(\lambda_k) e_{4s+2/p-1}(\lambda_k) , \\
 \xi(\vartheta_\ell) &= -e_{2/p-2}(\vartheta_\ell) .
 \end{aligned}
 \tag{8.4.23}$$

- (2) $\mathbf{p}_0 \leq \mathbf{p} < \mathbf{p}_1 \equiv -\frac{1}{2s}$: One spinon BS, $\lambda_0 = i(\frac{1}{2} - \frac{1}{p} - 2s)$, is allowed and is, as we will see when computing the finite-size spectrum, is energetically stable. Taking the imaginary root λ_0 into account in the BAE, we end up with new effective phase shifts

$$\begin{aligned}\phi(\lambda_k) &= e_{1-2/p}(\lambda_k)e_{4s+2/p-1}(\lambda_k)e_{-4s-2/p-1}(\lambda_k)e_{4s+2/p-3}(\lambda_k) , \\ \xi(\vartheta_\ell) &= -e_{2/p-2}(\vartheta_\ell)e_{4s+2/p}(\vartheta_\ell)e_{2-2/p-4s}(\vartheta_\ell) .\end{aligned}\tag{8.4.24}$$

- (3) $\mathbf{p}_1 \leq \mathbf{p} < \mathbf{p}_2 \equiv \mathbf{1}$: No BS is allowed and the BAE are the same as for the case (1).
- (4) $\mathbf{p}_2 \leq \mathbf{p} < \mathbf{p}_3 \equiv \mathbf{2}$: Another spin BS solution can be realised, different that the one of configuration (2) though. Absorbing the corresponding imaginary root, $\lambda_1 = i(\frac{1}{p} - \frac{1}{2})$, into the BAE we obtain the following modified phase shifts:

$$\begin{aligned}\phi(\lambda_k) &= e_{1-2/p}(\lambda_k)e_{4s+2/p-1}(\lambda_k)e_{2/p-3}(\lambda_k)e_{-2/p-1}(\lambda_k) , \\ \xi(\vartheta_\ell) &= -e_{2/p-2}(\vartheta_\ell) .\end{aligned}\tag{8.4.25}$$

- (5) $\mathbf{p} \geq \mathbf{p}_3$: No BS in the configuration, the situation is described by the BAE for region (1).

In order to analyse the thermodynamic properties of the system we shall from now on use the standard description in terms of root densities (cf Chap. 7 for example). The impurity contribution to the spin and charge densities are

$$\rho_{s,i}^{(R)}(\lambda) = \Phi^{(R)}(\lambda) - \int_{-A}^A d\nu a_2(\lambda - \nu)\rho_{s,i}^{(R)}(\nu) + \int_{-B}^B d\vartheta a_1(\lambda - \vartheta)\rho_{c,i}^{(R)}(\vartheta)\tag{8.4.26}$$

$$\rho_{c,i}^{(R)}(\vartheta) = \Xi^{(R)}(\vartheta) + \int_{-A}^A d\lambda a_1(\vartheta - \lambda)\rho_{s,i}^{(R)}(\lambda) .$$

Here (R) labels the different root configurations (or regions) associated to the ground state when p is varied. The driving terms appearing in Eq. 8.4.26 are given as follows: For $R = 1, 3$ and 5 , we have

$$\begin{aligned}\Phi^{(R)}(\lambda) &= a_{1-2/p}(\lambda) + a_{4s+2/p-1}(\lambda) \\ \Xi^{(R)}(\vartheta) &= a_{2/p-2}(\vartheta) .\end{aligned}\tag{8.4.27}$$

For $R = 2$, the driving terms are

$$\begin{aligned}\Phi^{(R)}(\lambda) &= a_{1-2/p}(\lambda) + a_{4s+2/p-1}(\lambda) - a_{4s+2/p+1}(\lambda) + a_{4s+2/p-3}(\lambda) \\ \Xi^{(R)}(\vartheta) &= a_{2/p-2}(\vartheta) + a_{4s+2/p}(\vartheta) + a_{2-4s-2/p}(\vartheta)\end{aligned}\tag{8.4.28}$$

and finally for $R = 4$

$$\begin{aligned}\Phi^{(R)}(\lambda) &= a_{1-2/p}(\lambda) + a_{4s+2/p-1}(\lambda) - a_{1+2/p}(\lambda) + a_{2/p-3}(\lambda) \\ \Xi^{(R)}(\vartheta) &= a_{2/p}(\vartheta) .\end{aligned}\quad (8.4.29)$$

The impurity contribution to the ground state energy is

$$\begin{aligned}\epsilon_{\text{imp}} &= \text{cst} - \pi \int_{-A}^A d\lambda \rho_{s,i}^{(R)}(\lambda) + \frac{1}{2} \left(\mu - \frac{H}{2} \right) \int_{-B}^B d\vartheta \rho_{c,i}^{(R)}(\vartheta) \\ &+ H \left(\frac{1}{2} \int_{-A}^A d\lambda \rho_{s,i}^{(R)}(\lambda) + \theta(p-p_0)\theta(p_1-p) + \theta(p-p_2)\theta(p_3-p) \right)\end{aligned}\quad (8.4.30)$$

In Fig. 8.5, a numerical integration of Eq. (8.4.30) is presented for the

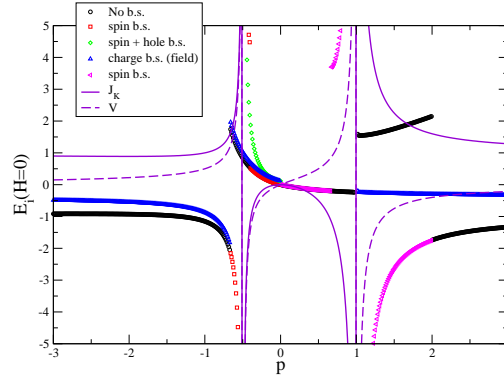


Figure 8.5: Impurity contribution to the energy for $H = 0$ and $s = 1$. Different root configurations are compared and the ground state appears to be realised by the ones described above from region (1) to (5). The Kondo coupling J_K and the potential V are also superimposed on the finite-size spectrum.

special case of zero-field and a spin-1 impurity. One can confirm on behalf of this graph that the five configurations we wrote previously correspond to the ground state of the system. Other bound states configuration leading to excitations in the spectrum are also depicted, but we will not comment any longer on their existence and will concentrate on the properties of the ground state. Super-imposed to this finite-size spectrum, are plotted the potential V and the Kondo coupling J_K . We can clearly see different regimes in the coupling constants themselves which will help us understanding physically the structure of bound states in the ground state. In region (1), $p < \frac{2}{1-4s}$, both V are small and positive: No bound states is expected in the ground state configuration. In region (2), $\frac{2}{1-4s} \leq p < -\frac{1}{2s}$, V and J_K grow to infinity

and surely a bound state should be occupied to insure a stable configuration. The first threshold appearing at the level of the BAE is in the spin sector. Therefore, the strong anti-ferromagnetic (AF) Kondo coupling will enforce the occupation of a spin bound state to minimise the energy. The region we called (3), $-\frac{1}{2s} \leq p < 1$, is, regarding the coupling constant, divided into two regimes: first, for $-\frac{1}{2s} \leq p < 0$, both V and J_K are negative. Since we explicitly chose a Sutherland description of the elementary excitations in terms of spinons and holons, neither an attractive V nor a ferromagnetic (F) J_K could leave to the formation of a bound state. The ground state is thus described by the bare BAE (8.3.21); second, if $0 \leq p < 1$, we see that the Kondo coupling remains ferromagnetic but the potential becomes large and repulsive as p approaches 1. Nevertheless, the analysis of the phase shift in the BAE shows that an holon BS is allowed only for $p \geq 1$, and the system will prefer to stay into a configuration without BS. This mechanism signals a competition between the potential and the Kondo terms in the boundary Hamiltonian. We pursue in region (4), $1 \leq p < 2$. Here, the Kondo coupling is large AF while the potential becomes attractive. The holon BS allowed as a solution of the BAE is therefore an excited state as we can confirm from the numerics in Fig. 8.5. Instead, the system finds preferable to relax the strong AF constraint by binding a spinon at the impurity site. In region (5), $p \geq 2$, both V and J_K stay small and the situation is the same as the one for region (1) i.e. the ground state root configuration contains no BS.

8.4.2 Impurity magnetization

Having the ground state configuration of the system clarified, let us study its magnetic properties. Just like in Chap. 7, the impurity magnetization can be expressed by means of the spin and charge densities (order $1/L$):

$$M_{\text{imp}} = s + \frac{1}{4} \int_{-B}^B d\vartheta \rho_{c,i}^{(\alpha)}(\vartheta) - \frac{1}{2} \int_{-A}^A d\lambda \rho_{s,i}^{(\alpha)}(\lambda) - \theta(p - p_0)\theta(p_1 - p) - \theta(p - p_2)\theta(p_3 - p) \quad (8.4.31)$$

For finite A and B , the various BAE can be solved numerically for the various root configurations discussed above. The computation of M_{imp} as a function of the magnetic field H and for different values of p (thus different bound states configurations) is shown in Fig. 8.6, for a spin-1/2 impurity, and in Fig. 8.7, for the spin-1 case. The hole doping is fixed to be $\delta = 0.2$

One immediately notices in both Figs. 8.6 and 8.7 that, depending on p , the magnetisation curves split into two groups: the first group with a residual spin s (i.e. $M_{\text{imp}}(H = 0) = s$) for values of p lying in region (3), the second group having a residual spin $s - 1/2$. For the first group of curves, the Kondo coupling is ferromagnetic whereas for the second group, J_K is anti-ferromagnetic leading to a screening of the impurity spin by the conduction

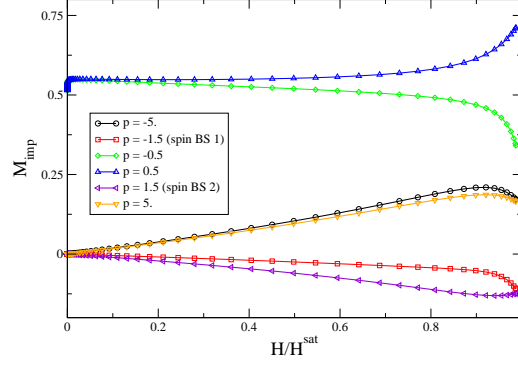


Figure 8.6: Impurity magnetization for $s = 1/2$ as a function of the uniform magnetic field. The hole concentration is fixed at $\delta = 20\%$

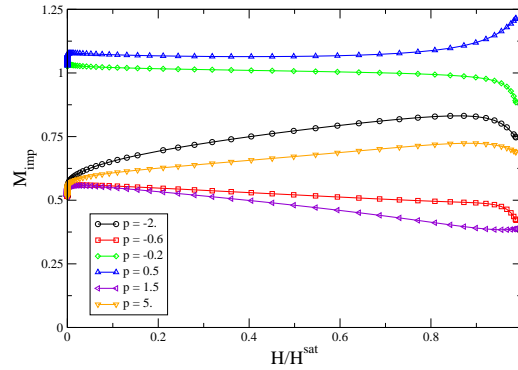


Figure 8.7: Impurity magnetization for $s = 1$ as a function of the uniform magnetic field. The hole concentration is fixed at $\delta = 20\%$

electrons. This screening mechanism has already been widely discussed in Chap. 5 in the conventional Kondo effect.

NB: Remark that M_{imp} calculated in this way can be larger than s . The reason is that the expression (8.4.31) takes all the $1/L$ -contributions from the impurity and the physical boundary into account. Those contributions are "entangled" due to the fact that we work on the projection line are cannot be substracted one from the other trivially.

Low-field behaviour: Wiener-Hopf analysis of the density equations

In order to get a better understanding of the magnetisation curves shown above, some analytical results will be useful. We first want to understand the difference between the spin-1/2 and the spin-1 case in the screening regime. We will restrict ourselves to the case of small AF Kondo coupling where signatures of the Kondo effect are expected. We shall then work in region (5) where the spectrum is described through the bare BAE (8.3.21). In the low-field regime, corresponding to $A \gg 1$, we remind that the following expression for H holds:

$$\pi A = -\ln(H/H_0) + \frac{1}{4 \ln H}, \quad H_0 = \sqrt{2\pi/e}(2\pi - C). \quad (8.4.32)$$

In this limit, it is convenient to rewrite the integral equation for ρ_s (in Fourier space) as follows

$$\begin{aligned} \rho_{s,i} = & \frac{a_{1-2/p} + a_{4s+2/p-1}}{1 + a_2} \\ & + \left(\int_{-\infty}^{-A} + \int_A^{\infty} \right) \frac{a_2}{1 + a_2} * \rho_{s,i} + \int_{-B}^B \frac{a_1}{1 + a_2} * \rho_{c,i} \end{aligned} \quad (8.4.33)$$

Therefore, using the definition (8.4.31), the low-field magnetization of the impurity is given by an integral over the density density only

$$\begin{aligned} M_{\text{imp}} &= s - \frac{1}{4} \int_{-\infty}^{\infty} d\lambda (a_{1-2/p}(\lambda) + a_{4s+2/p-1}(\lambda)) + \frac{1}{2} \int_A^{\infty} d\lambda \rho_s(\lambda) \\ &= \left(s - \frac{1}{2} \right) + \frac{1}{2} \int_A^{\infty} d\lambda \rho_s(\lambda), \quad p > 2. \end{aligned} \quad (8.4.34)$$

Introducing $g(z) = \rho_s(A + z)$ the evaluation of the impurity magnetization in the low-field limit boils down to the resolution of an integral equation for $g(z)$. This integral equation is of Wiener-Hopf type and its form is often met in dealing with impurity problems (see e.g. [129])

$$\begin{aligned} g(z) = & g_0(z) + \int_{-B}^B dz' G_0(z - z' + A) \rho_c(z') \\ & \int_0^{\infty} dz' G_1(z - z') g(z') + \int_0^{\infty} dz' G_1(2A + z + z') g(z'), \end{aligned} \quad (8.4.35)$$

with the function G_α being defined as

$$G_\alpha(x) = \mathcal{F}^{-1} \left[\frac{\exp(-\alpha|\omega|/2)}{2 \cosh(\omega/2)} \right] \quad (8.4.36)$$

and

$$g_0(z) = G_{-2/p}(A + z) + G_{4s+2/p-1}(A + z) \quad (8.4.37)$$

The leading contribution to the impurity magnetization in the large A limit is obtained by

$$M_{\text{imp}}^{A \gg 1} \simeq \left(s - \frac{1}{2} \right) + \frac{1}{2} \int_0^\infty dz g_1(z) \quad (8.4.38)$$

with

$$g_1(z) = g_0(z) + C_p G_0(A + z) + \int_0^\infty dz' G_1(z - z') g_1(z'). \quad (8.4.39)$$

C_p is a constant determined by the charge sector, $C_p = \int_{-B}^B dz \exp(\pi z) \rho_c(z)$.

For $s = 1/2$ the driving term in Eq. (8.4.39) becomes proportional to G_0 and gives a linear in H contribution to the impurity magnetization, i.e. proportional to $\exp(-\pi A)$ (cf Eq. 8.4.32).

$$M_{\text{imp}} = \left(2 \cos \frac{\pi}{p} + C_p \right) \frac{e^{-\pi A}}{\sqrt{2\pi e}} \quad (8.4.40)$$

This result, derived explicitly in App. C, explains what is seen in Fig. 8.6.

For $s > 1/2$, we have to deal with contributions involving driving terms of the form $G_\alpha(A + z)$, with $\alpha \neq 0$ which are a bit tricky. They give (see App. C for details) a contribution to the magnetization of the form

$$M_\alpha = \int_0^\infty dy \frac{\sin(\pi \tilde{\alpha} y)}{y} \Gamma\left(\frac{1}{2} - y\right) \left(\frac{y}{e}\right)^y e^{-2\pi A y} \quad (8.4.41)$$

where we have introduced

$$\tilde{\alpha} = \begin{cases} \alpha - 1 & \text{if } \alpha > 0 \\ \alpha + 1 & \text{otherwise} . \end{cases} \quad (8.4.42)$$

Collecting terms together gives the form of the low field contribution of the impurity to the magnetization:

$$M_{\text{imp}} = \left(s - \frac{1}{2} \right) + C_p \frac{e^{-\pi A}}{\sqrt{2\pi e}} + \frac{1}{2\pi^{3/2}} \int_0^\infty \frac{dy}{y} \left(\sin(\pi(1 - 2/p)y) + \sin(\pi(4s + 2/p - 3)y) \right) \Gamma\left(\frac{1}{2} - y\right) \left(\frac{y}{e}\right)^y e^{-2\pi A y} . \quad (8.4.43)$$

The non-trivial field dependence of the integral in (8.4.43) is responsible for the zero-field singularity in the magnetization (see Fig. 8.7).

To summarise, deep into the region where the impurity is screened ($p > 2$), a WH calculation allows to extract the correct behaviour of the magnetization in the low-field limit. For $s = 1/2$, M_{imp} is linear in H whereas for $s > 1/2$, M_{imp} diverges for $H \rightarrow 0$. This latter observation can be understood physically by saying that the impurity is underscreened, the conduction electrons carrying a spin-1/2. Therefore, in the Kondo regime, remains an effective spin $s - 1/2 > 0$, that is essentially free, obeying a Curie-law for the susceptibility.

To explain the difference in behaviour between the screened and unscreened case for $s = 1/2$, we should compare the results of the magnetization in region (3) and (5) for example. Again we shall start from the same equations for the densities with driving terms given by Eq. (8.4.27). In region (3), and without loss of generality for $0 < p < 1$, one has to solve the WH integral equation (8.4.39) with driving term

$$g_0(z) = -G_{2/p-2}(A+z) + G_{2/p}(A+z) . \quad (8.4.44)$$

This leads to the following expression for the magnetization of the impurity

$$M_{\text{imp}} = C_p \frac{e^{-\pi A}}{\sqrt{2\pi e}} + \frac{1}{\pi^{3/2}} \int_0^\infty dy \frac{\sin(\pi(2/p-1)y)}{y} \Gamma\left(\frac{1}{2}-y\right) \left(\frac{y}{e}\right)^y e^{-2\pi A y} . \quad (8.4.45)$$

The latter equation contains again this integral which is not present in Eq. (8.4.40). This particular term explains, formally, the difference between the low-field behaviour of the magnetization in the screened and un-screened regime.

NB: the later discussion can be extended to all regions (1) to (5). One has to carry out the WH calculation of M_{imp} with the appropriate driving terms.

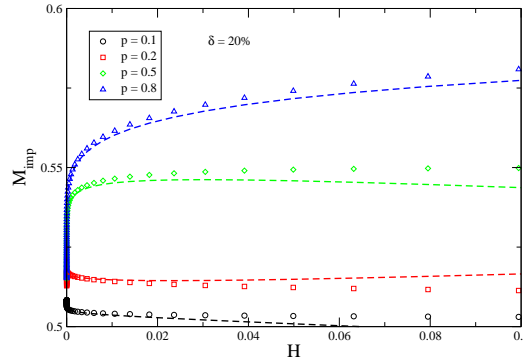


Figure 8.8: Zoom on the low-field behaviour of M_{imp} for $0 < p < 1$ (region (3)) and $s = 1/2$. The points have been obtained from a numerical resolution of the BAE and the lines are the WH expression (8.4.45)

Behaviour close to saturation

As we already mentioned in Chap. 7, the presence of a finite band-width in the host system induces that above the saturation field, $H^{\text{sat}} = 4 \cos^2(\pi\delta/2)$,

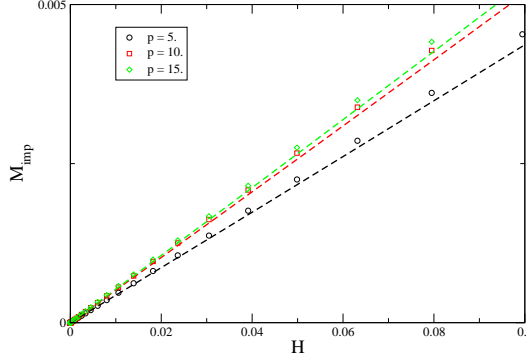


Figure 8.9: Zoom on the low-field behaviour of M_{imp} for $p > 2$ (region (5)) and $s = 1/2$. The points have been obtained from a numerical resolution of the BAE and the lines are the WH expression 8.4.40

the ground state is fully polarised. The regime of magnetic field values close to the saturation corresponds to $A \rightarrow A^{\text{sat}} = \frac{1}{2}\sqrt{4/H^{\text{sat}} - 1}$ while $B \rightarrow \infty$. In this limit, the equations for the densities (8.4.26) can be solved easily by Fourier transform. Since the analysis of the behaviour of the magnetization close to saturation is the same for all regions, let us, for the sake of clarity, focus on the region of low-boundary field $0 < p < 1$. In that case, one obtains the value of the impurity magnetization at saturation to be

$$M_{\text{imp}}^{\text{sat}} = s + \frac{1}{4} \left(1 - \int_{-A}^A d\nu \rho_{s,i}^{(R)}(\nu) \right). \quad (8.4.46)$$

In the limit $B \rightarrow \infty$, the spin density has a simple form:

$$\rho_s^{(R)}(\nu) = a_{4s+2/p-1}(\nu) \quad (8.4.47)$$

Performing the integral in Eq. (8.4.46) explicitly we can write

$$M_{\text{imp}}^{\text{sat}} = s + \frac{1}{4} \left(1 - \frac{2}{\pi} \arctan \frac{2Ap}{4sp + 2 - p} \right) \quad (8.4.48)$$

We notice that at maximum hole doping ($\delta = 1$) $M_{\text{imp}}^{\text{sat}}$ given by Eq. (8.4.48) is just equal to s , the strength of the impurity spin, as it should be.

To understand the effect of small doping on top of the fully polarised state let us have a look at the effective boundary Hamiltonian at saturation. If one imposes $s^z \equiv s$ and $S_1^z \equiv n_1/2$ in Eq. (8.3.19) we obtain

$$\mathcal{H}_{\text{sat}} = \tilde{V} n_1 \quad \tilde{V} = \frac{p}{2sp + 1}. \quad (8.4.49)$$

This means that at saturation the spectrum of the boundary impurity is essentially controlled by an effective local chemical potential \tilde{V} . It is interesting to notice that the result (8.4.48) can be obtained starting from the BAE of the t - J chain with a just a boundary potential, changing p to \tilde{V} . Using this analogy, one can compute the spin density in the limit $B \rightarrow \infty$ to be $\rho_{s,i}(\mu) = a_{1-2/\tilde{V}}(\mu)$ which is nothing than Eq. (8.4.47).

Slightly below H^{sat} a close formula for the impurity magnetization can be derived, just like we did in Chap. 7. Within our example, for $0 < p < 1$, an expansion in $1/B$ in the integral over $\rho_{c,i}^{(R)}$ in Eq. (8.4.26) leads to

$$M_{\text{imp}}^{B \gg 1} = 1 - \frac{1}{\pi} \left(2 - \frac{1}{2} \frac{\pi\delta}{\arctan \sqrt{\frac{4-h}{h}}} \right) \arctan \left(\frac{p\sqrt{\frac{4-h}{h}}}{2 + 4sp - p} \right) + \frac{p-1}{p} \left(1 - \frac{1}{2} \frac{\pi\delta}{\arctan \sqrt{\frac{4-h}{h}}} \right) \quad (8.4.50)$$

which captures the behaviour of the impurity magnetization in the "large field" limit. In Fig. 8.10 we compare this asymptotic to a numerical calculation and the agreement is excellent.

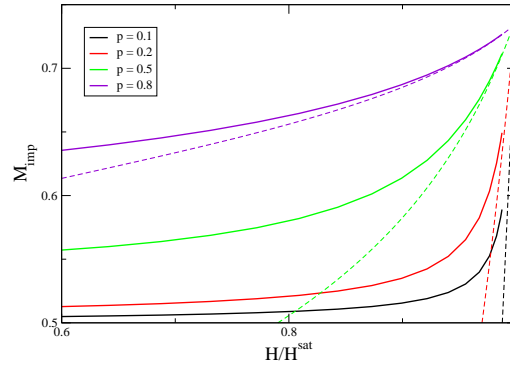


Figure 8.10: Zoom on the high-field behaviour of M_{imp} for $0 < p < 1$ (region (3)) and $s = 1/2$. The solid curves are the result of a numerical calculation and the dashed lines are the asymptotic expression (8.4.50)

8.5 Summary and Outlook

In this Chapter, we constructed and studied an integrable model of a pure Kondo spin in an open t - J chain. Using the techniques we have learned

from Chapters 6 and 7, we were able to combine an inhomogeneity together with a boundary chemical potential p . Remarkably, when the parameters characterising the impurity, such as the spin strength s or the spectral shift t , are adjusted in a particular way with respect to p , the charge fluctuations are completely suppressed and the impurity becomes purely magnetic. This 'projection' has the consequence of breaking the standard p - h symmetry at the level of the bare BAE. Instead, we have seen that the equivalence of the Bethe ansätze obtained from different reference states relies on the proper choice of bound states configurations to select the relevant sector (spin s or spin $(s - 1/2)$).

Having clarified the way the spectrum of the Kondo impurity problem should be described, we made use of the techniques introduced in Chapter 7 to calculate the contribution of the impurity to the magnetisation. Here we were able to identify essentially two different regimes: First, if the Kondo coupling entering the effective Hamiltonian is ferromagnetic then the impurity spin is free and have a diverging Curie-like susceptibility for zero field. Second if the Kondo coupling is antiferromagnetic (AF), then screening of the impurity is effective at small energies and signatures of the Kondo effect are likely. In the non-trivial AF-regime, a clear distinction between the $s = 1/2$ impurity and the $s > 1/2$ case appears. The $s = 1/2$ situation corresponds to the standard Kondo effect where the impurity is exactly screened by the host electrons. The low-field magnetization is linear in H in this case. In the $s > 1/2$ scenario the impurity is only partially screened and the residual spin $s - 1/2$ acts like a free spin. The magnetization exhibits a zero-field singularity in this case.

Note that despite the striking similarity with the textbook Kondo effect we discussed in Chapter 5, the ground state here is always a non-Fermi liquid since the bulk is strongly correlated. It would be, in our opinion, interesting to analyse the situation of an over-screened Kondo impurity within this integrable lattice model approach. In that particular case if the spin density of the bulk electrons is higher than the impurity spin, a non-Fermi liquid fixed point is expected even without interaction in the bulk. Practically, one could study the situation where the bulk is constructed from a $[s]_+$ representation while the impurity relies on $[s']_+$, with $s > s'$. A bulk Hamiltonian obtained from the $[s > 1/2]_+$ representation has already been studied in connection with the physics of doped one-dimensional magnets [48]. But the extension to the impurity problem we are arguing raises several new issues: 1) Open boundary conditions should be incorporated. 2) One would have to verify the existence of simple c -numbered solution of the RE in this case. 3) Is a simple projection condition discarding one spin multiplet still holds? 4) Finally, the question of the emergence of a bound states spectrum should be answered.

Appendix A

The (super)algebra $gl(2|1)$

A.1 Generators

Apart from the generators $1, S^z, S^\pm$ forming an (ungraded) $gl(2)$ subalgebra, $gl(2|1)$ has an additional generator B of even parity (charge), commuting with the spin operators, and four odd parity generators V^\pm and W^\pm . The commutation relations between even and odd generators are listed below:

$$\begin{aligned} [S^z, V^\pm] &= \pm \frac{1}{2} V^\pm, & [S^\pm, V^\pm] &= 0, & [S^\mp, V^\pm] &= V^\mp, \\ [S^z, W^\pm] &= \pm \frac{1}{2} W^\pm, & [S^\pm, W^\pm] &= 0, & [S^\mp, W^\pm] &= W^\mp, \\ [B, V_\pm] &= \frac{1}{2} V_\pm, & [B, W_\pm] &= -\frac{1}{2} W_\pm. \end{aligned}$$

The odd generators satisfy anticommutation relations

$$\begin{aligned} \{V^\pm, V^\pm\} &= \{V^\pm, V^\mp\} = \{W^\pm, W^\pm\} = \{V^\pm, W^\mp\} = 0, \\ \{V^\pm, W^\pm\} &= \pm \frac{1}{2} S^\pm, & \{V^\pm, W^\mp\} &= \frac{1}{2} (S^z \pm B). \end{aligned}$$

These relations are visualised graphically in the root diagram of the superalgebra $gl(2|1)$ (cf Fig. A.1)

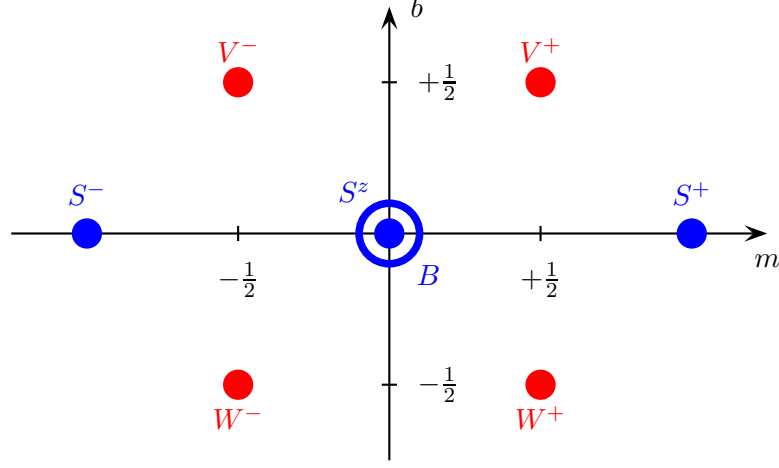
A.2 Irreducible representations

The irreducible representations of $gl(2|1)$ can be classified into typical and atypical ones [120, 105]. With respect to the even parity $U(1)$ and $SU(2)$ subalgebras they can be decomposed into spin multiplets and are conveniently labelled by the eigenvalues of the even parity operators B, \mathbf{S}^2 and S^z .

A.2.1 $[b, s]$

The typical $8s$ -dimensional representation $[b, s]$ contains four spin-multiplets

$$\begin{aligned} \{&|b, s, m\rangle, m = -s, \dots, s\}, \\ \{&|b, s - 1, m\rangle, m = -s + 1, \dots, s - 1\}, \\ \{&|b \pm \frac{1}{2}, s - \frac{1}{2}, m\rangle, m = -s + \frac{1}{2}, \dots, s - \frac{1}{2}\}. \end{aligned}$$

Figure A.1: Root diagram of $gl(2|1)$.

Explicitly, for $s = 1/2$, we have for the bosonic generators

$$S^+ = c_{\uparrow}^{\dagger} c_{\downarrow} \quad (\text{A.2.1})$$

$$S^- = c_{\downarrow}^{\dagger} c_{\uparrow} \quad (\text{A.2.2})$$

$$S^+ = \frac{1}{2}(c_{\uparrow}^{\dagger} c_{\uparrow} - c_{\downarrow}^{\dagger} c_{\downarrow}) \quad (\text{A.2.3})$$

$$B = b + \frac{1}{2}(1 - N) \quad (\text{A.2.4})$$

and

$$V^+ = \frac{1}{2}[\sqrt{2b+1}(1 - n_{\uparrow}) + \sqrt{2b-1}n_{\uparrow}]c_{\downarrow} \quad (\text{A.2.5})$$

$$V^- = -\frac{1}{2}[\sqrt{2b+1}(1 - n_{\downarrow}) + \sqrt{2b-1}n_{\downarrow}]c_{\uparrow} \quad (\text{A.2.6})$$

$$W^+ = \frac{1}{2}[\sqrt{2b+1}(1 - n_{\downarrow}) + \sqrt{2b-1}n_{\downarrow}]c_{\uparrow}^{\dagger} \quad (\text{A.2.7})$$

$$W^- = \frac{1}{2}[\sqrt{2b+1}(1 - n_{\uparrow}) + \sqrt{2b-1}n_{\uparrow}]c_{\downarrow}^{\dagger} \quad (\text{A.2.8})$$

for the fermionic ones.

A.2.2 $[s]_{\pm}$

As $b \rightarrow \pm s$ these representations degenerate into two atypical ones. Atypical representations are denoted by $[s]_{\pm}$ and contain $4s + 1$ states in two spin

multiplets

$$\begin{aligned} & \{|\pm s, s, m\rangle, m = -s, \dots, s\}, \\ & \{|\pm(s + \frac{1}{2}), s - \frac{1}{2}, m\rangle, m = -s + \frac{1}{2}, \dots, s - \frac{1}{2}\} \end{aligned}$$

respectively. When no confusion is possible we denote the $SU(2)$ highest weight states in the atypical representation $[s]_+$ by $|s, s, s\rangle \equiv |s\rangle$ and $|s + \frac{1}{2}, s - \frac{1}{2}, s - \frac{1}{2}\rangle \equiv |s - \frac{1}{2}\rangle$.

An important particular example is the three-dimensional $[1/2]_+$ case which is the 'natural' representation on which is constructed the t - J model. doublet $(1/2, 1/2)$ and singlet $(1, 0)$. We make the association $|\uparrow\rangle = |\frac{1}{2}, \frac{1}{2}, \frac{1}{2}\rangle$, $|\downarrow\rangle = |\frac{1}{2}, \frac{1}{2}, -\frac{1}{2}\rangle$ for the doublet and $|0\rangle = |1, 0, 0\rangle$ for the singlet. The generators are obtained by taking $b = 1/2$ above... N.B. :The superalgebra $gl(2|1)$ has two Casimir operators, we have used the quadratic one

$$C_2 = B^2 - \mathbf{S}^2 + W_- V_+ - W_+ V_- + V_- W_+ - V_+ W_- \quad (\text{A.2.9})$$

to express the \mathcal{L} -operator and the Hamiltonian in the main text. On a typical representation $[b, s]$, C_2 takes the value $b^2 - s^2$ while it vanishes on the atypical ones for any s .

A.3 Matrix representation

A.3.1 $[b, s]$

$$S^\pm |b, s, m\rangle = \sqrt{(s \mp m)(s \pm m + 1)} |b, s, m \pm 1\rangle \quad (\text{A.3.10})$$

on $(b, s), (b - \frac{1}{2}, s - \frac{1}{2}), (b + \frac{1}{2}, s - \frac{1}{2}), (b, s - 1)$

$$V^\pm = \begin{pmatrix} 0 & \epsilon \sqrt{s \pm m + \frac{1}{2}} & 0 & 0 \\ 0 & 0 & 0 & 0 \\ \pm \alpha \sqrt{s \mp m} & 0 & 0 & \tau \sqrt{s \pm m} \\ 0 & \pm \zeta \sqrt{s \mp m - \frac{1}{2}} & 0 & 0 \end{pmatrix} \quad (\text{A.3.11})$$

$$W^\pm = \begin{pmatrix} 0 & 0 & \gamma \sqrt{s \pm m + \frac{1}{2}} & 0 \\ \pm \beta \sqrt{s \mp m} & 0 & 0 & \omega \sqrt{s \pm m} \\ 0 & 0 & 0 & 0 \\ 0 & 0 & \pm \delta \sqrt{s \mp m - \frac{1}{2}} & 0 \end{pmatrix} \quad (\text{A.3.12})$$

The parameters α, \dots, ω satisfy

$$\begin{pmatrix} \alpha & \zeta \\ \omega & \gamma \end{pmatrix} \cdot \begin{pmatrix} \epsilon & \delta \\ \tau & \beta \end{pmatrix} = 0 \quad \alpha\gamma = \zeta\omega = \frac{s+b}{4s} \quad \beta\epsilon = \delta\tau = \frac{s-b}{4s} \quad (\text{A.3.13})$$

A.3.2 $[\frac{1}{2}]_+$

In the natural basis $\{|\downarrow\rangle = |\frac{1}{2}, \frac{1}{2}, -\frac{1}{2}\rangle, |\uparrow\rangle = |\frac{1}{2}, \frac{1}{2}, -\frac{1}{2}\rangle, |0\rangle = |1, 0, 0\rangle\}$ the bosonic generators take the following matrix form

$$S^+ = \begin{pmatrix} 0 & 1 & 0 \\ 0 & 0 & 0 \\ 0 & 0 & 0 \end{pmatrix} \quad (\text{A.3.14})$$

$$S^- = \begin{pmatrix} 0 & 0 & 0 \\ 1 & 0 & 0 \\ 0 & 0 & 0 \end{pmatrix} \quad (\text{A.3.15})$$

$$S^z = \begin{pmatrix} \frac{1}{2} & 0 & 0 \\ 0 & -\frac{1}{2} & 0 \\ 0 & 0 & 0 \end{pmatrix} \quad (\text{A.3.16})$$

$$B = \begin{pmatrix} \frac{1}{2} & 0 & 0 \\ 0 & \frac{1}{2} & 0 \\ 0 & 0 & 1 \end{pmatrix} \quad (\text{A.3.17})$$

and the fermionic generators

$$V^+ = \begin{pmatrix} 0 & 0 & 0 \\ 0 & 0 & 0 \\ 0 & \frac{1}{\sqrt{2}} & 0 \end{pmatrix} \quad (\text{A.3.18})$$

$$V^- = \begin{pmatrix} 0 & 0 & 0 \\ 0 & 0 & 0 \\ -\frac{1}{\sqrt{2}} & 0 & 0 \end{pmatrix} \quad (\text{A.3.19})$$

$$W^+ = \begin{pmatrix} 0 & 0 & \frac{1}{\sqrt{2}} \\ 0 & 0 & 0 \\ 0 & 0 & 0 \end{pmatrix} \quad (\text{A.3.20})$$

$$W^- = \begin{pmatrix} 0 & 0 & 0 \\ 0 & 0 & \frac{1}{\sqrt{2}} \\ 0 & 0 & 0 \end{pmatrix} \quad (\text{A.3.21})$$

Appendix B

Density equations for the open t - J chain

In this appendix we derive the equations for the densities in a general open t - J chain with boundary terms.

Starting from the BAE (7.2.7), we choose the roots $\{\lambda_j\}_{j=1,\dots,M_s}$ and $\{\vartheta_\gamma\}_{\gamma=1,\dots,M_c}$ to be real. Taking the logarithm of the BAE gives

$$\begin{aligned} \frac{2\pi}{L} I_j &= \left(2 + \frac{1}{L}\right) \theta(\lambda_j) - \frac{1}{L} \sum_k \theta\left(\frac{\lambda_j - \lambda_k}{2}\right) + \theta\left(\frac{\lambda_j + \lambda_k}{2}\right) \\ &\quad + \frac{1}{L} \sum_\beta \theta(\lambda_j - \vartheta_\beta) + \theta(\lambda_j + \vartheta_\beta) + \frac{1}{L} \kappa(\lambda_j), \\ \frac{2\pi}{L} J_\gamma &= \frac{1}{L} \sum_k \theta(\vartheta_\gamma - \lambda_k) + \theta(\vartheta_\gamma + \lambda_k) + \frac{1}{L} \omega(\vartheta_\gamma). \end{aligned} \quad (\text{B.0.1})$$

Here, I_j , J_γ are integers and $\theta(x) = 2 \arctan(2x)$. The functions $\kappa(\lambda_j)$ and $\omega(\vartheta_\gamma)$ are the real part of the logarithm of $\Phi_s(\lambda_j)$ and $\Phi_c(\vartheta_\gamma)$ respectively. The ground state for given magnetic field H and chemical potential μ is obtained by filling all vacancies for the integers I_j from 1 to $I_{\max} = M_s$ and all vacancies for the integers J_γ between 1 and $J_{\max} = M_c$. Inserting this description into the Bethe equations (B.0.1) and then subtracting subsequent equations for j and $j + 1$ and γ and $\gamma + 1$ we obtain the following equations for the densities $\varrho_s(\lambda_j) = \frac{1}{L(\lambda_{j+1} - \lambda_j)}$ and $\varrho_c(\vartheta_\gamma) = \frac{1}{L(\vartheta_{\gamma+1} - \vartheta_\gamma)}$

$$\begin{aligned} \varrho_s(\lambda_j) &= 2a_1(\lambda_j) - \frac{1}{L} \sum_\beta a_2(\lambda_j - \lambda_k) + a_2(\lambda_j + \lambda_k) \\ &\quad + \frac{1}{L} \sum_\beta a_1(\lambda_j - \vartheta_\beta) + a_1(\lambda_j + \vartheta_\beta) + \frac{1}{L} \left(\frac{\kappa'(\lambda_j)}{2\pi} + a_1(\lambda_j) \right) \\ \varrho_c(\vartheta_\gamma) &= \frac{1}{L} \sum_\alpha a_1(\vartheta_\gamma - \lambda_k) + a_1(\vartheta_\gamma + \lambda_k) + \frac{1}{2\pi L} \omega'(\vartheta_\gamma). \end{aligned} \quad (\text{B.0.2})$$

Now we follow [46] and rewrite (B.0.2) in terms of a set of “doubled” variables

$$\begin{aligned} \nu_j &= \begin{cases} -\lambda_{M_s-j} & j = 0, \dots, M_s \\ \lambda_{j-M_s} & j = M_s + 1, \dots, 2M_s \end{cases} \\ \nu_\gamma^{(1)} &= \begin{cases} -\vartheta_{M_c-\gamma} & \gamma = 0, \dots, M_c \\ \vartheta_{\gamma-M_c} & \gamma = M_c + 1, \dots, 2M_c \end{cases}, \end{aligned} \quad (\text{B.0.3})$$

where we defined $\lambda_0 = 0$ and $\vartheta_0 = 0$. Now we take the thermodynamic limit of the equations (B.0.2) written in the new variables. This is done by using the Euler-Maclaurin formula to turn sums into integrals. Note that we should subtract explicitly terms depending on the spectral parameters located at zero. After some manipulations we arrive at following coupled integral equations for the densities $\rho_s(\nu_j) = \frac{1}{L(\nu_{j+1}-\nu_j)}$ and $\rho_c(\nu_\gamma^{(1)}) = \frac{1}{L(\nu_{\gamma+1}^{(1)}-\nu_\gamma^{(1)})}$

$$\begin{aligned} \rho_s(\lambda) &= 2a_1(\lambda) - \int_{-A}^A d\mu a_2(\lambda - \mu) \rho_s(\mu) + \int_{-B}^B d\vartheta a_1(\lambda - \vartheta) \rho_c(\vartheta) \\ &\quad + \frac{1}{L} \left(\frac{\kappa'(\lambda)}{2\pi} + a_2(\lambda) \right) \\ \rho_c(\vartheta) &= \int_{-A}^A d\lambda a_1(\vartheta - \lambda) \rho_s(\lambda) + \frac{1}{L} \left(\frac{\omega'(\vartheta)}{2\pi} - a_1(\vartheta) \right), \end{aligned} \quad (\text{B.0.4})$$

where A and B are the spectral parameters corresponding to the maximal taken integers I_j and J_γ plus $\frac{1}{2}$. Higher order terms in the Euler-Maclaurin expansion have been dropped as they turn out to not contribute to the surface energy.

Appendix C

The Wiener-Hopf method

The Wiener-Hopf (WH) technique is widely used as a method to solve integral equations. We have seen throughout this thesis that the Bethe-Ansatz equations giving the properties of an integral model, are, in the continuum limit, expressed in terms of integral equations for the Bethe root densities.

C.1 Wiener-Hopf factorization

In the examples we have met so far (Lai and Yang or t - J model), the WH-type integral equation we were confronted to is the form

$$g(z) = g_0(z) + \int_0^\infty dz' G_1(z - z')g(z') \quad (\text{C.1.1})$$

where we should define

$$G_\beta(x) = \int_{-\infty}^\infty \frac{d\omega}{2\pi} e^{-i\omega x} \frac{e^{-\beta|x|/2}}{2 \cosh \frac{\omega}{2}}. \quad (\text{C.1.2})$$

The first key-step of the WH technique is to find a proper factorization of the Fourier transformed kernel $G_1(\omega)$

$$[1 - G_1(\omega)]^{-1} = G^+(\omega)G^-(\omega), \quad \lim_{\omega \rightarrow \infty} G^\pm(\omega) = 1 \quad (\text{C.1.3})$$

into functions $G^\pm(\omega)$ which are analytic for $\text{Im} \omega > 0$ (< 0), respectively. For the t - J model these techniques have been applied before [121, 39] and the factorization of the kernel is known to be

$$G^-(\omega) = G^+(-\omega) = \frac{\sqrt{2\pi}}{\Gamma(\frac{1}{2} + i\frac{\omega}{2\pi})} \left(\frac{i\omega}{2\pi e} \right)^{\frac{i\omega}{2\pi}}. \quad (\text{C.1.4})$$

C.2 Applications

In this section we want to solve the function g and to compute its integral in four relevant types of driving terms g_0 .

C.2.1 $g_0(z) = G_0(A + z)$

This kind of driving term already appears in the calculation of bulk quantities such as the dressed energies for the t - J model. Following Refs. [121, 39] we find for g

$$g^+(\omega) = iG^+(\omega)G^-(-i\pi)\frac{e^{-\pi A}}{\omega + i\pi} \equiv \mathcal{G}(\omega). \quad (\text{C.2.5})$$

Using the explicit expressions (C.1.4) we obtain

$$\int_0^\infty dz g(z) = g^+(\omega = 0) = \sqrt{\frac{2}{e\pi}}e^{-\pi A}, \quad (\text{C.2.6})$$

which will be necessary to compute the impurity's magnetization.

C.2.2 $g_0(z) = G_\beta(z + A) + G_{-\beta}(z + A)$

In this case, the analysis of the WH equation is completely analogous to the first case and we find

$$g^+(\omega) = 2iG^+(\omega)G^-(-i\pi)\frac{e^{-\pi A}}{\omega + i\pi} \cos\left(\frac{\pi\beta}{2}\right) = 2 \cos\left(\frac{\pi\beta}{2}\right)\mathcal{G}(\omega). \quad (\text{C.2.7})$$

C.2.3 $g_0(z) = G_\alpha(z + A)$

In the case of a driving of the form $g_0(z) = G_\alpha(z + A)$ with $\alpha \neq 0$ the situation is a little more involved. The Fourier transform of the driving term is easily $g_0^{(R)}(\omega) = \text{sgn}(\alpha)G_\alpha(\omega)e^{-i\omega A}$. One encounters a similar WH equation with such a driving term in the exact solution of the s - d exchange model. There, α plays the role of the impurity spin. Following the work of Tsvetick and Wiegmann [129] one obtains

$$g^+(\omega = 0) = \text{sgn}(\alpha)\frac{i}{2\pi^{3/2}} \int_{-\infty}^\infty d\omega \frac{\Gamma(\frac{1}{2} + i\omega)}{\omega + i0^+} e^{2i\pi\omega A} f_+^{\alpha+1}(\omega) f_-^\alpha(\omega) \quad (\text{C.2.8})$$

where Γ is the Gamma function. The right-hand side of Eq. (C.2.8) can be evaluated by contour integration. This leads to the following result for the integral over g

$$\int_0^\infty dz g(z) = \text{sgn}(\alpha)\frac{1}{2\pi^{3/2}} \int_0^\infty dy \frac{\sin(\pi\tilde{\alpha}y)}{y} \Gamma\left(\frac{1}{2} - y\right) \left(\frac{y}{e}\right)^y e^{-2\pi Ay} \quad (\text{C.2.9})$$

where we have introduced

$$\tilde{\alpha} = \begin{cases} \alpha - 1 & \text{if } \alpha > 0 \\ \alpha + 1 & \text{otherwise.} \end{cases} \quad (\text{C.2.10})$$

$$\mathbf{C.2.4} \quad g_0(z) = \int_0^\infty dz' G_1(2A + z + z')G_0(A + z')$$

Finally, the driving term we would like to consider is a the form: $g_0(z) = \int_0^\infty dz' G_1(2A + z + z')G_0(A + z')$. This particular driving term enters in the computation of sub-leading contribution to the thermodynamics in the t - J model and, in particular, the characterization of the logarithmic singularity in the low-field susceptibility. Following Ref. [39], we perform a Laplace transform of $g_0(z)$ to obtain:

$$g_0(z) \simeq \frac{1}{4\pi} \int_0^\infty dx e^{-2Ax} e^{-|z|x} \mathcal{G}(ix) (x + \dots), \quad (\text{C.2.11})$$

where we have used the asymptotic expansion of the function $G_1(z) \sim 1/4\pi z^2 + \mathcal{O}(z^{-4})$. Now the solution of the Wiener–Hopf equation is given by

$$g^+(\omega) \simeq G^+(\omega) \frac{i}{4\pi} \int_0^\infty dx e^{-2Ax} (x + \dots) \frac{G^+(ix) \mathcal{G}(ix)}{\omega + ix} \quad (\text{C.2.12})$$

The presence of the rapidly decaying factor $\exp(-2Ax)$ (remember that $A \gg 1$ at small field) in the integrand suggests the following expansion around $x = 0$

$$\mathcal{G}(ix)G^+(ix) (x + \dots) \sim 2 \frac{e^{-\pi A}}{\sqrt{e\pi}} x + \mathcal{O}(x^2). \quad (\text{C.2.13})$$

From this expression we obtain

$$\int_0^\infty dz g(z) = g^+(\omega = 0) = \sqrt{\frac{2}{e\pi}} \frac{e^{-\pi A}}{4\pi A} + \mathcal{O}\left(\frac{1}{A^2}\right). \quad (\text{C.2.14})$$

Appendix D

Derivation of the Hamiltonian (8.1.4)

In this Appendix, we give all the hints and formulas required to reproduce the boundary Hamiltonian (8.1.4). This Hamiltonian is essentially the derivative of the dressed K -matrix with respect to the spectral parameter and evaluated at the 'shift point' $\lambda = 0$. Formally we write

$$H_{\text{bimp}} = \frac{1}{2i} \frac{\partial}{\partial \lambda} \text{str}_0 \mathcal{K}_-(\lambda) \Big|_{\lambda=0}, \quad (\text{D.0.1})$$

We remind that

$$\mathcal{K}_-(\lambda) = \mathcal{L}_{\text{imp}}(\lambda + t) K_-^p(\lambda) (\mathcal{L}_{\text{imp}}(-\lambda + t))^{-1}. \quad (\text{D.0.2})$$

and

$$K_-^p(\lambda) = \text{diag} \left(1, 1, -\frac{p\lambda + i}{p\lambda - i} \right) \quad (\text{D.0.3})$$

NB: To streamline the notations, let us call $K_-^p(\lambda)$ simply $K(\lambda)$ and \mathcal{L}_{imp} simply \mathcal{L} .

Applying the chain rule for the derivative, we see that the boundary Hamiltonian is the sum of three terms,

$$\begin{aligned} H_{\text{bimp}} = & \underbrace{\mathcal{L}_{s,1}(-t) K'(0) \mathcal{L}_{s,1}(t)}_{(a)} \\ & + \underbrace{\mathcal{L}'_{s,1}(-t) K(0) \mathcal{L}_{s,1}(t)}_{(b)} \\ & + \underbrace{\mathcal{L}_{s,1}(-t) K'(0) \mathcal{L}_{s,1}(t)}_{(c)}, \quad (\text{D.0.4}) \end{aligned}$$

where we have used the normalization of \mathcal{L}

$$\mathcal{L}(\lambda) \mathcal{L}(-\lambda) = \mathbb{1}. \quad (\text{D.0.5})$$

Furthermore, we have performed the super-trace over the auxiliary space to obtain \mathcal{L} -matrices directly acting on the physical sites s (impurity) and 1 (bulk). The representation space on which \mathcal{L} acts is thus $[s]_+ \otimes [1/2]_+$ which can be decompose [105] as a direct sum of an atypical and a typical representation of $gl(2|1)$, namely

$$[s]_+ \otimes [1/2]_+ = [s + 1/2]_+ \oplus [s + 1, s] . \quad (\text{D.0.6})$$

Using this decomposing of the quantum space, the \mathcal{L} -operator can be written as [48]

$$\mathcal{L}_{s,1} = \frac{\lambda + i(s + 1/2)}{\lambda - i(s + 1/2)} \mathcal{P}_{[s+1/2]_+} - \mathcal{P}_{[s+1,s]} , \quad (\text{D.0.7})$$

where $\mathcal{P}_{[s+1/2]_+}$ (resp. $\mathcal{P}_{[s+1,s]}$) is the projector onto the representation $[s + 1/2]_+$ (resp. $[s + 1, s]$). In terms of the quadratic Casimir of $gl(2|1)$ (cf Eq. (A.2.9)), these projectors are expressed in the following way:

$$\begin{aligned} \mathcal{P}_{[s+1/2]_+} &= \mathbb{1} + \frac{C_2^{s1}}{2s + 1} \\ \mathcal{P}_{[s+1,s]} &= \frac{C_2^{s1}}{s^2 - (s + 1)^2} = -\frac{C_2^{s1}}{2s + 1} . \end{aligned} \quad (\text{D.0.8})$$

We are now in position to compute explicitly each term (a), (b) and (c) entering Eq. (D.0.4). Using the relations (D.0.7) and noticing that $K'(0) = \mathbb{1}$, we can show, after some algebra that

$$\begin{aligned} (b) &= \frac{i(2s + 1)}{t^2 + (s + 1/2)^2} + \frac{2s + 1}{(-t + i(s + 1/2))(t^2 + (s + 1/2)^2)} C_2^{(s1)} \\ &+ \frac{i}{t^2 + (s + 1/2)^2} C_2^{s1} - \frac{1}{(-t + i(s + 1/2))(t^2 + (s + 1/2)^2)} (C_2^{(s1)})^2 \end{aligned} \quad (\text{D.0.9})$$

and

$$\begin{aligned} (c) &= \frac{i(2s + 1)}{t^2 + (s + 1/2)^2} + \frac{2s + 1}{(t + i(s + 1/2))(t^2 + (s + 1/2)^2)} C_2^{(s1)} \\ &+ \frac{i}{t^2 + (s + 1/2)^2} C_2^{s1} - \frac{1}{(t + i(s + 1/2))(t^2 + (s + 1/2)^2)} (C_2^{(s1)})^2 . \end{aligned} \quad (\text{D.0.10})$$

Combining (D.0.9) and (D.0.10) together, and using the fundamental property of the Casimir, i.e.

$$(C_2^{(s1)})^2 = (2s + 1)C_2^{(s1)} \quad (\text{D.0.11})$$

we end up with the simple form

$$(b) + (c) = 2i \left[\frac{2s + 1}{t^2 + (s + 1/2)^2} + \frac{C_2^{(s1)}}{t^2 + (s + 1/2)^2} \right] . \quad (\text{D.0.12})$$

Concerning the (a) -term which will generate the bulk-impurity interaction, the computation is much lengthy but, again, all the ingredients are there, in the relations above. Formally, it reads

$$(a) = \text{cst} + \frac{2s+1}{t^2 + (s+1/2)^2} K'(0) C_2^{(s1)} + \frac{1}{t^2 + (s+1/2)^2} C_2^{(s1)} K'(0) C_2^{(s1)} . \quad (\text{D.0.13})$$

Using the expression for the Casimir (A.2.9) in terms of the generators of $gl(2|1)$ and $K'(0) = \text{diag}(0, 0, -2ip)$ we finally arrive to

$$\begin{aligned} \frac{(a)}{2i} = & -2p \left(B_1 - \frac{1}{2} \right) - \frac{2p}{t^2 + (s+1/2)^2} \left(it[B_1, C_2^{(s1)}] \right. \\ & \left. - (s + \frac{1}{2}) \{ B_1, C_2^{(s1)} \} + C_2^{(s1)} B_1 C_2^{(s1)} \right) \quad (\text{D.0.14}) \end{aligned}$$

Appendix E

Lai and Sutherland BAE

There are three different BAE for the $gl(2|1)$ supersymmetric t - J model depending on the choice of grading in the algebra that contains two fermions and one boson [42]. Here we will focus on two equivalent constructions of the spectrum of the t - J model with an $[s]_+$ -impurity which differ in the choice of the highest-weight state used for the pseudo vacuum in the algebraic Bethe ansatz. Either one can construct the Bethe states starting from the so-called Lai vacuum $|\Omega_L\rangle = |0\rangle^{\otimes L} \otimes |s + \frac{1}{2}, s - \frac{1}{2}, s - \frac{1}{2}\rangle_{imp}$ or from the so-called Sutherland vacuum $|\Omega_S\rangle = |\uparrow\rangle^{\otimes L} \otimes |s, s, s\rangle_{imp}$. The two approaches are perfectly equivalent for the description of the system's spectrum. In the case of the homogeneous chain with periodic boundary conditions, the equivalence of the Lai and Sutherland BAE has been proven in Ref. [16] using a p - h transformation introduced by Woyrnarovich [137]. The aim of this Appendix is to generalize this technique to open boundary conditions including the possibility of having boundary fields and impurity phase shifts. Nevertheless the spirit of the proof is very similar to the one derived in the periodic case.

If one starts from the Sutherland vacuum, the resulting BAE for a t - J model with boundaries are given by:

$$\begin{aligned}
 (e_1(\lambda_k))^{2L} \eta(\lambda_k) &= \prod_{j \neq k}^{N_h + N_\downarrow} e_2(\lambda_k - \lambda_j) e_2(\lambda_k + \lambda_j) \prod_{\ell=1}^{N_h} e_{-1}(\lambda_k - \vartheta_\ell) e_{-1}(\lambda_k + \vartheta_\ell), \\
 1 &= \xi(\vartheta_\ell) \prod_{j=1}^{N_h + N_\downarrow} e_1(\vartheta_\ell - \lambda_j) e_1(\vartheta_\ell + \lambda_j).
 \end{aligned}
 \tag{E.0.1}$$

where η and ξ are phase factors (rational functions in their arguments) describing the boundary and inhomogeneity scattering (see Eqs. (8.2.6)). From

the second set of these equations we find that ϑ_ℓ are zeroes of the polynomial

$$\begin{aligned}
P(w) &= \xi_+(w) \prod_{j=1}^{N_h+N_\downarrow} (w - \lambda_j + \frac{i}{2})(w + \lambda_j + \frac{i}{2}) \\
&\quad - \xi_-(w) \prod_{j=1}^{N_h+N_\downarrow} (w - \lambda_j - \frac{i}{2})(w + \lambda_j - \frac{i}{2}) \equiv 0. \quad (\text{E.0.2})
\end{aligned}$$

Here ξ_+ (resp. ξ_-) stands for the numerator (resp. denominator) of the function ξ . $P(w)$ is of degree $2(N_h + N_\downarrow) + \delta$ where δ is determined by the degree and the parity of $\xi_\pm(w)$. Hence, in addition to the first $2N_h$ roots of $P(w)$ which we identify with the roots $\{\vartheta_\ell\}$ of the BAE (E.0.1) there are $2N_\downarrow + \delta$ additional zeroes $\{x_\ell\}$. Notice that $P(w)$ is an odd polynomial in all cases considered in this paper. Consequently, the zeroes of P come in pairs $\vartheta_\ell = -\vartheta_{-\ell}$ and $x_\ell = -x_{-\ell}$ except from a single root at $x_0 = 0$. Using the residue theorem we obtain:

$$\begin{aligned}
&\sum_{\ell=1}^{N_h} \frac{1}{i} \ln \left(\frac{\lambda_k - \vartheta_\ell - \frac{i}{2}}{\lambda_k - \vartheta_\ell + \frac{i}{2}} \frac{\lambda_k + \vartheta_\ell - \frac{i}{2}}{\lambda_k + \vartheta_\ell + \frac{i}{2}} \right) \\
&= \sum_{\ell=1}^{N_h} \frac{1}{2\pi i} \oint_{\mathcal{C}_\ell} dz \frac{1}{i} \ln \left(\frac{\lambda_k - z - \frac{i}{2}}{\lambda_k - z + \frac{i}{2}} \right) \frac{d}{dz} \ln P(z) \\
&= - \sum_{\ell=1}^{N_\downarrow} \frac{1}{i} \ln \left(\frac{\lambda_k - x_\ell - \frac{i}{2}}{\lambda_k - x_\ell + \frac{i}{2}} \frac{\lambda_k + x_\ell - \frac{i}{2}}{\lambda_k + x_\ell + \frac{i}{2}} \right) \\
&\quad - \frac{1}{i} \ln \left(\frac{\lambda_k - \frac{i}{2}}{\lambda_k + \frac{i}{2}} \right) + \frac{1}{i} \ln \left(\frac{P(\lambda_k - \frac{i}{2})}{P(\lambda_k + \frac{i}{2})} \right) \quad (\text{E.0.3})
\end{aligned}$$

(the last sum runs over the nonzero x_ℓ). The contour \mathcal{C}_ℓ is chosen such that it encloses both zeroes ϑ_ℓ and $-\vartheta_\ell$ carefully avoiding the logarithm's branch cut between $\lambda_k - i/2$ and $\lambda_k + i/2$ (see Fig. E.1). By definition of P (E.0.2) we evaluate its value at both ends of the branch cuts,

$$\begin{aligned}
P(\lambda_k - \frac{i}{2}) &= -\xi_-(\lambda_k - \frac{i}{2}) \prod_{j=1}^{N_h+N_\downarrow} (\lambda_k - \lambda_j - i)(\lambda_k + \lambda_j - i), \\
P(\lambda_k + \frac{i}{2}) &= \xi_+(\lambda_k + \frac{i}{2}) \prod_{j=1}^{N_h+N_\downarrow} (\lambda_k - \lambda_j + i)(\lambda_k + \lambda_j + i). \quad (\text{E.0.4})
\end{aligned}$$

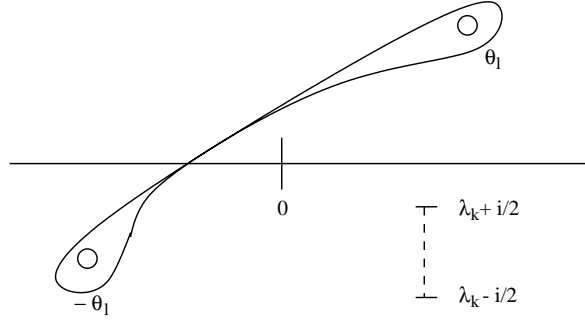


Figure E.1: The Contour \mathcal{C}_ℓ used in Eq. (E.0.3) encloses the points ϑ_ℓ and $-\vartheta_\ell$. The branch cut of the logarithm in the integrand is depicted as the dashed line connecting from $\lambda_k - i/2$ to $\lambda_k + i/2$.

Exponentiating Eq. (E.0.3) we obtain

$$\prod_{\ell=1}^{N_h} e_{-1}(\lambda_k - \vartheta_\ell) e_{-1}(\lambda_k + \vartheta_\ell) = -e_1(\lambda_k) \frac{\xi_-(\lambda_k - \frac{i}{2})}{\xi_+(\lambda_k + \frac{i}{2})} \times \prod_{\ell=1}^{N_1} e_1(\lambda_k - x_\ell) e_1(\lambda_k + x_\ell) \prod_{j=1}^{N_h+N_1} e_{-2}(\lambda_k - \lambda_j) e_{-2}(\lambda_k + \lambda_j). \quad (\text{E.0.5})$$

The last product appearing on the r.h.s. can be reexpressed as

$$\prod_{j=1}^{N_h+N_1} e_{-2}(\lambda_k - \lambda_j) e_{-2}(\lambda_k + \lambda_j) = -e_{-1}(\lambda_k) \prod_{j \neq k}^{N_h+N_1} e_{-2}(\lambda_k - \lambda_j) e_{-2}(\lambda_k + \lambda_j) \quad (\text{E.0.6})$$

since $e_{-2}(2\lambda_k) = e_{-1}(\lambda_k)$. Then, using Eq. (E.0.5) in the first of Eqs. (E.0.1) we obtain:

$$\eta(\lambda_k) [e_1(\lambda_k)]^{2L} = \frac{\xi_-(\lambda_k - \frac{i}{2})}{\xi_+(\lambda_k + \frac{i}{2})} \prod_{\ell=1}^{N_1} e_1(\lambda_k - x_\ell) e_1(\lambda_k + x_\ell) \quad (\text{E.0.7})$$

(cf. the first of the Lai equations (E.0.8)). Starting from Eq. (E.0.7), it is straightforward to apply the same procedure as before to derive the second Lai type equation.

To summarize the main result of this Appendix let us write the relation connecting the boundary phase factors within BAE in the Sutherland repre-

sentation (E.0.1) and those in the Lai representation:

$$\begin{aligned} \Phi(w_k)[e_1(w_k)]^{2L} &= \prod_{\ell=1}^{N_{\downarrow}} e_1(w_k - x_{\ell})e_1(w_k + x_{\ell}), \\ \Xi(x_{\ell}) \prod_{j=1}^{N_e} e_1(x_{\ell} - w_j)e_1(x_{\ell} + w_j) &= \prod_{m \neq \ell}^{N_{\downarrow}} e_2(x_{\ell} - x_m)e_2(x_{\ell} + x_m). \end{aligned} \quad (\text{E.0.8})$$

Comparing the result of the particle-hole transformation applied to (E.0.1) with (E.0.8) we find

$$\eta(\lambda) \frac{\xi_+(\lambda + \frac{i}{2})}{\xi_-(\lambda - \frac{i}{2})} = \Phi(\lambda), \quad \xi^{-1}(x) = \Xi(x) \frac{\Phi_-(x + \frac{i}{2})}{\Phi_+(x - \frac{i}{2})}. \quad (\text{E.0.9})$$

Bibliography

- [1] A. A. Abrikosov, *Physics* **2** (1965), 5.
- [2] I. Affleck, *Phys. Rev. Lett.* **56** (1986), 746.
- [3] I. Affleck and A. Ludwig, *Nucl. Phys. B* **352** (1991), 849.
- [4] ———, *Nucl. Phys. B* **360** (1991), 641.
- [5] ———, *Phys. Rev. Lett.* **67** (1991), 161.
- [6] ———, *Phys. Rev. B* **48** (1993), 7297.
- [7] I. Affleck and A. W. W. Ludwig, *Nucl. Phys. B* **352** (1991), 849.
- [8] E. Altman, E. Demler, and M. D. Lukin, *Phys. Rev. A* **70** (2004), 013603.
- [9] P. W. Anderson, *Phys. Rev.* **115** (1959), 2.
- [10] ———, *J. Phys. C* **3** (1970), 2436.
- [11] N. Andrei, *Phys. Rev. Lett.* **45** (1980), 379.
- [12] N. Andrei, K. Furuya, and J. H. Lowenstein, *Rev. Mod. Phys.* **55** (1983), 331.
- [13] N. Andrei and H. Johannesson, *Phys. Lett. A* **100** (1984), 108.
- [14] S. Aubin, M. H. T. Extavour, S. Myrskog, L. J. LeBlanc, J. Estève, S. Singh, P. Scrutton, D. McKay, R. McKenzie, I. D. Leroux, A. Stummer, and J. H. Thywissen, *J. Low Temp.* **140** (2005), 377.
- [15] Assa Auerbach, *Interacting Electrons and Quantum Magnetism*, Springer, 1994.
- [16] P. A. Bares, J. M. P. Carmelo, J. Ferrer, and P. Horsch, *Phys. Rev. B* **46** (1992), 14624–14654.
- [17] M. T. Batchelor, M. Bortz, X. W. Guan, and N. Oelkers, *Phys. Rev. A* **72** (2005), 061603.

- [18] G. Bedürftig, F. H. L. Essler, and H. Frahm, *Phys. Rev. Lett.* **77** (1996), 5098–5101.
- [19] ———, *Nucl. Phys. B* **489** (1997), 697–736.
- [20] G. Bedürftig and H. Frahm, *J. Phys. A* **32** (1999), 4585–4591.
- [21] N. Beisert, C. Kristjansen, and M. Staudacher, *Nucl. Phys. B* **664** (2003), 131–184.
- [22] N. Beisert and M. Staudacher, *Nucl. Phys. B* **670** (2003), 439–463.
- [23] ———, *Nucl. Phys. B* **676** (2004), 3–42.
- [24] A. A. Belavin, A. M. Polyakov, and A. B. Zamolodchikov, *Nucl. Phys. B* **241** (1984), 333.
- [25] H. Bethe, *Z. Physik* **31** (1931), 205.
- [26] H. W. Blöte, J. L. Cardy, and M. P. Nightingale, *Phys. Rev. Lett.* **56** (1986), 742.
- [27] M. Bortz and J. Sirker, *J. Stat. Mech.: Theor. Exp.* (2006), P01007.
- [28] J. S. Caux and J. M. Maillet, *Phys. Rev. Lett.* **95** (2005), 077201.
- [29] M. A. Cazalilla and A. F. Ho, *Phys. Rev. Lett.* **91** (2003), 150403.
- [30] V. V. Cheianov, H. Smith, and M. B. Zvonarev, *Phys. Rev. A* **71** (2005), 033610.
- [31] I. V. Cherednik, *Theor. Math. Phys.* **61** (1984), 977.
- [32] A. J. Daley, C. Kollath, U. Schollwöck, and G. Vidal, *J. Stat. Mech.: Theor. Exp.* (2004), P04005.
- [33] K. K. Das, *Phys. Rev. Lett.* **90** (2003), 170403.
- [34] W. J. de Haas and J. de Boer, *Physica* **1** (1934), 609.
- [35] W. J. de Haas, J. de Boer, and G. J. van den Berg, *Physica* **1** (1934), 1115.
- [36] H. J. de Vega and A. González-Ruiz, *J. Phys. A* **27** (1994), 6129–6137.
- [37] R. Egger and A. Komnik, *Phys. Rev. B* **57** (1998), 10620.
- [38] S. Eggert, I. Affleck, and M. Takahashi, *Phys. Rev. Lett.* **73** (1994), 332.
- [39] F. H. L. Essler, *J. Phys. A* **29** (1996), 6183–6203.

- [40] F. H. L. Essler and H. Frahm, *Phys. Rev. B* **56** (1997), 6631.
- [41] F. H. L. Essler, H. Frahm, F. Göhmann, A. Klümper, and V. E. Korepin, *The One-Dimensional Hubbard Model*, Cambridge University Press, Cambridge, 2005.
- [42] F. H. L. Essler and V. E. Korepin, *Phys. Rev. B* **46** (1992), 9147.
- [43] J. Estève, C. Aussibal, T. Schumm, C. Figl, D. Maily, I. Bouchoule, C. I. Westbrook, and A. Aspect, *Phys. Rev. A* **70** (2004), 043629.
- [44] S. Richard et al., *Phys. Rev. Lett.* **91** (2003), 010405.
- [45] H. Fan, M. Wadati, and R. H. Yue, *J. Phys. A* **33** (2000), 6187–6202.
- [46] P. Fendley and H. Saleur, *Nucl. Phys. B* **428** (1994), 681–693.
- [47] M. Flicker and E. H. Lieb, *Phys. Rev.* **161** (1967), 179.
- [48] H. Frahm, *Nucl. Phys. B* **559** (1999), 613–636.
- [49] H. Frahm and V. E. Korepin, *Phys. Rev. B* **42** (1990), 10553.
- [50] ———, *Phys. Rev. B* **43** (1991), 5653.
- [51] H. Frahm and G. Palacios, *Phys. Rev. A* **72** (2005), 061604(R).
- [52] ———, *Phys. Rev. B* **73** (2006), 214419.
- [53] ———, *Theor. Math. Phys.* **150** (2007), 338–352.
- [54] H. Frahm, M. Pfannmüller, and A. M. Tsvelik, *Phys. Rev. Lett.* **81** (1998), 2116.
- [55] H. Frahm and N. A. Slavnov, *J. Phys. A* **32** (1999), 1547–1555.
- [56] ———, *Nucl. Phys. B* **575** (2000), 485–503.
- [57] P. Fröjdh and H. Johannesson, *Phys. Rev. Lett.* **75** (1995), 300.
- [58] P. Fröjdh and H. Johannesson, *Phys. Rev. B* **53** (1996), 3211–3236.
- [59] A. Furusaki and N. Nagaosa, *Phys. Rev. Lett.* **72** (1994), 892.
- [60] M. Gaudin, *Phys. Lett. A* **24** (1967), 55.
- [61] F. Gerbier, J. H. Thywissen, S. Richard, M. Hugbart, P. Bouyer, and A. Aspect, *Phys. Rev. A* **67** (2003), 051602(R).
- [62] T. Giamarchi, *Quantum Physics in One-Dimension*, Oxford Science Publications, Oxford, 2004.

- [63] M. Girardeau, *J. Math. Phys.* **1** (1960), 516.
- [64] A. O. Gogolin, A. A. Nersesyan, and A. Tsvelik, *Bosonization and Strongly Correlated Systems*, Cambridge University Press, Cambridge, 1998.
- [65] F. Göhmann, M. Bortz, and H. Frahm, *J. Phys. A* **38** (2005), 10879.
- [66] F. Göhmann and V. E. Korepin, *J. Phys. A* **33** (2000), 1199–1220.
- [67] F. Göhmann and H. Schulz, *J. Phys. Condens. Matter* **2** (1990), 3841–3854.
- [68] D. Goldhaber-Gordon, J. Göres, M. A. Kastner, Hadas Shtrikman, D. Mahalu, and U. Meirav, *Phys. Rev. Lett.* **81** (1998), 5225–5228.
- [69] D. Goldhaber-Gordon, H. Shtrikman, D. Mahalu, David Abusch-Magder, U. Meirav, and M. A. Kastner, *Nature* **391** (1998), 156–159.
- [70] A. González-Ruiz, *Nucl. Phys. B* **424** (1994), 468–486.
- [71] S. Groth, P. Krüger, S. Wildermuth, R. Folman, T. Fernholz, J. Schmiedmayer, D. Mahalu, and I. Bar-Joseph, *Applied Physics Letters* **85** (2004), 2980.
- [72] K. Günter, T. Stöferle, H. Moritz, M. Köhl, and T. Esslinger, *Phys. Rev. Lett.* **96** (2006), 180402.
- [73] F. D. M. Haldane, *Phys. Rev. Lett.* **47** (1981), 1840.
- [74] W. Hänsel, P. Hommelhoff, T. W. Hänsch, and J. Reichel, *Nature* **413** (2001), 498.
- [75] A. C. Hewson, *The Kondo Problem to Heavy Fermions*, Cambridge University Press, Cambridge, 1993.
- [76] A. Imambekov and E. Demler, *Phys. Rev. A* **73** (2005), 021602.
- [77] ———, *Annals of Physics* **321** (2006), 2390–2437.
- [78] E. Jeckelmann, *Phys. Rev. B* **66** (2002), 045114.
- [79] C. L. Kane and Matthew P. A. Fisher, *Phys. Rev. B* **46** (1992), 15233–15262.
- [80] ———, *Phys. Rev. Lett.* **68** (1992), 1220–1223.
- [81] N. Kawakami and A. Okiji, *Phys. Lett. A* **86** (1981), 483.
- [82] N. Kawakami and S.-K. Yang, *J. Phys. C* **3** (1991), 5983.

- [83] S. Kehrein, *The Flow Equation Approach to Many-Particle Systems*, Springer-Verlag, Berlin-Heidelberg, 2006.
- [84] T. Kinoshita, T. Wenger, and D. S. Weiss, *Phys. Rev. Lett.* **95** (2005), 190406.
- [85] N. Kitanine, J. M. Maillet, and V. Terras, *Nucl. Phys. B* **554** (1994), 647–678.
- [86] J. Kondo, *Physica* **1** (1934), 609.
- [87] R. M. Konik, H. Saleur, and A. Ludwig, *Phys. Rev. B* **66** (2002), 125304.
- [88] V. E. Korepin, N. M. Bogoliubov, and A. G. Izergin, *Quantum Inverse Scattering Method and Correlation Functions*, Cambridge University Press, Cambridge, 1993.
- [89] L. P. Kouwenhoven and L. I. Glazman, *Phys. World* **14** (2001), 33.
- [90] P. P. Kulish, *J. Sov. Math.* **35** (1986), 2648.
- [91] C. K. Lai, *J. Math. Phys.* **15** (1974), 1675.
- [92] C. K. Lai and C. N. Yang, *Phys. Rev.* **3** (1971), 393.
- [93] B. Lake, D. A. Tennant, C. D. Frost, and S. E. Nagler, *Nat. Mater.* **4** (2005), 329.
- [94] D.-H. Lee and J. Toner, *Phys. Rev. Lett.* **69** (1992), 3378.
- [95] F. Lesage, H. Saleur, and S. Skorik, *Phys. Rev. Lett.* **76** (1996), 3388–3391.
- [96] M. Lewenstein, L. Santos, M. Baranov, and H. Fehrmann, *Phys. Rev. Lett.* **92** (2004), 050401.
- [97] J. Li, W.-D. Schneider, R. Berndt, and B. Delley, *Phys. Rev. Lett.* **80** (1998), 2893.
- [98] E. H. Lieb, *Phys. Rev.* **130** (1963), 1616.
- [99] E. H. Lieb and W. Liniger, *Phys. Rev.* **130** (1963), 1605.
- [100] E. H. Lieb and F. Y. Wu, *Phys. Rev. Lett.* **20** (1968), 1445–1448.
- [101] A. Ludwig and I. Affleck, *Phys. Rev. Lett.* **67** (1991), 3160.
- [102] S. Lukyanov, *Nucl. Phys. B* **522** (1998), 533–549.
- [103] V. Madhavan, W. Chen, T. Jamneala, M. F. Crommie, and N. S. Wingreen, *Science* **280** (1998), 567.

- [104] J. M. Maldacena, *Adv. Theor. Math. Phys.* **2** (1998), 231–252.
- [105] M. Marcu, *J. Math. Phys.* **21** (1980), 1277.
- [106] L. Mathey, E. Altman, and A. Vishwanath, *cond-mat/0507108*.
- [107] L. Mathey, Wang, Hofstetter, M. Lukin, and E. Demler, *Phys. Rev. Lett.* **93** (2004), 120404.
- [108] P. Mehta and N. Andrei, *cond-mat/0702612*.
- [109] P. Mehta and N. Andrei., *Phys. Rev. Lett.* **96** (2006), 216802.
- [110] K. Mølmer, *Phys. Rev. Lett.* **80** (1998), 1804.
- [111] P. Nozières, *J. Low Temp. Phys.* **17** (1974), 31.
- [112] Jesper Nygaard, David Henry Cobden, and Poul Erik Lindelof, *Nature* **408** (2000), 342–346.
- [113] M. Ogata, M. U. Luchini, S. Sorella, and F. F. Assaad, *Phys. Rev. Lett.* **66** (1991), 2388.
- [114] M. Ogata and H. Shiba, *Phys. Rev. B* **41** (1990), 2326.
- [115] H. Ott, J. Fortagh, G. Schlotterbeck, A. Grossmann, and C. Zimmermann, *Phys. Rev. Lett.* **87** (2001), 230401.
- [116] G. Yuval P. W. Anderson and D. R. Hamann, *Phys. Rev. B* **1** (1970), 4464.
- [117] B. Paredes, A. Widera, V. Murg, O. Mandel, S. Fölling, I. Cirac, G. V. Shlyapnikov, T. W. Hänsch, and I. Bloch, *Nature* **429** (2004), 277.
- [118] T. M. Rice and F. C. Zhang, *Phys. Rev. B* **39** (1989), 815.
- [119] H. Saleur, private communication.
- [120] M. Scheunert, W. Nahm, and V. Rittenberg, *J. Math. Phys.* **18** (1977), 155.
- [121] P. Schlottmann, *Phys. Rev. B* **36** (1987), 5177.
- [122] P. Schlottmann and A. A. Zvyagin, *Phys. Rev. B* **55** (1997), 5027–5036.
- [123] E. K. Sklyanin, *J. Phys. A* **21** (1988), 2375–2389.
- [124] E. K. Sklyanin, *Quantum Inverse Scattering Method. Selected Topics*, In: *Quantum Group and Quantum Integrable Systems (Nankai Lectures in Mathematical Physics)*, 1992, pp. 63–97.

- [125] T. Stöferle, H. Moritz, C. Schori, M. Köhl, and T. Esslinger, *Phys. Rev. Lett.* **92** (2004), 130403.
- [126] H. Suhl, *Phys. Rev.* **138** (1965), A515.
- [127] B. Sutherland, *Phys. Rev. B* **12** (1975), 3795.
- [128] L. Tonks, *Phys. Rev.* **50** (1936), 955.
- [129] A. M. Tsvelik and P. W. Wiegmann, *Adv. in Phys.* **32** (1983), 453.
- [130] G. Vidal, *Phys. Rev. Lett.* **91** (2003), 147902.
- [131] ———, *Phys. Rev. Lett.* **93** (2004), 040502.
- [132] Y. Wang, J. H. Dai, Z. N. Hu, and F. C. Pu, *Phys. Rev. Lett.* **79** (1997), 1901–1904.
- [133] Y. Wang and J. Voit, *Phys. Rev. Lett.* **77** (1996), 4934–4937.
- [134] P. B. Wiegmann, *Sov. Phys. JETP Lett.* **31** (1980), 392.
- [135] ———, *Phys. Lett. A* **31** (1981), 163.
- [136] K. G. Wilson, *Rev. Mod. Phys.* **47** (1975), 773.
- [137] F. Woynarovich, *J. Phys. C* **16** (1983), 6593.
- [138] C. N. Yang, *Phys. Rev. Lett.* **19** (1967), 1312.
- [139] ———, *Prog. Theor. Phys.* **55** (1967), 67.
- [140] C. N. Yang and C. P. Yang, *J. Math. Phys.* **10** (1960), 1115.
- [141] H. Q. Zhou, X. Y. Ge, and M. D. Gould, *J. Phys. A* **32** (1999), L137–L142.
- [142] H. Q. Zhou, X. Y. Ge, J. Links, and M. D. Gould, *Nucl. Phys. B* **546** (1999), 779.

Lebenslauf

Name Guillaume Palacios

Geburtsdatum 20. März 1980

Nationalität Französisch

Forschungsgebiete

Exakt lösbare Modelle

Stark korrelierte Elektronen

Kalte Gase in niedrigen Dimensionen

Verschränkung und Quanten-Phasenübergänge

Ausbildung

seit 09/2004 Doktorand – Kondensierte Materie Theorie – ITP Hannover
Direktor: Prof. Dr. H. Frahm

2002–2003 DEA (Master) in Quantenphysik
Ecole Normale Supérieure (ENS) – Université Pierre et Marie Curie –
Paris VI

2001–2002 Maîtrise (MSc) in Physik
Université Pierre et Marie Curie – Paris VI

Bisherige Anstellungen

01/2001–06/2001 System- und Netzwerk-Administrator
Cap Gemini – Ernst & Young (CGEY), Paris La Défense